OSTEOCYTES AND BONE DISEASES

A Dissertation

by

YINSHI REN

Submitted to the Office of Graduate and Professional Studies of
Texas A&M University
in partial fulfillment of the requirements for the degree of

DOCTOR OF PHILOSOPHY

Chair of Committee:	Jian Q. Feng
Committee Members:	Kathy Svoboda
	Paul Dechow
	Yongbo Lu
	Yi-Shing Lisa Cheng
Head of Department:	Paul Dechow

May 2015

Major Subject: Biomedical Sciences

ABSTRACT

For many centuries, the osteoblast is considered to be responsible for bone formation. It is also believed that an imbalance of osteoblasts (weak) and osteoclasts (strong) is the main cause for bone diseases such as osteomalacia and osteoporosis and periodontal diseases, globally the most prevalent dental disease. Most studies are aimed at these two surface cells, although neither of them penetrates into the deep bone matrix. Osteocytes, terminally differentiated osteoblasts, are buried deep in the bone and account for up to 95% of all bone cells. Due to the high mineral density around osteocytes, most people consider them "quiescent" cells. Only recent research revealed more profound and important roles of osteocytes, such as mechano-sensors.

In this study, we developed the innovative "FITC-Imaris technique", which combines FITC (Fluorescein isothiocyanate), confocal microscopy and Imaris software. With this method, we could visualize the 3-D morphology of embedded osteocytesand statistically quantitate the osteocyte structure cell surface total cell volume, and dendrite numbers. We examined Dmp1 (dentin matrix protein 1) mutant mice, an established osteomalacia animal model, and showed both significant morphological and statistical differences in the osteocyte structure between the Dmp1-null mice and their age-matched control littermates, suggesting a high correlation between osteocytes and osteomalacia.

Then, we studied periostin knockout mice, a periodontal disease mouse model, and found that osteocyte' morphological and pathological changes are closely linked to alveolar bone loss. Monoclonal anti-SOST antibody) restores not only bone loss, but also osteocyte morphology, suggesting osteocytes may be responsible for bone loss in periostin mutant mice.

Lastly, we examined OVX rats as an osteoporosis model and showed that Ocys failed to maintain their shape, dendrite number and size in response to estrogen deficiency. Abnormalities in blood vessel morphology and bone matrices also developed, resulting in osteoporotic changes in both compact and trabecular bone. Similarly, administering

SOST antibody normalized osteocyte morphology and recovered bone loss from osteoporosis.

Altogether, we demonstrated that Ocy maturation was directly linked to a slow mineralization process. Minerals were constantly “pumped” via Ocy-dendrites to the surrounding matrix and to the bone surface. These study results expanded our understanding of how osteocytes regulate bone development and mineralization. These findings have clinical relevance, as SOST antibody improved bone phenotypes in all osteomalacia, periodontal disease and osteoporosis animal models, holding great potential for treating human bone disease.

DEDICATION

I thank God for listening to my prayers and healing my heart all the time. My thesis could not have been completed without God's glory. Also to my parents and especially to my sister, thank you for accompanying dad and helping him out when he was fighting cancer for the last two years. I would also like to thank my wife for her understanding and support through my 5 years at Baylor College of Dentistry. Lastly, I thank Dr. Jerry Feng who accepted me as his graduate student, which led me to the path of bone research.

ACKNOWLEDGEMENTS

I would like to thank my committee chair, Dr. Jerry Feng; I could not have completed my dissertation without his mentoring. During my Ph.D. program, Dr. Feng not only served as my supervisor, but also his hardworking and exceptional work ethic always provided a role model for all the lab personal. He sets high standards for the lab and keeps pushing himself to the limit in the scientific field. I am proud to be one of his students and will adopt his spirit and attitude towards science in my future research life. Deepest thanks also go to my committee members, Dr. Kathy Svoboda, Dr. Paul Dechow, Dr. Yongbo Lu, and Dr. Lisa Cheng, for their guidance and support throughout the course of this research. I also want to express the gratitude to Dr. Xiaofang Wang, Dr. Feng Tao and Dr. Philip Kramer who guided me through my cognate exams and helped me expand my knowledge of the calcium channel and Wnt signaling. I sincerely thank Dr. Shuxian Lin, Dr. Yan Jing and Dr. Xianglong Han for their assistance with the whole project and research analysis.

Last but not least, I would also like to convey my gratitude to Priscilla Hooks and Gerald Hill for their coordination and great help in animal breeding. Also, sincere appreciation goes to Nancy Anthony, Marge Palma and Jeanne Santa Cruz, who assisted me both with my study and research from the very first day in Baylor through my graduation. Thanks also go to my friends and colleagues and the department faculty and staff for making my time at Baylor College of Dentistry, Texas A&M University, a great experience. Finally, special thanks to NIH for the support to fund my research.

NOMENCLATURE

AB	Alveolar bone
ALP	Alkaline phosphatase
APC	Adenomatous polyposis coli
BSP	Bone sialoprotein
BSEM	Backscattered scanning electron microscopy
BrdU	5-Bromo-2’-deoxyuridine
µCT	Microcomputed tomography
Ca	Calcium
CEJ	Cementum-Enamel Junction
CK1	Casein Kinase 1
CKO	Conditional knockout
Con	Control group
Dapi	4',6-diamidino-2-phenylindole
DMP1	Dentin matrix protein 1
DKK1	Dickkopf-related protein 1
DKO	Double knockout
DSPP	Dentin sialophosphoprotein
Dsh (DVL)	Dishevelled
ECM	Extracellular matrix
ER	Endoplasmic reticulum
FITC	[2, 5]- Fluorescein isothiocyanate
FGF23	Fibroblast growth factor-23
FZD	Frizzled
GSK	Glycogen synthase kinase
Het	Heterozygous
HE	Hematoxylin & Eosin
Hyp	loss-of-function mutation of *Phex*
IHC	Immunohistochemistry

IP3	Inositol 1,4,5-trisphosphate
KO	Knockout
LacZ	β-Galactosidase
LRP5/6	Low-density lipoprotein receptor-related protein 5/6
MEPE	Matrix extracellular phosphoglycoprotein
MAPK	Mitogen-activated protein kinase
NIH	National Institutes of Health
Ob	Osteoblast
OCN	Osteocalcin
Ocy	Osteocyte
OPG	Osteoprotegerin
OPN	Osteopontin
OPPG	Osteoporosis-pseudoglioma syndrome
OSX	Osteorix
OVX	Ovariectomized
PCP	Planar cell polarity
PDL	Periodontal ligament
Phex	Phosphate-regulating neutral endopeptidase, X-linked
Pi	Phosphorus
PIP2	Phosphatidylinositol 4,5-bisphosphate
PKO	Periostin knockout
PTH	Parathyroid hormone
Rankl	Receptor activator of nuclear factor kappa-B ligand
Runx2	Runt-related transcription factor 2
SEM	Scanning electron microscope
SOST	Sclerostin
SE	Standard error of the mean
WT	Wild type

TABLE OF CONTENTS

Page

Page

LIST OF FIGURES

Page

Page

Page

CHAPTER I

INTRODUCTION AND LITERATURE REVIEW

Specific Aims

An imbalance of osteoblast and osteoclast activity attributes may be the main reason for the cause of periodontal disease, osteomalacia and osteoporosis, as it has long been assumed that osteoblasts build mineral and play a central role in recruiting osteoclasts. Recently, Tomoki Nakashima et al.(60) discovered that osteocytes are actually the main cells responsible for RANKL production and osteoclast recruitment. As the major cell type (more than 90% of cells in mature bone) (6,66), osteocytes also have a much longer life span (up to 20 years; some researchers even claim certain osteocytes remain alive the entire individual's life) than any other cell types. It is hard to be convinced that osteocytes remain quiescent the whole period. Moreover, osteocytes are found in the perfect place (totally buried in the mineral) to sense mineral changes; they are well connected with each other and with blood vessels through the canaliculi system.

To dissect osteocytes' direct role in bone mineralization and their pathological involvement, we used Dmp1 null mice, periostin null mice, OVX rats and osteoporosis patient cadavers in our osteomalacia, periodontal disease and osteoporosis study. Interestingly, we found that osteocytes have great morphological changes in all disease types, together with mineral loss around osteocyte lacunae. Applying an antibody against SOST (inhibitory gene of bone formation, mainly expressed in mature osteocytes) successfully recovers osteocytes and lost bone mass. Surprisingly, SOST antibody also induces blood vessel formation in animal models. Osteoblasts are responsible for collagen production as an abundant ER and Golgi complex in the cytoplasm; however, the way mineral is transported and laid down still remains unknown. By double labeling and DAPI staining (a novel technique developed in this lab), we visualized a great amount of new mineral along blood vessels, osteocyte lacuna, osteocyte dendritic processes and the

mineral front. Unexpectedly, a huge gap was present between osteoblast lining cells and the mineral front (also confirmed by backscatter imaging on the bone surface), which may indicate that osteoblasts do not directly participate in mineral deposition. Dmp1 (21,28) is mainly expressed in osteocytes (22,34,82). Dmp1 KO mice (88,89) and Dmp1 human mutations (20,25,47,48) cause striking defects in bone (51,91). Primary mouse calvarial cell (osteoblasts) culture from Dmp1-lacZ knock-in mice also confirm that mineralized nodules only form around lacZ positive cells (mainly fully developed osteocytes) rather than undifferentiated osteoblasts. Based on both *in vivo* and *in vitro* data, we propose that osteocytes are the main cells responsible for mineral transportation, deposition and maintaining bone homeostasis; thus, osteocytes could be a potential target for treating bone diseases such as osteomalacia, periodontitis or osteoporosis. To address our hypothesis, three specific aims are proposed:

Specific Aim 1: To investigate osteocyte changes (cell surface, cell volume and dendritic numbers) both qualitively and quantitively by introducing a novel technique combining FITC staining, confocal microscope and Imaris quantification software in Dmp1 null mice, using an osteomalacia animal model. The osteocyte-canaliculi system in the bone is stained by FITC and the 3-dimensional structure is captured by confocal microscopy. Finally, osteocyte changes are quantitively analyzed by Imaris (a software initially developed for neuron cell studies). We hypothesized that there would be a sharp reduction of surface area and dendrite numbers in Dmp1 null mice compared with age-matched control groups. Successful development of this technique will provide a great tool to study deep embedded cells like osteocytes and help us understand osteocytes' role in bone diseases like periodontal disease and osteoporosis (Aim 2 and Aim 3).

Specific Aim 2: To determine the role of the PDL (periodontal ligament) and osteocytes in periodontal disease and bone development. Periostin null mice were utilized as our periodontal disease model, and histological and biochemical studies were done to analyze the PDL's role in alveolar bone formation and the origin of periodontal disease in this particular mouse model. Meantime, anti-SOST monoclonal antibodies were

administrated and studied for their potential as a periodontal disease treatment. We hypothesize that the PDL is the major cell reservoir for postnatal alveolar bone formation; Scl-Ab treatment successfully reverses both alveolar bone defects and loss of PDL integrity in periostin null mice; osteocyte changes in periostin null mice are highly correlated with periodontal disease.

Specific Aim 3: To define the essential role of osteocytes in building and maintaining mineralized bone. Our hypothesis is that bone mineralization is a long process, in which the osteocyte plays a key role in orchestrating the mineral within an organic matrix; and that the osteoblast reciprocally supports osteocyte function in mineralization. To test this hypothesis, we will 1) use mandibular and femur bone from newborn to 5 months to map the maturation of the mineralization matrix and its close relationship with osteocyte maturation with both biological and physicochemical approaches; 2) both qualitively and quantitively analyze osteocyte change (cell surface, cell volume, dendrite numbers) in OVX rat, monkey animal models and osteoporosis patients; 3) using osteocyte-less (Dmp1 DTR) Tg mice to specifically delete osteocytes to determine if blocking mineral transportation through osteocytes alone has an effect on bone mineralization.

Together these aims will be a major paradigm shift over the understanding of bone mineralization from osteoblast-oriented to osteocyte-oriented bone modeling. Elucidating the relationship of osteocytes and bone development provide new perspective in treating and understanding various bone diseases such as osteomalacia, periodontal disease and osteoporosis. Furthermore, successful rescue of bone defects by Scl-Ab administration in all three disease types will provide evidence for new drug discovery and patient treatment.

Literature Review

Canonical and Non-canonical Wnt Signaling Pathways

Wnt is a group of secreted, highly-conserved glycosylated proteins that are often found to have lipid modifications (palmitoylation of cysteines) necessary for secretion and

signal transduction. Wnt, first identified as int1 in early mouse oncogenetic studies, was then known as Wingless (Wg) in Drosophilia, a segment polarity gene involved in body axis development in a morphogenetic manner. By now, Wnt signaling has been well studied in various areas - from embryo development to tissue regeneration. In this short discussion, we will focus on the role of Wnt signaling in bone development.

Wnt signaling is classified mainly into two categories: the canonical signaling pathway (Wnt-β catenin pathway) and the non-canonical pathway (including the Wnt-PCP and Wnt-Ca2+ pathways). Although the Wnt planar cell polarity (PCP) pathway is believed to cascade along small G-protein Rho and down-streaming Rac or to modify actin polymerization and regulate cell polarization through an alternative rac1-JNK way, its role in bone development is not known. The Wnt-Calcium pathway activates phospholipases C through Dsh, then the plasma component PIP2 can be cleaved to IP3 through the function of activated phospholipases C. IP3 subsequently regulates the calcium release from the endoplasmic reticulum (ER). The released calcium is responsible for cell migration and adhesion, and it is also suggested to have functions in ventral patterning. Recent research has indicated that the Wnt non-canonical pathway, especially the Wnt-calcium pathway, may be integrated with the β-catenin-initiated canonical pathway through Wnt 5a.

The Wnt β-catenin canonical pathway is initiated by various Wnt proteins; the well-studied ones include Wnt3a, Wnt5a, Wnt10b and Wnt 14. In the absence of Wnt signaling, β-catenin is sequestered in a complex including tumor suppressor Axin, adenomatous polyposis (APC), glycogen synthase kinase (GSK) 3β and casein kinase 1 (CK1). B-catenin subsequently will be phosphorylated and targeted for polyubiquitination, polyubiquitinated β-catenin will be transported to proteasomes and then degraded in this complex. When the Wnt β-catenin pathway is turned off, downstream T-cell factor/lymphoid enhancer factor (TCF/LEF) will remain repressed by Groucho. Once Wnt is present, it will form a receptor complex with Wnt co-receptor low-density lipoprotein receptor-related proteins 5 and 6 (Lrp 5/6) and a seven-transmembrane receptor FZD (Frizzleds). This complex will recruit Axin through interaction with

disheveled (DVL), which will free β-catenin from the destruction complex. Accumulating evidence has shown that a certain amount of β-catenin will still be phosphorylated but cannot be polyubiquitinated, resulting in excessive β-catenin that can be subsequently translocated into the nucleus. Nuclearized β-catenin will replace TCF/LEF repressor groucho and initiate downstream gene expression.

Wnt Signaling (SOST) and Bone Formation

Wnt signaling pathway has been extensively studied for its role in bone formation, and it is generally believed to be positively correlated with bone growth. The relationship of Wnt signaling with bone came to people's attention over a decade ago with discoveries that mutations in Wnt signaling in 4 different groups of patients resulted in severely altered bone strength and density, of which three of the groups saw a dramatically increased bone formation while the other one had an osteopenia phenotype. Remarkably, two of the mutations occurred in Lrp5, low density lipoprotein receptor-related protein 5, which proved to be an important co-receptor for the Wnt-β catenin signaling pathway. A loss of function mutation in Lrp5 led to osteoporosis-pseudoglioma syndrome (OPPG), resembling a low bone mass phenotype; on the other hand, a gain of function mutation of Lrp5 resulted in high bone mass. The other two groups of patients had mutations affecting the expression of SOST, or sclerostin, an antagonist of Wnt signaling that usually binds to Lrp4, 5 and 6 to prevent Wnt's association with the receptors. These two groups of patients were later known as sclerosteosis and Van Buchem disease, all leading to a high bone mass phenotype. Ever since the association of the Wnt canonical pathway and bone formation was illuminated, multiple transgenic mouse models were created to explore and exploit the possible role of Wnt signaling in bone development.

One group of well-studied transgenic animal models was related to the SOST gene. Sclerostin, the protein product of the SOST gene, is highly expressed by osteocytes and long and is hypothesized to be an essential molecule secreted at the bone surface by osteocyte, to regulate osteoblast activities. Overexpression of sclerostin led to low bone

mass as reported by Kramer et al., 2010. Deletion of SOST in mice is fully fertile and showed an increase bone formation, bone strength and density by increasing osteoblast numbers. Lrp 5 deficient mice are the animal model of OPPG syndrome, showing decreased bone density and an osteoporosis-like phenotype. Interestingly, deletion of SOST in Lrp 5 null mice fully reversed skeletal fragility, and the treatment of Lrp5 null mice with neutralizing sclerostin antibody rescued reduced bone mass and bone density. In fact, SOST is one of the few Wnt pathway genes selectively expressed in bone tissue, which makes it a promising target for drug design to treat bone-related diseases such as osteoporosis.

Dkk1 (Dickkopf-related protein 1), like sclerostin, binds with Lrp receptors to inhibit Wnt signaling. Dkk1 is highly expressed in osteoblasts, conventional knockout of Dkk1 lead to embryo death since DKK1 is an important molecule for head induction; however, Dkk1+/- heterozygote mice showed increased bone mass. Overexpression of Dkk1 led to osteopenia in the long bone, retarded mandibular tooth formation and demineralized calvaria. Dkk1 neutralizing antibody has been developed and showed increased bone formation at the endosteal side in an ovariectomy-induced osteopenia mouse model. Unlike SOST, Dkk1 expression is not limited to bone, so a systematic attribution of Dkk1 antibody may result in unwanted effects.

β-catenin is believed to be the essential molecule that determines mesenchymal cell fate and couples bone formation with bone resorption. The conditional knockout of β-catenin at an early osteoblast stage by using Osx-cre developed cranial ossification defects and increased chondrogenesis. The late osteoblast stage oblation of β-catenin by 2.3 col1-cre resulted in both increased osteoblasts and osteoclasts; however, the Opg/RankL ratio was significantly lower, which led to reduced bone mass. The osteocyte stage oblation of β-catenin by Dmp1-cre also produced impaired bone quality and decreased bone formation with decreased Opg expression and more active osteoclasts. Current research proved that exon 3 of β-catenin encodes for a region consisting of several serine and threonine sites for phosphorylation by Gsk3β, which will direct β-catenin to be polyubiquitinated and degraded. Multiple clinical cases revealed that the deletion of exon

3 in β-catenin is the cause for tumor genesis by stabilizing β-catenin in the cytoplasm. Numerous exon 3 conditional deletion mice were developed to study the role of constitutive activation of β-catenin (CA- β-catenin) in bone development. Osx-cre induced CA- β catenin resulted in early embryo death and premature ossification with increased proliferation of pre-osteoblasts. Interestingly, cranial ossification in this cKO mice was delayed while the overall skeleton showed early mineralization. This may due to the fact that β-catenin has different functions in modulating intramembranous bone formation versus endochondral bone formation. 2.3 Col1-cre induced CA- β-catenin led to postnatal lethality and osteopetrosis with decreased osteoclast numbers. Osteocyte stabilization of β-catenin by Dmp1-cre produces phenotypes similar to those of 2.3 Col1-cre: 1) Delay of teeth eruption due to a decreased number of osteoclasts; 2) stunted mandibular tooth root formation; 3) immature osteocytes (OSX staining positive) with a flattened and cuboid cell body and reduction of dendritic processes; and 4) trabecularization of cortical bone.

In conclusion, the β-catenin-mediated Wnt canonical pathway is a pivotal signaling pathway for bone formation, which is tightly controlled and interplays with multiple other signaling pathways such as Bmp, IHH and FGF signaling. Inhibited Wnt signaling in bone led to osteoporosis or osteopenia while increased Wnt signaling may lead to osteopetrosis and premature bone formation. Meantime, although being very promising, the idea of utilizing Wnt signaling-based drugs, for instance, the anti-sclerostin neutralizing antibody and anti-Wnt small molecule inhibitors, must be closely modulated to evaluate not only the effectiveness but also side-effects. In addition, Wnt β-catenin signaling may have different functions in different origins and types of bone development (intramembranous bone formation vs. endochondral bone formation). Further research will need to be done to illustrate how Wnt signaling is fine tuned to achieve balanced bone formation during development.

Summary

Osteocytes make up over 90-95% of bone cells (6,66). Evidence is accumulating that osteocytes are more active than previously thought (13,15); they regulate osteoclast

formation in bone (60,87) and play a key role in the mechanical strain reaction and coordination of adaptive bone remodeling responses (6). However, there are major gaps in our knowledge of osteocyte function during mineralization because: a) it is extremely difficult to study these cells, as they are buried in the mineralized matrix; b) currently no clear pathways have been identified that are in charge of the maturation from osteoblasts to osteocytes; and c) few diseases and animal models are linked to osteocyte functions. In this study, we first developed a new FITC-confocal-Imaris analysis technique that enables both qualitative and quantitative analysis of osteocytes, we also identified the Wnt canonical pathway to be responsible for the maturation of osteoblasts (an increased amount of Wnt-β-catenin is the key causative factor in the development of osteomalacia, which blocks the transformation of Ob into Ocy), and thus maintains overall healthy bone homeostasis. Last we utilized three different animal models (Dmp1 null mice as osteomalacia disease model, Periostin null mice as the periodontal disease model, and OVX rat as an osteoporosis model) to study the role of osteocytes in bone disease development. The inhibition of SOST function by Scl-Ab injection (activation of Wnt β-catenin signaling) restores bone loss and improved bone quality in all three animal models, which provides insights into new targets for drug development to treat patients with bone disease.

CHAPTER II

A NOVEL WAY TO STATISTICALLY ANALYZE MORPHOLOGIC CHANGES IN DMP1-NULL OSTEOCYTES*

Synopsis

Recent studies have revealed multiple roles of osteocytes in bone metabolism. However, detailed analyses of the embedded osteocytes in bone structure are still limited because of the high mineral content around these cells. In this study, we developed an innovative technique, the "FITC-Imaris technique", which combines FITC ([2, 5]-Fluorescein isothiocyanate), confocal microscopy and Imaris software. With this method, we could not only visualize the 3-D morphology of embedded osteocytes, but more importantly, we were able to statistically quantitate the osteocyte structure in the cell surface, total cell volume, and dendrite numbers. Furthermore, we made a side-by-side comparison of the new method with the acid-etched SEM imaging technique, a common imaging method for studies of osteocyte morphology with a much smaller cell depth (< 3 μm). Finally, we used the FITC-Imaris technique to show both the morphological and statistical differences in the osteocyte structure between the Dmp1-null mice (the osteomalacia model) and their age-matched control littermates. We expect that this newly developed technique will become a powerful tool to disclose more roles that osteocytes play in bone health and diseases(71).

Introduction

Osteocytes account for more than 90% of the total number of cells in mineralized bone. However, most bone studies have focused on the surface cells, such as osteoblasts

---

*Reprinted with permission from "A novel way to statistically analyze morphologic changes in Dmp1-null osteocytes" by Y Ren, S.Lin, Y. Jing, et al, 2014. Connective Tissue Research PVol.55 Suppl 1pp:129-133, Copyright [2014] by Informa Healthcare.

and osteoclasts, partly because these cells are more active in metabolism and are technically easier to access. However, recent studies have revealed more profound and important roles of osteocytes in addition to their role as mechanosensors. These roles include regulation of bone formation by secreting sclerostin proteins (5,32), bone resorption through the production of a great amount of RankL(60), control of phosphate homeostasis through FGF23 (25), and regulation of primary lymphoid organs and fat metabolism. Therefore, analyzing osteocytes in a more efficient and precise way is vital and necessary in bone biology studies.

One of the traditional methods of evaluating mineral-embedded bone cells is known as “acid-etched SEM” (25). Resin is packed into the non-mineralized structures during sample embedding; after acid treatment, the mineral is removed to expose the underlying resin-filled structures. Although a high-resolution, acid-etched SEM image can reveal the osteocyte-canalicular system, this technique has several limitations: 1) The optimal acid concentration and treatment time vary among samples, depending on the sample hardness and structure (thus, the process is time consuming). Oftentimes when the condition is optimized for mineralization defect samples like Dmp1-null bones, the mineral cannot be fully removed from the control samples under the same conditions; 2) The SEM technique can only be applied efficiently when the sample surfaces are polished so that all scratches are eliminated, although polishing removes many dendrites protruding from the osteocytes; and 3) Only the top layer of the osteocyte is uncovered, while cell processes deeply embedded in mineral remain hidden. Thus, a true 3-D analysis technique for osteocytes needs to be developed to enhance the understanding of the detailed osteocyte structure.

FITC is a small fluorescent molecule that penetrates all non-mineralized tissues. In bone studies, this molecule fills in the entire prospective osteocyte-canalicular system, surrounding blood vessels and osteoid layers, as well as surface cells such as osteoblasts and osteoclasts. However, there is a lack of good quantitative methods for defining the cell surface, volume, dendrite number, and average length of the dendrite.

Dentin matrix protein 1 (DMP1) has been shown to be a key factor in osteocyte biology and bone development. Functional studies have revealed that DMP1 is essential for the maturation and function of osteocytes via both local and systemic mechanisms (22,25,89). Genetic research identified that DMP1 mutations in humans or its deletion in mice lead to autosomal recessive hypophosphatemic rickets, characterized by severe osteomalacia bone changes with significant reductions in bone mineralization (22). Although the osteocytes of Dmp1-null mice have been characterized by SEM, immunohistochemical staining and other methods, the morphologic changes in them still have not been quantified and analytically documented.

In this study, we developed an innovative technique, which we call the "FITC-Imaris technique", because it combines FITC, confocal microscopy and Imaris software to statistically quantitate the osteocyte structure in the cell surface, total cell volume, and dendrite numbers. Our results revealed for the first time the statistical analysis of the detailed cell structures in healthy and Dmp1-null osteocytes. We predict that this study will have great impact on future studies of osteocyte roles in bone diseases such as osteoporosis.

Experimental Procedure

Mouse, rat and human specimens

Eight-week-old Dmp1 null mice and Dmp1 heterozygote littermates were analyzed in this study. After they were sacrificed, the right side of the tibia was removed for testing and evaluation. In addition, the technique is further demonstrated through the use of human and rat bone. All animal protocols were approved by the Animal Welfare Committee at Texas A&M University Baylor College of Dentistry.

FITC sample preparation and staining for confocal imaging

The muscle was removed from the mouse tibia, and the tibia bone was rinsed in PBS, followed by fixation in 70% ethanol for two days at room temperature with a one-time change of 70% ethanol. The bone samples were slowly dehydrated in 95% ethanol for one day and 100% ethanol for one day. The samples were stained with 1% FITC (Sigma, cat. no. F7250) in 100% ethanol overnight, followed by continuous dehydration with 100% ethanol for one more day and acetone for 2 days; they also underwent the plastic embedding process described previously (19). Notably, during the FITC staining process, additional dehydration, and the plastic embedding process, the bones were kept away from light by wrapping them in aluminum foil. The human specimen obtained from femur cortical bone and the rat tibia were cut to cubic size by a diamond saw for dehydration, which followed the same procedure as described above.

The embedded plastic blocks were sectioned using a water-cooled diamond-impregnated circular saw (Isomet, Buehler) into approximately 1-2-mm-thick slices. These slices were further sanded down to < 100 μm thickness using six grades (80, 200, 400, 600, 800, and 1200 grit) of sanding papers, and polished on a soft cloth rotating wheel with 1-μm alumina alpha micropolish II solutions (Buehler, no. 406323016). After polishing, the slides were immersed in a water-soluble mounting medium for confocal imaging and then covered with a plastic coverslip.

Confocal microscope imaging

The SP5 Leica confocal microscope located at Baylor College of Dentistry was used to gather Z-stack images. The FITC samples were subjected to 488-nm wave length excitation using an argon laser and emission at 520 nm. All the images were captured at light ranging from 500 to 540-μm wavelengths. Multiple stacked images were taken at 200 Hz and 1024x1024 dimensions using 63X glycerol objective lense at 1.5 times magnification. For both the Dmp1 HET and the null mice, a thickness of 32 μm was

obtained with a pixel size of 0.1542 μm x 0.1542 μm x 0.49 μm from the tibia cortical bone midshaft area. The ideal cubic pixel size was revised from 0.1542 x 0.1542 x 0.1542 μm to 0.1542 x 0.1542 x 0.49 μm in order to reduce possible fluorescence bleaching from prolonged exposure of tissues to laser light. For the human and rat specimens, a thickness of 35 μm was obtained for imaging using the same parameters.

Image J, Autoquant and Imaris analyses

To obtain good optical image quality, the stacked confocal images stored as Tiff files were converted to a multilayer Tiff file using Image J software. The images were uploaded to Autoquant software for deconvolution. The dimensions for the pictures entered into Autoquant were set at 0.1542 x 0.1542 x 0.49 μm. Blind 3-D deconvolution was performed after selecting the magnification and the optical medium for confocal imaging. The Autoquant output file was then imported into Imaris for filament tracing and statistical quantification. The same threshold parameters were set for the osteocyte body (7.85 μm for the filament tracing start point) as well as the dendrite length (0.485 μm for the end point) for both the Dmp1 heterozygote (HET) and Dmp1-null specimens. The computed cell bodies were then manually corrected according to the FITC confocal images. After tracing, the filament surface area, volume, length, and terminal point number were all collected and selected for statistical analyses.

Data analyses

Osteocytes (20-25) from the middle of the tibia cortical bone region were chosen to be quantitatively analyzed. Statistical significance was determined by an independent-sample t-test using SPSS 12.0. A p value of < 0.05 was considered statistically significant.

Results

Comparison between the acid-etched SEM and FITC imaging techniques

To better understand the advantage of the FITC-confocal imaging technique, we did a side-by-side comparison of both images. As shown in Fig 1-1 a, the maximum thickness of the osteocyte-lacuna image on the bone surface was less than 3 μm, which equals approximately half the thickness of the osteocyte. Therefore, this image could not be used for quantification. In contrast, an approximately 30-μm thickness of the stacked image could be obtained using the FITC-confocal technique with no distortion of the osteocyte structure using one photon laser beam (Fig 1-1 b, which is a diagram showing the difference of the imaging area covered by both techniques). Fig 1-1 c gives an example of the rat tibia cortical bone (approximately 5 μm thick; note that only the middle 10 slices of the series picture from the confocal microscope are stacked, to give a better view of the cell structure), in which the osteoblast lining cells, osteoclasts, and osteocytes are well documented in the same frame. Fig 1-1 d illustrates an osteon (the basic bone unit in mammalian compact bone) from a 30-year-old human male femur; the detailed structure, approximately 35 μm thick, includes the Haversian canal; many osteocytes, plus a large amount of dendrites, are visible.

Dmp1 null mice showed a significant increase in osteoid accumulation associated with a sharp reduction in dendrites and cell volume in osteocyte structure.

Imaris is Bitplane's scientific software that was originally developed for neuronal visualization and interpretation of 3D microscopy datasets. We have adapted this software for analyzing osteocyte FITC images qualitatively and quantitatively. As an example, we took separate FITC images of the HET and Dmp1-null compact bones (Fig. 1-2 a, step 1). Next, the osteocyte and its dendrites were traced using this software (Fig. 1-2 b, step 2), and the original images were then removed (Fig. 1-2 c, step 3). Finally, the data were

processed for statistical comparison (Fig. 1-2 d, step 4), which showed significant reductions in cellular surface, total volume, and dendrite length and numbers, supporting the notion that DMP1 is essential for osteocyte maturation in the structure

Discussion

In the present study, we developed a novel technique combining FITC confocal imaging and Imaris software, which not only enables the visualization of the true 3-D morphology of non-decalcified compact bone cells, but also statistically analyzes the morphologic differences among the healthy and the Dmp1-null osteocytes. This technique shares many similarities with the acid-etched SEM imaging technique, such as sample preparation and visualization of the 3-D osteocyte structure. The technique offers the following advantages: 1) much broader bone areas can be evaluated, including cells on the bone surface (osteoblasts and osteoclasts) and the interior structures, including both osteocytes and the osteon structure; 2) no extra physical and chemical treatments are required; thus, a natural cell distribution with essentially no tissue distortions can be seen; and 3) most importantly, the buried osteocytes and their dendrites can be precisely analyzed both qualitatively and quantitatively.

CHAPTER III

VITAL ROLES OF OSTEOCYTES IN RESTORATION OF BONE AND PDL DEFECTS IN PERIODONTITIS*

Synopsis

The development of an effective treatment for bone loss and PDL (periodontal ligaments) damage in periodontitis has been a longstanding aim in dentistry and medicine. Osteocytes account for over 90% of bone cells, although their relationship with the PDL and periodontitis is largely unknown. In this study, we initially documented a 2- and 3-fold faster rate in the PDL than in the periosteum and endosteum, respectively. Further, we demonstrated the origin of alveolar bone cells from PDL progenitor cells using the Cre-loxP technique. We then identified ectopic ossification in the PDL and pathological changes in osteocyte morphologies from spindle to round with sharp reductions in dendrites in a severe periodontitis patient. A similar osteocyte change plus increases in SOST (Wnt inhibitor) occurred in periostin-null mice. Subsequently, we showed that removing *Sost* or blocking SOST by the SOST antibody rescued the bone phenotype and made improvements in the PDL morphologies and expressions of biglycan and decorin in periostin-null mice. We propose that (1) PDL functions as the key reservoir for alveolar bone formation; (2) The osteocyte defect is responsible for bone loss in periodontitis; and (3) blocking SOST function restores bone loss is in part through enhancing PDL progenitor cells.

Introduction

The periodontal ligament (PDL), positioned between the bone forming the socket wall and the cementum covering the tooth root, was named in part because of rich of fibers

---

*Part of this chapter is reprinted with permission from "Removal of SOST or blocking its product sclerostin rescues defect in the periodontitis mouse model" by Y Ren, X Han, SP HO, et al, 2015. FASEB J, pii: fj.14-265496, Copyright [2015] by The FASEB Journal.

in this unique structure. These fibers connect the tooth to the jaw bone, support the tooth in the socket, and buffer loads imposed on the tooth, thus protecting the tooth and adapting to tooth movement and occlusal function. Because PDL contains osteogenic progenitor cells, it is widely believed that these cells, like bone marrow cells, contribute to alveolar bone formation before molecular biology era. However, there is a lack of in depth in vivo studies on the basic role of PDL in alveolar bone formation.

Periodontitis, the most common disorder known to mankind, is defined as a set of complex diseases that include different types of gingivitis and periodontitis. The real causes of these diseases are still largely unknown, as they could be of developmental, inflammatory, traumatic, neoplastic, genetic, or metabolic origin, although pathogenic microflora in the biofilm or dental plaque are the common causes. Gingivitis, the mildest form of periodontal disease, affects 50–90% of adults worldwide. Inflammation that extends deep into the tissues and causes loss of supporting connective tissue and alveolar bone is known as periodontitis (67). The advanced form results in loss of connective tissue and bone and accounts for 10-15% of adults in population studies (17,29,30) who suffer from tooth loss. Moderate periodontitis is estimated to affect even more people (68). Furthermore, there are afew pieces of evidence that supporta two-way relationship between periodontitis and diabetes (i.e., diabetes increases the risk for periodontitis, and periodontitis negatively disturbs glycemic control (9,35,39,57,68,78). Because the early or moderate condition is typically asymptomatic, many patients are unaware till the disease progresses to affect the teeth. Development of an effective treatment for bone loss in these diseases has been a longstanding aim (67).

Sclerostin, a potent inhibitor of Wnt signaling, is highly expressed in an osteocyte (Ocy). The sclerostin antibody (Scl-Ab) has been shown to have great efficacy in the treatment of a number of pre-clinical models for osteoporosis and bone fracture healing (1,38,42). Recent studies showed that this monoclonal antibody can be used to prevent bone loss in a model of inflammation-induced bone loss (18), and in an experimental periodontitis rat model (81). However, it is not known how and why blocking Scl works in inflammation-induced bone loss.

Genetic animal models are widely used not only to prove causes and consequences of genes and disease relationships, but also to test the potential of drug therapeutics. For example, Periostin is highly expressed in PDL cells during adult life as demonstrated by in situ hybridization and immunohistochemistry (74,75,85), and Periostin-knockout (KO) mice have been used for studies of periodontal diseases (73,75,76), as this animal model recaptures many characteristics of human periodontal diseases, including early onset of periodontal bone loss, PDL inflammation and pocket formation. In contrast, Sost-KO mice have a dramatic increase in bone mass with no apparent abnormality in morphology (45). In this study, we sought to investigate the biological significance of PDL in normal alveolar bone formation and the possible impact on chronic periodontitis with a focus on the intervention of the Sost gene or its function in periostin KO mice at the cellular and molecular levels. Our findings support the novel concept that the PDL plays a far more important physiological role than that of the periosteum and the endosteum in alveolar bone formation. We also found a surprising pathological change (from spindle to round with a sharp reduction in dendrites) in the osteocyte (the cell accounting for over 90% of bone cells) in the periostin KO mandible. Translational studies have showed that the deletion of Sost or treatment with Scl-Ab fully prevented or reversed bone loss in periostin KO mice, likely through reversing osteocyte structure and function. Furthermore, these interventional approaches greatly improved the PDL structure, which raised new hope for the future treatment of patients with periodontitis, as there is currently no surgical or drug method that can be used to restore the PDL structure.

Materials and Methods

Mice, dog and human tissue

Periostin, sclerostin double knockout mice were created by mating periostin and sclerostin null mice. Ten-month-old dog mandibles were generously offered by Dr. Peter Bushang in the Orthodontic department at Baylor College of Dentistry. Human tooth and mandible bone specimens were provided by Dr. Zhengguo Cao from Wuhan University

in China. All animal protocols were approved by the Animal Welfare Committee at Texas A&M Health Science Center Baylor College of Dentistry.

Scl-Ab injection into periostin null mice

To evaluate the function of anti-sclerostin monoclonal antibody in periodontal disease treatment, WT and periostin null mice were both injected with 25 mg/kg Scl-Ab twice a week for 8 weeks; control mice were injected with saline as placebos in both WT and periostin null mice. Injection started at 4 weeks and 12 weeks of age; after injection, the mice were sacrificed at 12 weeks and 20 weeks of age, respectively.

Adeno-virus injection into Rosa-26 mice

One-month-old Rosa-26 mice were subjected to adeno-virus injection. The virus was injected in the periodontal ligament around both molars and incisor using a 0.2 mm fine needle. Samples were collected at 5 days and 10 days post-injection for lacZ staining to trace the migration and development of the PDL cells.

Double fluorochrome labeling

To analyze the difference in the bone formation rate in the periosteum, endosteum and PDL in the mandible, double fluorescence labeling was performed as described previously (50,58). Briefly, calcein (5 mg/kg i.p.; Fluka) was administered 7 days before sacrifice, and alizarin red (20mg/kg i.p; Sigma) was injected for the 2nd labeling at 2 days before sacrifice. The mandibles were removed and fixed in 70% ethanol for 48 h. The specimens were dehydrated through a graded series of ethanol (70–100%) and embedded in methyl-methacrylate (MMA, Buehler, Lake Bluff, IL) without decalcification. Fifty-μm sections were cut using a Leitz 1600 saw microtome. Then the plastic sections were

viewed under a Leica-Sp5 confocal microscope. The mean distance between the two fluorescent labels was determined and divided by the number of days between labels to calculate the deposition rate of bone from different origins (periosteum vs. endosteum vs. PDL)(70).

Histology

The teeth (mice, dog and human) were all fixed in freshly prepared 4% paraformaldehyde in phosphate-buffered saline (pH 7.4), decalcified, and embedded in paraffin using standard histological procedures as previously described (22). The tissue blocks were cut into 4-μm thick mesio-distal serial sections to compare the tissue samples from the experimental and control groups and were then mounted on glass slides. The sections were used for H&E staining, trap staining, Sirius red staining and immunohistochemistry (Dmp1: 1:400, provided by Dr. Chunlin Qin from Baylor; Mepe: 1:400; Biglycan and Decorin: 1:1000, provided by Dr. Larry Fisher from NIH; Periostin: 1:1000, Innovative Research; OSX: 1:400, abcam; SOST: 1:400, R&D).

Backscattered scanning electron microscopy (SEM) and resin-casted SEM

The mandibles were dissected and fixed in 70% ethanol at room temperature for 24 h. The tissue specimens were dehydrated in ascending concentrations of ethanol (from 70% to 100%), embedded in MMA without decalcification and sectioned through the center of the first mandibular molar using a water-cooled diamond-impregnated circular saw (Isomet, Buehler). The cut surface was polished using 1, 0.3 and 0.05 μm alumina alpha micropolish II solutions (Buehler) on a soft cloth rotating wheel (58). Each sample was placed in an ultrasonic bath between steps and immediately following the polishing steps. The dehydrated specimens were then sputter-coated with carbon and scanned with a backscattered electron detector in a JEOL JSM-6300 scanning electron microscope (JEOL, Japan). The parameters were kept constant while the backscattered SEM images

were taken. Next, the carbon-coated samples were repolished, as described above. The surfaces were acid-etched with 37% phosphoric acid for 2-10 seconds, followed by 5% sodium hypochlorite for 20 minutes. The samples were then sputter-coated with gold and palladium, as described previously (25,54), and examined in the scanning electron microscope.

FITC staining and Imaris Analysis

FITC staining (10)- Fluorescein isothiocyanate, a small molecular dye, fills in the PDL cells/fibers as well as the cementoblast and cementocyte cells but does not enter the mineral matrix. Thus, the dye provides a visual representation of the organization of the PDL and osteocytes under the confocal microscope. After harvesting and dissection, the jaw bones were stained by FITC (Sigma, cat. no. F7250) overnight during the dehydration and embedding process at room temperature and then processed to obtain cortical sections and cancellous bone blocks. Cross section (300-400 μm thick) were cut with a diamond-bladed saw (Buehler, Lake Bluff, IL), and the plastic sections were then sanded and ground to a final thickness of 30-50 μm for confocal imaging. Stacked pictures were processed to Autoquant (Mediacybernetics, Rockville, MD) for deconvolution and subsequently to Imaris (Bitplane, Switzerland) to quantify the cell surface area, volume and dendrite ending points of the osteocytes as previously described by Ren et.al.

Micro-CT and CEJ-Bone level area quantification

The mandibles from 4 different groups in both age sets (12 weeks old and 20 weeks old when sacrificed) were dissected from the mice and analyzed by x-ray radiography (piXarray 100, Micro Photonics) and a μ-CT35 imaging system (Scanco Medical, Basserdorf, Switzerland). The μ-CT analyses included: 1) a medium-resolution scan (7.0 μm slice increment) of the whole mandible from the mice for an overall assessment of the shape and structure; 2) a high-resolution scan (3.5 μm slice increment) of the alveolar bone

(teeth were set upright during scan, 400 slices were chosen starting from the alveolar bone level) for analysis of the alveolar bone around the 1st molar. The data acquired from the high-resolution scans were used for quantitative analyses. Bone volume to total volume ratio (BV/TV) was obtained and analyzed using the Scanco software. The data are reported as mean ± S.E.

To quantify the area within CEJ (Cementum-Enamel junction) and bone level before and after treatment in all groups, 4 mandibles in each of the 4 groups (named the WT group, WT + Ab group, Periostin KO group, Periostin KO + Ab group) both 12-weeks- and 20-weeks-old were scanned by micro-CT (Scanco-35, Switzerland) in high resolution to quantitate periodontal bone loss. Similar to previous reports by De souza (79) and Kuhr(41), the lost bone area was restricted by the alveolar bone crest (ABC), the cementum-enamel junction (CEJ), the mesial root of the 1st molar and the distal root of the 3rd molar. The 3-D mandible images were firstly virtually sectioned to expose both root canals of the 3 molars in order to align the mandible perpendicularly, and then the 3D images were restored for quantification. Lost bone area was contoured and calculated by Image J (NIH, USA).

Statistical analysis

Statistical significance was determined by One-Way ANOVA followed by Bonferroni post hoc comparisons between two groups using SPSS 13.0. A P value of < 0.05 was considered statistically significant.

Results

Patients with periodontitis display ectopic bone formation and severe inflammation in the PDL

Bone loss and inflammation are key characteristics of patients with periodontitis, which is routinely diagnosed by an oral pocket formation using X-ray and local

examinations with no biopsy required. To explore actual pathological changes in this disease, we initially analyzed the extracted teeth, in which the PDL and alveolar bone tissues were attached, from the two cases of patients with severe periodontitis. As expected, both alveolar bone samples displayed chronic inflammation with large amounts of plasma cells, a few lymphocytes, and TRAP (tartrate-resistant acid phosphatase) positive cells, as well as bone loss (Fig. 2-S1 a). Unexpectedly, in the first case the radiograph and H&E images revealed ectopic ossifications in the PDL regions adjacent to the acellular cementum layer (Fig. 2-S1 b). The enlarged H&E image documented Ocy-like cells in the ectopic bone region (Fig 2-1 a). These bone-like cells expressed low levels of DMP1 (Fig 2-1 b, the gene highly expressed in Ocy) and MEPE (Fig 2-1 c, the gene expressed in Ob and Ocy) with an extremely low level of perisotin (Fig 2-1d, the gene that is essential for the integrity of PDL (74,75)). The FITC (Fluorescein isothiocyanate)-confocal images (8) showed fibers only in the patient PDL (Fig 2-1 e), dramatic changes in Ocy cell shape (from spindle to expanded round), and cell distribution (a loss of osteon, the basic bone formation unit) in the alveolar bone (Fig 2-1 f-g). The above data indicate that human PDL progenitor cells may directly contribute to the ectopic bone formation, and that the loss of PDL progenitor cells and pathological changes of osteocytes can explain in part the failure for the compensation of bone loss in the periodontitis patient.

The PDL progenitor cells are the key for alveolar bone formation

Although it was speculated that the PDL could form alveolar bone long before the molecular biology era, there is no in vivo experimental evidence supporting this assumption. To test this hypothesis we initially compared the bone formation rate on the PDL-alveolar bone surface, periosteum bone surface, and endosteum surface using pre-labeled fluorochrome specimens (Calcein injection first, and Alizarin Red injection second 5 days apart) from one-month-old mouse jaw bones. The double labelling confocal image demonstrated a statistically significant difference among these regions with the fastest deposition rate on the PDL-alveolar bone surface, which is 2- and 3-fold faster rate

in the PDL than in the periosteum and endosteum, respectively (Fig. 2-2 a, $P < 0.05$). In the enlarged view, a double labeling layer was observed around an OCY, indicating a direct mineral contribution from the OCY cell (Fig. 2-2 b). Further, we observed a small amount of minerals (yellow color, overlaid with green and red color) in the PDL area adjacent to the bone surface, supporting the mineralization started from the PDL adjacent to the alveolar surface. A similar indication that OCYs come from the PDL progenitor cells was confirmed by the FITC-confocal technique (Fig 2-2 c). In addition, we used the acid-etched SEM technique, a sensitive method for revealing trace amounts of minerals in bone matrices (29), and the close relationship between the mineral sheet and the osteocyte-canalicular system, indicating contributions of osteocytes in mineralization (Fig. 2-2 d). For the definite confirmation of the progenitor resource of alveolar bone cells from the PDL progenitor cells, a local injection of adenovirus CMV-CRE into the PDL and periosteum (as a positive control) regions of the Rosa26 jaw bone were carried out and followed by X-gal stains of these samples 5 days after injection. The blue cells in the mandible cortical bone and alveolar bone regions indicated their origins were from the periosteum (Fig 2-2 d, left) and the PDL (Fig 2-2 d, right) respectively. Taken together, the above data support the notion that alveolar bone is formed from three different progenitor cell pools: PDL, periosteum and endosteum; and that the PDL progenitor cells play a far more important role in alveolar bone formation.

Removing the Sost gene or treatment with Scl-ab fully prevented or greatly improved bone loss in periostin KO mice

Previously, we showed that periostin KO mice develop a periodontitis-like phenotype due to the loss of the PDL integrity (74,75). Here we re-examined this KO mouse line and found an unpredicted change of Ocys from spindle-to-round shape in the jaw bone (Fig. 2-S2 a-b) but with no apparent changes in the periostin KO long bone (Fig. 2-S2 c). Moreover, there was a sharp increase in SOST expression in the periostin KO jaw bone (Fig. 2-S2 d) with no apparent change in SOST in the KO tibia (Fig. 2-S2 e). These

data support the notion that the local changes in Ocy in morphology and SOST expression is partly responsible for the periostin KO bone loss.

Because deletion of Sost led to a great increase of bone volume in long bone (45), we studied the Sost KO jawbone phenotype and showed a similar bone volume increase in alveolar bone plus the development of the osteon, the basic bone unit that occurs only in mammals but not in rodents (Fig. 2-S3). Then, we reasoned that removing Sost in periostin KO mice could rescue the Ocy and bone-loss phenotype. To test this hypothesis we first generated double KO (DKO) mice and showed the full prevention of the bone phenotype by radiography (Fig 2-3 a) and μCT techniques qualitatively and quantitatively (Fig 2-3 b-c). We also demonstrated the prevention of the following pathological changes in the bone matrix and Ocy morphology in the DKO mice: i) poor bone mineral matrices in the jaw bone as reflected by a mixed appearance of grey (low mineral) and white (high mineral) color with a lack of white rings surrounding the Ocy cell bodies; ii) the Ocy shape change from spindle to round; and iii) a full prevention of both bone matrices and cell shapes in the DKO bone using backscattered SEM (Fig 2-3 d) and acid etching SEM (Fig 2-3 e) approaches.

We next asked whether treatment of periostin KO mice with Scl-Ab, a clinical trial drug that is used for treatment of osteoporosis (55,65), can prevent or rescue the bone loss in this mouse model. To achieve this goal, the animals were i.p. injected with Scl-Ab starting from the age of one month when animals display no apparent phenotype (for prevention purposes) or three months when the animals had already developed the periodontitis-like phenotype (74,75) (for treatment purposes) for 8 weeks, separately. In the prevention group, the radiographic images (Fig. 2-S4 a) and μCT images (Fig. 2-S4 b) showed no apparent changes in alveolar bone volume compared to the control group. The quantitative uCT analysis confirmed a full prevention of bone loss in the early-treated KO group (Fig. 2-S4 c).

To address whether the prevention of bone loss was directly linked to the Ocy morphological change, we developed a novel approach combining FITC images with IMARIS software (which was originally developed for neuronal visualization and

quantitation of 3D datasets) to quantify the Oyc-laculo-canalicular system in vivo (Ren et al. in press). In these non-decalcified mandibles, we randomly examined the FITC images from a WT, a non-treated and a treated group at age of 3 months, and traced 20 Ocys and their dendrites qualitative and quantitative comparisons. In the non-treated periostin KO samples there were significant reductions in Ocy volume, length and number of dendrites (Fig 2-4). These pathological changes were fully prevented in the Scl-ab treated cortical bone, supporting the notion that the direct role of Scl-ab on Ocy morphology is the key to prevention of bone loss in this animal model.

In further support of the above hypothesis, we took the same approaches and compared the effectiveness of the Scl-ab on the treatment of bone loss in the 3-month-old periostin KO group. Both the radiographic image (Fig 2-5 a) and μCT data (Fig 2-5 b) showed a great rescue of alveolar bone loss. The cementum-enamel junction (CEJ) to bone level area reflected by μCT images, a new method developed for estimating the degree of alveolar bone loss, revealed a significant amount of alveolar bone loss in the periostin KO mice and great improvement in the Scl-Ab treated group (Fig 2-5 c). The backscattered SEM images (Fig 2-5 d) and acid-etched SEM images revealed a severe bone volume reduction in the entire alveoli and a great loss in minerals surrounding the Oyc-laculo-canalicular system in the periostin KO alveolar bone (mid), which was fully restored in the Scl-Ab-treated jaw bone (right), supporting a close correlation between the changes of Ocy morphologies and matrix mineral contents, and the key role of Ocys in the developmental bone loss and treatment in this periodontitis animal model.

Removing the Sost gene or blocking SOST function restored cellular and molecular readouts in the periostin KO alveolar bone and PDL

To define the impact of removing the Sost gene or blocking SOST function on cellular and molecular changes in the periostin KO alveolar bone and PDL, we did a series of histological and immunohistochemical analyses. In the periostin KO mice, both bone resorption (as reflected by TRAP expression in Fig 2-6 a, middle) and formation (a

compensated reaction, as revealed by levels of osterix (59), Fig 2-6 b, middle) were high, although the bone quality was poor, reflecting a low level of DMP1 (Fig 2-6 c, middle). Further, in the periostin KO PDL, the expression of biglycan (Fig 2-6 d), decorin (Fig 2-6 e), and collagen (as reflected by polarized light, Fig 2-6 f, middle) were greatly reduced. All these pathological changes were fully reversed when Sost was removed (Fig 2-6, right images, double KO). Similarly, 8-week-treatment of periostin KO with Scl-ab achieved the same rescue effect (Fig. 2-S5, right images), supporting the notions that Scl-ab not only restores the bone phenotype but also greatly improve PDL phenotype in the periostin KO mice.

Discussion

Control of chronic periodontal disease, the most common human disease, has been the focus of intense investigation for many decades because of the destruction of the PDL and the loss of bone and teeth in these patients. In this study, we took a totally different strategy and focused on osteocytes in both the patient bone sample and animal studies, instead of concentrating on changes of cytokine and inflammation processes as commonly performed. For example, we first identified extensive ectopic bone-like tissues in the patient PDL region adjacent to the acellular cementum (Fig. 2-1 and Fig. 2-S1 b). This finding agrees with the in vitro studies that human PDL cells express bone markers and form mineral-nodules (2,44). Next, we demonstrated enormous pathological changes in the PDL and osteocyte, including the loss of PDL cells, a shape change of the osteocytes from spindle to round, a huge increase in the cell body but a sharp reduction in the dendrite number and length, and a change in the cell distribution from surrounding the Haversian canal arrangement in the osteon structure to a totally disorganized cluster pattern (Fig. 2-1 e-f). In combination with our previous report that the osteocyte played a critical role in mineralization (25), we propose that both a loss of PDL progenitor cell and defects in

osteocyte morphologies account for in part a severe bone loss in the patient with severe periodontitis.

To further support the critical role of PDL in the human disease case, we compared the PDL's contribution to alveolar bone formation with other well-established bone progenitor resources (periosteum and endosteum) in one month old mice. It is clear that the bone formation rate originating from PDL progenitor cells is even faster than the periosteum and endosteum. Both the cell lineage assay and FITC imaging data are in agreement with the notion that the PDL cells play a far more important role in alveolar bone formation than is commonly believed (Fig. 2-2).

The pathological changes in osteocytes in the periodontitis patient are not predictable. To directly link this change to bone loss was initially challenging, since we know very little about this cell in bone mineralization. Because there was a sharp reduction in the expression of periostin in the patient PDL (Fig. 2-1 d), and the periostin KO mice develop many characteristics of the human periodontitis phenotype such as early onset of periodontal bone loss, PDL inflammation and pocket formation (73,75,76), we studied their osteocyte morphologies using multiple techniques. Again, this animal model developed the same osteocyte phenotype as in the human patient (Figs. 2-3-5). Further, because of a great increase in SOST in the periostin KO mice (Fig. 2-S2) and the close correlation between the optimal change in osteocyte morphologies and the increase in alveolar bone volume (Fig. 2-S3), we generated double KO mice. The full prevention of osteocyte and bone loss phenotype in these double KO mice not only confirmed our hypothesis but also triggered our next step to address whether blocking SOST function rescues osteocytes and the bone phenotype in the periostin KO mice using the monoclonal Scl-ab. The data obtained from the prevention group (early treatment before the bone phenotype appeared) and the rescue group (the treatment initiated after the bone loss) are exciting, as both osteocyte and bone loss phenotypes are prevented or greatly rescued. What's more, the PDL phenotype is greatly improved in the double KO and Scl-ab treated mice (Fig. 2-6, and Fig 2-S5). At this stage, we do not know why and how the PDL phenotype is reversed by blocking SOST function, as periostin is mainly expressed in PDL

and SOST is highly expressed in alveolar bone. However, based on a close association between the Sharpe's fibers and osteocytes in the alveolar bone regarding their structural connection and gene expression patterns (Fig 2-S6), we speculate that there might be an interaction among them in this special environment, which is altered during periodontitis, leading to local changes in osteocyte morphologies. On the other hand, deletion of Sost or blocking SOST function may send a positive signal to PDL progenitor cells for repairing damages in both the PDL itself and alveolar bone through Sharpe fibers. In other words, the Sharpe fibers not only connect the PDL and alveolar bone but also function as a bridge between these two tissues in signaling interaction.

In summary, in this study we demonstrated that (1) the PDL functions as the most important reservoir for alveolar bone formation; (2) Morphological changes in osteocytes are responsible for bone loss in both the patient with periodontitis and the periostin KO mice; (3) Deletion of Sost or blocking SOST function prevents/restores bone loss via reversing osteocyte morphologies; and (4) Restoration of the PDL phenotype by Scl-ab treatment in the periostin KO mice shed a new light on future drug development, as there is no success in repairing PDL damage in patients with chronic periodontitis.

CHAPTER IV

THE OSTEOCYTE IS THE KEY TO BONE MINERALIZATION

Synopsis

The theory that osteoblasts (Obs) form bone is the cornerstone of bone biology, although the role of the osteocyte (Ocy), the most abundant bone cell with a half-life of decades, remains speculative despite its ideal location to initiate and maintain mineralization. Using comprehensive imaging techniques, we demonstrated that Ocys, whose maturation is directly linked to a slow mineralization process, constantly "pump" minerals via their dendrites not only to the surrounding matrix, but to the bone surface as well. Next, we showed that mineralization defects occurred when Obs failed to form Ocys in Dmp1-null mice with osteomalacia. Mechanism studies of Dmp1-null mice revealed a surprising increase in β-catenin in bone, which is responsible for abnormal mineralization. On the other hand, when Ocys failed to maintain their shape, dendrite number and size in response to estrogen-deficiency, abnormalities in blood vessel morphology and bone matrices developed, resulting in osteoporotic changes in both compact and trabecular bone. These findings demonstrate that Ocys are the key cells in bone mineralization, and defective Ocy maturation and function may underlie abnormal mineralization in osteomalacic diseases (Supplementary Fig. 3-1)

Introduction

The osteocyte, defined as the terminally differentiated cells derived from osteoblasts located within the bone matrix, comprises more than 90% to 95% of all bone cells in the adult skeleton. Previously, osteocytogenesis was considered a passive process, during which osteoblasts produced a matrix/osteoid and became trapped under new osteoid over the embedded cells (31,61). However, in the last decade, there was a virtual

explosion of data on the molecular biology and function of osteocytes. Far from being the "passive placeholder in bone", this cell type has demonstrated numerous functions, such as remodeling the bone (3), producing hormones such as the parathyroid hormone (4,72,77) and estrogen (40,86), acting as a mechanosensory cell (80), regulating bone resorption via osteoclasts (63,87), and working as an endocrine cell via connections with the vascular system (14). More clinical observations indicated that osteocytes were important for bone mineralization and maintenance. For example, the functional disorder of osteocytes leads to osteoporosis, a disease affecting 55% of Americans aged 50 or above and is responsible for millions of fractures annually (53,62,90). The differentiation of osteoblasts into osteocytes occurs in several stages, including osteoid osteocyte (or newly formed osteocyte), mineralized osteocyte, and mature osteocyte (7). Therefore, the osteocyte was one of the key cells involved in skeleton development and homeostasis, and the identification of the mechanisms underlying its differentiation and maturation process helped to further the understanding of bone biology in order to develop skeletal disease therapy.

Subjects and Methods

Animals

All animal studies were performed in accordance with the guidelines of the Baylor College of Dentistry, TX A&M Health Science Center, and Amgen IACUS review board. Thehuman cadavers used were from the BCD anatomy teaching lab and exempted from the IRB of Baylor College of Dentistry. C57BL/6 Dmp1-null mice (24) and Hyp mice, which were purchased from Jackson Labs, were used in this study (6 weeks old, 4 in each group, no blinding or randomization is performed during sampling). Previous examination of these mice showed no apparent differences between sexes, between heterozygous (Het) and wild-type (WT) mice in any parameters measured to date, representative data were shown in this paper. The 12-year-old cynomolgus monkey humorous bone samples 48

months after OVX or sham treatment were generously provided by Dr. Cynthia J. Lees (Department of Pathology, Wake Forest University School of Medicine, Winston-Salem, NC, USA) from previous studies(43). Rat OVX and sham bone samples with and without 8-week Scl-ab treatment were from previous studies (46,64). The rabbit dye injection (5% sodium metaperiodate with a molecular weight at 214, Fisher Scientific) was carried out through the abdominal aorta catheter approximately onminute apart from the dye injection and fixation. The midshaft of the femur was decalcified and used for TEM analysis as described previously (25).

Preparation and analyses of bone samples:

Procedures for bone sample preparation and high resolution X-ray, uCT, TEM, FITC-Confocal, and SEM were described previously (25). For TEM images the thin sections were cut and stained with uranyl acetate and lead citrate and examined using a Philips CM12 in STEM mode. For resin-casted osteocyte-lacuno-canalicular SEM, the surface of methylmethacrylate embedded bone was polished followed by acid etching with 37% phosphoric acid for 2-10 seconds, 5% sodium hypochlorite for 5 minutes, then coated with gold and palladium, and examined by FEI/Philips XL30 Field emission environmental SEM (Hillsboro, OR). Standard methods for H&E, Goldner's Masson Trichrome staining, polarized light microscopy imaging, immunohistochemistry, and in situ hybridization using digoxigenin-labeled cRNA probes have been described previously(91). To analyze the role of osteocytes in mineralization, mice were injected 5 days apart with calcein (5 mg/kg i.p, 1st), and alizarin red (20 mg/kg i.p, 2nd), and dogs were injected 10 days apart with the same reagents and dosages plus one more time of calcein injection (i.e., 3-time-injections). The animals were sacrificed 2 days after the final injection. The 10 μm non-decalcified samples from these animals were photographed using a Leica TCS SP5-II upright microscope for fluorochrome labeling combined with and without DAPI staining of nuclei of osteocytes.

Visualization of the osteocyte-canalicular system by Fluorescein isothiocyanate (FITC), a small molecular dye, will fill in all cells, dendrites and blood vessels (but will not enter the mineral matrix) followed by a MMA embedding method previously described (8) (Ren et al., in press). Thus, the dye provides a visual representation of the organization of the osteocyte-canalicular system and blood vessels under the confocal microscope. A cross section with around 1 mm thickness were cut with a diamond blade saw (Buehler, Lake Bluff, IL), and the sections were then sand ground to final thickness of ~50 μm for confocal images.

Statistics

All datasets were independent two tailed normally distributed with equal variances (levene's test). Student t-test was carried to compare mean differences between two groups, if there were more than 2 groups for comparison, one-way ANOVA was used and bonferroni adjustment was applied to measure differences between each one. All were performed by using SPSS 13.0 and all data were recorded as mean+s.e.m (standard error of the mean), a P value <0.05 was considered statistically significant (*, $p < 0.05$; **, $p < 0.01$; ***, $p<0.001$).

Results

To test the hypothesis that Ocys are essential for bone mineralization, we initially used electron microscopic techniques and found a close association between slow Ocy maturation and the lengthy mineralization process, reflected by the gradual transition of the mineral content from an extremely low level at the osteoid layer through the early mineral layer with a poorly organized sphere-like mineral structure the mature matrix layer, in which the Ocys were fully mature and the mineral was continuous (Supplementary Fig. 3-S2). We then confirmed the apparent role of Ocys in mineralized bone formation using a confocal FITC imaging technique, which showed that the poorly

organized, irregularly shaped Ocys with few dendrites were present in trabecular bone having relatively low mineral content, whereas well organized spindle-shaped Ocys with numerous dendrites were present in cortical bone with relatively high mineral content. These observations were further affirmed upon examination of human osteoporotic bone, which displayed dramatic changes in the Ocys, from a spindle shape to a round shape with few dendrites (Supplementary Fig. 3-S3) , indicating a close association between Ocy structures and status of mineralization.

While the mineralization process has been well characterized in vitro, we have little information regarding the in vivo mechanisms that regulate mineralization (84). In the present study, we showed that the absence of mineralization in the newborn calvarial matrix occurred in association with the presence of nascent Ocys that had few dendrites. After 10 days, however, the appearance of plump young–Ocys heralded progressive mineralization in the calvarium. By 3 weeks, the Ocys transformed into a spindle shape surrounded by a solid mineral matrix. At 5 months, fully mature Ocys, reduced to one-half their original size, exhibited the replacement of depleted cytoplasm by mineral (Fig. 3-1 a). Similarly, the mineralization of long bones closely correlated with Ocy maturation and a gradual reduction of the Ocy volume. The resulting vacant space was filled by mineral, leading to bone growth (Fig. 3-1 b).

To confirm the functional role of Ocys in the mineralization process, we examined double-labeled fluorochrome specimens under confocal microscopy, which revealed small amounts of mineral surrounding the cells and dendrites. As shown in Figs. 3-1 c (cortical bone), 3-1 d (trabecular bone), Supplementary Figs. 3-S4-S5, there was a double label not only at the bone surface, but in the bone matrix surrounding the Ocys as well, although there was no fluorescent label surrounding the Obs at the bone surface as predicted. These data support the novel concept that Ocys embedded in the bone matrix, not Obs on the bone surface, directly contribute to the mineralization of the surrounding matrices and the bone surfaces. Thus, in patients with osteomalacia, the abundant unmineralized osteoid is

not related to the Obs at the bone surface (3) but to the embedded Ocys that fail to pump mineral to the surface (Supplementary Fig. 3-S1).

The ability of the Ocy to form mineralized bone is, of course, dependent upon the appropriate transfer of oxygen and nutrients from blood circulation. However, it is widely believed that there are few blood vessels in mineralized bone and that the canalicular fluid outside the Ocys transports nutrients to the Ocys (7). Interestingly, however, the acid-etched SEM (Fig. 3-2 a-b) and FITC images (Fig. 3-2 c) showed evidence of high blood vessel density, plus numerous connections between the blood vessels and the Ocys. Indeed, a single dye injection assay, via a catheter inserted into a rabbit abdominal aorta, documented large amounts of dye in the cytoplasm of the Ocy bodies and their dendrites in < 2 minutes (Fig. 3-2 d and Supplementary Fig. 3-S6), indicating a rapid exchange and delivery of mineral between the capillary and Ocys.

To understand the molecular mechanisms by which Obs are transformed into Ocys and the role of Ocys in bone formation, we studied Dmp1-null mice, an animal model of osteomalacia, in which Obs fail to form Ocys (91). Initially we confirmed that the deletion of the Dmp1 gene, which is highly expressed in Ocys (26,82), leads to severe defects in Ocy morphology and mineralization (Supplementary Fig. 3-7). Unexpectedly, however, we found numerous Ob-like cells buried in the osteoid of the null-bone matrix, with no evidence of peri-cellular mineral deposition (Fig. 3-3 a-b). These Dmp1-lacZ-positive cells divide (Fig 3-3 c-d), produce abundant collagen (Fig 3-3 e) and express high levels of Ob-markers, such as Runx2, Osx, Cox-2, osteocalcin (OC) and Tcf1. The Ocys present in the bone matrix are irregularly shaped plump cells, consistent with arrested maturation, which are surrounded, in part, by poorly mineralized tissue (3-3 f-j). These data suggest that: 1) although producing collagen, Obs apparently do not directly contribute to mineral deposition; and 2) the arrested transition of Obs to Ocys and failure of Ocy maturation likely result in abnormal mineralization. Furthermore, DMP1 appears to be a key molecule

controlling the transition of Obs into Ocys, along with their maturation (Supplementary Fig. 3-S1).

Although the mechanism by which DMP1 effects the above changes is unclear, our previous data showed that sclerostin (a potent inhibitor of Wnt-β-catenin), which is highly expressed in mature Ocys (83), was sharply reduced in the immature Dmp1-null Ocys (Supplementary Fig 3-S8)(91)(51). Consistent with the reduced sclerostin expression, we found evidence from immunochemical and x-gal staining of a sharp increase in the Wnt-β-catenin levels in the Dmp1 null mouse bone (Figs 3-4 a-b). Quantitative bone RT-PCR data showed greater than10-fold increases in β-catenin in the Dmp1-null mice compared to the control mice ($n = 8$, $P < 0.01$). In addition, the bone displayed a high level of TCF1 (Fig. 3-3 j), a key downstream molecule of β-catenin (16). To assure that the observations in the Dmp1-null mouse were independent of the elevation of Fgf23 mRNA, we generated and studied the offspring of a cross between Dmp1-Cre (49) and Ctnnb1ex3flox (36) mice, in which high levels of β-catenin in the bone were confirmed (data not shown). The osteomalacia phenotype was documented by multiple microscopic and staining criteria (Figs 3-4e-k, Supplementary Fig. 3-S8) and low serum Pi levels (8.11 mg% compared to 11.61 mg% in control, $n=4$, $P <0.01$) with no changes in FGF23 levels (171 pg% compared to 195.7 pg% in control, $n=4$, $P =0.7$). These findings not only demonstrate the vital role of DMP1 in controlling the maturation of Obs into Ocys but also identify the key pathological role of Wnt-β-catenin in osteomalacia.

.

Discussion

For over a century, the osteoblast has been viewed as the cell responsible for bone formation. Furthermore, it has been widely believed that an imbalance of osteoblast (weak) and osteoclast (strong) function is the main cause for osteoporosis, a common disease affecting the senior population in particular. Most, if not all, studies are thus aimed at these two bone surface cells, although neither of them can penetrate into the deep bone

matrix. In fact, over 90-95% of bone cells are osteocytes, which are derived from osteoblasts. Our understanding of the function of these long-lived (for decades) cells is extremely limited. One of the most difficult challenges in studying in vivo osteocytes is how to quantitatively and qualitatively define the osteocyte changes in healthy, diseased, and different unloading conditions. To this end, we have developed a novel approach combining FITC images with IMARIS software (which was originally developed for neuronal visualization and quantitation of 3D datasets) to study osteocytes and bone vessels. In this manuscript, we examined the FITC images from a 30 years old white male control and a 98 years old osteoporosis patient bone (all from cadavers), in which the osteocytes (which were altered from a spindle to a round shape) had greatly increased in the cell bodies but sharply decreased in dendrite numbers. To quantitate the difference, the osteocytes and their dendrites were traced using this software, and the original images were then removed. Finally, the data were processed for statistical comparison, which showed significant reductions in volume, length and number of dendrites but great increases in the number of cell bodies with a reduction in the actual contact surface between osteocytes and matrices. This sharp pathological change is likely responsible for bone loss in the osteoporosis.

In this manuscript, we also attempted various approaches, including a critical novel method (double labeling plus DAPI stain), to demonstrate that osteocytes are the key cells in building mineralized bone and maintaining bone homeostasis. We also identified Dmp1, to be the critical molecule during the process of osteoblast maturation into osteocyte. As deletion of Dmp1 led to osteoblast-like cells instead of mature and well-differentiated osteocytes. Meantime, increased osteoblast and decreased osteocyte activities in Dmp1 null mice led to under-mineralized osteomalacia phenotype, suggesting robust osteoblast function alone does not guarantee balanced bone homeostasis.

In the search for the molecular mechanism and potential treatment of bone loss in osteoporosis, we found a sharp increase in SOST expression in the osteoporosis patient bone, likely responsible for bone loss in the osteoporosis. Because a loss of the sclerostin gene in mice (SOST KO) or treatment of WT mice with SOST-Ab all result in great

increases in bone volume. SOST (sclerostin) is the antagonist for canonical Wnt-β-catenin signaling pathway. Administration of anti-SOST monoclonal antibody has successfully restored bone loss, as well as altered osteocyte morphology in OVX rat-an osteoporosis animal model, which may give people great hints in future anti-osteoporosis drug design and test.

In summary, our studies indicate that Ocys are the key cells for bone mineralization. Therefore, defective Ocy function likely underlies osteomalacia and possibly other disorders of bone formation, such as osteoporosis.

CHAPTER V

CONCLUSION

For over the last several decades, bone biologists have widely accepted the idea that osteoblasts are responsible for building bone based on its location on the bone surfaces. Without doubt, osteoblasts possess abundant rough ER and Golgi complex, which contributes to the collagen synthesis and assemble during bone formation. Meantime, however, both collagen and mineral are needed to construct a solid bone structure, and there is no evidence supporting osteoblasts' role in mineral secretion or transportation. Our prelimary data strongly suggests that, osteocytes play an equal role as osteoblasts, if not more important, in bone mineralization during development. Osteocytes are well connected with each other and get nutrient supply from blood vessels through lacunae-caniliculi system, also by which, mineral is transported from vessel to each individual osteocyte and to the bone mineral front (which is supported by our confocal-double labeling imaging technique, all the lacunae, dendritic processes and mineral front are labelled with calcein green and alizarin red, Fig 3-1). Dmp1 is essential for the maturation of osteoblast to osteocytes, Dmp1 deletion will lead to similar osteomalacia phenotypes with osteoblast-like osteocytes failing to maintain and build mineral, which is identified with abundant osteoid formation. Failure to maintain osteocytes' function in Dmp1 null osteomalacia model, Periostin null mice model, OVX rat animal model and osteoporosis human specimen all revealed failure to sustain normal bone hemostasis, indicating osteocytes play a vital role in bone remodeling. Application of SOST antibody not only restores normal osteocyte morphology, as well as normal bone mass, mineralization defect and several gene expressions. Close correlation between osteocytes function and bone quality underlies a key role for osteocytes in bone diseases progressing and its prospective in drug design.

Sclereostin (SOST) is the ligand for LRP5/6 receptor and antagonist of Wnt-β-catenin signaling pathway. It has been studied for the possible function of regulating osteoblast activity through osteocyte. However, with a higher concentration of SOST and

10X greater surface area osteocyte has over osteoblast, as well as a better understanding of the mineralizing function of osteocytes, we reason that osteocytes are actually the main target cell of SOST and SOST works as an endocrine-like factor locally to regulate bone mineralization through osteocytes rather than osteoblasts. Successful completion of this study enabled us to clarify SOST function on bone formation, proved its new involvement in blood vessel development, as well as evaluated anti-SOST monoclonal antibody itself as a new clinical treatment to bone/vessel related diseases.

Dmp1 Mediates The Maturation of Osteoblast to Osteocyte Through Wnt-β-catenin Signaling Pathway

N-linked Glycoprotein (SIBLINGs) family belongs to numerous non-collagenous proteins (NCPs), which makes an important component of bone and dentin extracellular matrix (ECM). The SIBLINGs family shares similar intron/exon properties, conserved protein biochemical properties and specific peptide motifs (e.g., phosphorylation and integrin-binding RGD). To date five members in this SIBLINGs family have been identified: Dentin matrix protein 1 (DMP1), osteopontin (OPN), bone sialoprotein (BSP), matrix extracellular phosphoglycoprotein (MEPE), and dentin sialophosphoprotein (DSPP) (27). DMP1 was originally identified by cDNA cloning from the rat dentin matrix (33) and was initially believed to be dentin specific but was later proved to be largely produced by bone (12,26). Studies suggested that DMP1 initiates its expression at E15.5 and resides mainly in osteoblasts during embryonic development. However, postnatally Dmp1 is mainly expressed by differentiated osteocytes in the bone (22,82). The *Dmp1* gene was mapped at 4q21 (the long (q) arm of chromosome 4 at position 21) in humans and at 5q21 in mice. *Dmp1* has 6 exons and 80% of its coding information reside in exon 6. Two promoter control domains for Dmp1 have been identified: a proximal one located between the -2.4 kb and the +4 kb region, and a distal one between the -2.4 kb and -9.6 kb

region. The proximal domain controls DMP1 expression at early stages, and the distal domain controls the later stages (52).

Mutations of Dmp1 in humans or its deletion in mice have been identified to cause a novel disease: autosomal recessive hypophosphatemic rickets (ARHR), which is characterized as inadequate or delayed mineralization of osteoid in mature or spongy bones; hypophosphatemia (which is mainly due to renal phosphate wasting); and ultimately a deficiency or impaired metabolism of Vitamin D, phosphate and calcium. Based on the reported cases, the primary clinical symptoms of ARHR show "lower limb deformities (bowed legs or knock-knees), waddling gait, short stature or stunted growth, tooth abscesses or early loss of teeth, bone and muscle pain, biochemical abnormalities (hypophosphatemia with normal levels of serum calcium and parathyroid hormone). More severely afflicted patients may also suffer from nerve deafness, facial and dental abnormalities, learning disabilities, joint pain, and contracture and immobilization of the spine. Patients diagnosed with ARHR display symptoms in their early childhood that are likely to have a wide spectrum of severity, depending on the site and size of the mutations and the severity and chronicity of the associated phosphate depletion."(23).

Dmp1-null mice do not show obvious abnormalities during embryo bone development. However, the bones are severely impaired postnatally which are characterized by short and widened long bones, flared and irregular metaphyses, and delayed ossification centers (89). *Dmp1*-null animals displayed significantly lower serum phosphorus levels than the wild type controls when compared with the human cases, which is due to increased urinary phosphate excretion accompanied with increased FGF23. Furthermore, the levels of 1,25-dihydroxyvitamin D [$1,25(OH)_2D_3$] were inappropriately normal, whereas the serum PTH level significantly increased in the *Dmp1*-null mice (25,51,91). Bone histological studies demonstrated that the *Dmp1*-null mice displayed severe osteomalacia bone changes with significant defect in bone mineralization. Moreover, the *Dmp1*-null mice showed increased osteoid area and more porous cortical bone. Under higher-magnification back-scattered scanning electron microscopic images, the minerals, which are evenly distributed around the osteocyte lacunae in normal

condition, were either absent or sparsely located in regions surrounding the *Dmp1*-null osteocytes. The scanning transmission electron microscopic images indicated a much lower content of mineral, calcium, and phosphorus in the *Dmp1*-null mineralized matrix (25,51,91)

Compared with normally differentiated osteocytes, *Dmp1*-null osteocytes display bulky and coarse microstructural features, as well as abnormally enlarged and round-shaped osteocytes accompanied by a reduction in dendrite numbers (25,51,91). Dmp1 was identified as a key regulator of the differentiation and maturation of osteocytes from osteoblasts (69,91). However, how this molecule regulated this process, or which signaling pathways control it were largely unknown. In our separate study, we evidenced that there is a sharp increase of β-catenin in Dmp1 null mice (Fig 4-1). To prove the essential role of Wnt-β-catenin signaling pathway during osteocyte maturation, we crossed the *Dmp1-Cre* mice with β-cat$^{ex3loxP/loxP}$ mice, which introduced a constitutive stabilization of β-catenin in the osteocytes. The off springs recaptured osteomalacia phenotype as observed in Dmp1 null mice, as well as altered osteocyte morphology and function (Fig 4-2). Similarly, normalizing Wnt-β-catenin activity in Dmp1 null mice by crossing Dmp1 null with DKK1 transgenic mice greatly improved hypophosphatemic rickets/osteomalacia phenotype (Fig 4-3). Our pioneer data strongly suggest Dmp1 regulate bone mineralization and osteocyte maturation likely through Wnt-β-catenin signaling pathway.

SOST Mainly Targets Osteocytes for Its Anabolic Effect on Bone

Bones have two unique features: high mineral content and non-stop remodeling lifespan. For many decades, the osteoblast has been widely considered as the cell responsible for bone formation, while the osteoclast's function is bone resorption. Based on studies in the physiological effects of spaceflight on the body, bone loss is the most adverse effect, which takes a long time to reverse. The common belief is that an imbalance between osteoblast and osteoclast activity during spaceflight contributes to bone loss with

the mechanism similar to the aging-caused osteoporosis. Although great efforts have been made to solve this critical issues, there has been no real breakthrough, partly due to the fact that most studies focus only on these two short-lived bone surface cells.

It is well documented that loading increases bone volume via the reduction of SOST in osteocytes, and unloading results in bone loss due to an increase in the Sost expression in the osteocytes. It is also known that Sost-knockout mice maintain a much larger bone volume compared to control mice in the tail suspended model (62). The current belief is that as a mechanosensor, the osteocyte secretes more sclerostin in the paracrine manner into bone marrow under mechanical unloading and that SOST reduces Wnt/β-catenin signaling and inhibits bone formation in the bone marrow, resulting in bone loss.

SOST, or sclerostin, has been well studied for its potent role as an inhibitor of Wnt-β-catenin signaling and a negative regulator of bone formation (38). And the Sclerostin antibody (Scl-Ab) treatment has been shown to have great efficacy in the treatment of a number of pre-clinical animal models and clinical trials of osteoporosis and bone fracture healing (11,37,46,56,64). However, how SOST function and what cells SOST target have been a myth over decades.

Although it has been suggested SOST might be targeted on osteoblast and is a potential molecule through which the osteocytes can control bone remodeling. However, as stated earlier, SOST is not a growth factor, and it doesn't seems logical for this potent inhibitory factor produced in the osteocyte to "travel" to the bone marrow, in which SOST inhibits osteogenesis. Our preliminary data have already demonstrated that it is the osteocyte and not the osteoblast that forms mineralized bone. Thus, it is important to demonstrate that SOST directly regulates osteocyte activity in an autocrine manner in the mechanical unloading condition.

Here we proved that SOST modulate bone metabolism mainly through osteocytes in an autocrine manner rather than targeting on osteoblasts (Fig 4-4). By tracing SOST LacZ staining in SOST null heterozygote, in-situ hybridization and western blot, we confirmed that there is constitutive expression of SOST from osteo-progenitor cells in the bone marrow through mature osteocyte with an increased level (Fig 4-5), suggesting that

sclerostin is not secreted from osteocytes to the bone surface but is produced by progenitor cells and osteoblasts themselves, and sclerostin production increases over time as progenitor cells mature to osteocytes. In vitro study also evidenced that only osteocyte responds to anti-sclerostin antibodies but not osteoblast, Scl-Ab greatly reduced SOST production in MLOY4 cells, and decreased RankL and increased Dmp1 significantly. But there are no apparent changes of these genes expression levels in MC3T3 cell line (Fig 4-6). We have reasoned that SOST mainly targets on osteocyte to modulate bone homeostasis by regulating RankL production.

REFERENCES

1. Agholme, F., Li, X., Isaksson, H., Ke, H. Z., and Aspenberg, P. (2010) Sclerostin antibody treatment enhances metaphyseal bone healing in rats. *Journal of bone and mineral research : the official journal of the American Society for Bone and Mineral Research* **25**, 2412-2418
2. Arceo, N., Sauk, J. J., Moehring, J., Foster, R. A., and Somerman, M. J. (1991) Human periodontal cells initiate mineral-like nodules in vitro. *Journal of periodontology* **62**, 499-503
3. Baylink, D. J., and Wergedal, J. E. (1971) Bone formation by osteocytes. *The American journal of physiology* **221**, 669-678
4. Belanger, L. F., and Robichon, J. (1964) Parathormone-Induced Osteolysis in Dogs. A Microradiographic and Alpharadiographic Survey. *The Journal of bone and joint surgery. American volume* **46**, 1008-1012
5. Bellido, T. (2006) Downregulation of SOST/sclerostin by PTH: a novel mechanism of hormonal control of bone formation mediated by osteocytes. *Journal of musculoskeletal & neuronal interactions* **6**, 358-359
6. Bonewald, L. F. (2006) Mechanosensation and Transduction in Osteocytes. *Bonekey* **3**, 7-15
7. Bonewald, L. F. (2011) The amazing osteocyte. *Journal of bone and mineral research : the official journal of the American Society for Bone and Mineral Research* **26**, 229-238
8. Cao, Z., Zhang, H., Zhou, X., Han, X., Ren, Y., Gao, T., Xiao, Y., de Crombrugghe, B., Somerman, M. J., and Feng, J. Q. (2012) Genetic evidence for the vital function of Osterix in cementogenesis. *Journal of bone and mineral research : the official journal of the American Society for Bone and Mineral Research* **27**, 1080-1092

9. Chavarry, N. G., Vettore, M. V., Sansone, C., and Sheiham, A. (2009) The relationship between diabetes mellitus and destructive periodontal disease: a meta-analysis. *Oral health & preventive dentistry* **7**, 107-127
10. Ciani, C., Doty, S. B., and Fritton, S. P. (2009) An effective histological staining process to visualize bone interstitial fluid space using confocal microscopy. *Bone* **44**, 1015-1017
11. Costa, A. G., Bilezikian, J. P., and Lewiecki, E. M. (2014) Update on romosozumab : a humanized monoclonal antibody to sclerostin. *Expert opinion on biological therapy* **14**, 697-707
12. D'Souza, R. N., Cavender, A., Sunavala, G., Alvarez, J., Ohshima, T., Kulkarni, A. B., and MacDougall, M. (1997) Gene expression patterns of murine dentin matrix protein 1 (Dmp1) and dentin sialophosphoprotein (DSPP) suggest distinct developmental functions in vivo. *Journal of bone and mineral research : the official journal of the American Society for Bone and Mineral Research* **12**, 2040-2049
13. Dallas, S. L., and Bonewald, L. F. (2010) Dynamics of the transition from osteoblast to osteocyte. *Annals of the New York Academy of Sciences* **1192**, 437-443
14. Dallas, S. L., Prideaux, M., and Bonewald, L. F. (2013) The osteocyte: an endocrine cell ... and more. *Endocrine reviews* **34**, 658-690
15. Dallas, S. L., Veno, P. A., Rosser, J. L., Barragan-Adjemian, C., Rowe, D. W., Kalajzic, I., and Bonewald, L. F. (2009) Time lapse imaging techniques for comparison of mineralization dynamics in primary murine osteoblasts and the late osteoblast/early osteocyte-like cell line MLO-A5. *Cells Tissues Organs* **189**, 6-11
16. DasGupta, R., and Fuchs, E. (1999) Multiple roles for activated LEF/TCF transcription complexes during hair follicle development and differentiation. *Development* **126**, 4557-4568

17. Douglass, C. W., and Fox, C. H. (1993) Cross-sectional studies in periodontal disease: current status and implications for dental practice. *Advances in dental research* **7**, 25-31

18. Eddleston, A., Marenzana, M., Moore, A. R., Stephens, P., Muzylak, M., Marshall, D., and Robinson, M. K. (2009) A short treatment with an antibody to sclerostin can inhibit bone loss in an ongoing model of colitis. *Journal of bone and mineral research : the official journal of the American Society for Bone and Mineral Research* **24**, 1662-1671

19. Erben, R. G. (1997) Embedding of bone samples in methylmethacrylate: an improved method suitable for bone histomorphometry, histochemistry, and immunohistochemistry. *The journal of histochemistry and cytochemistry : official journal of the Histochemistry Society* **45**, 307-313

20. Farrow, E. G., Davis, S. I., Ward, L. M., Summers, L. J., Bubbear, J. S., Keen, R., Stamp, T. C., Baker, L. R., Bonewald, L. F., and White, K. E. (2009) Molecular analysis of DMP1 mutants causing autosomal recessive hypophosphatemic rickets. *Bone* **44**, 287-294

21. Fedarko, N. S., Fohr, B., Robey, P. G., Young, M. F., and Fisher, L. W. (2000) Factor H binding to bone sialoprotein and osteopontin enables tumor cell evasion of complement-mediated attack. *Journal of Biological Chemistry* **275**, 16666-16672

22. Fen, J. Q., Zhang, J., Dallas, S. L., Lu, Y., Chen, S., Tan, X., Owen, M., Harris, S. E., and MacDougall, M. (2002) Dentin matrix protein 1, a target molecule for Cbfa1 in bone, is a unique bone marker gene. *Journal of bone and mineral research : the official journal of the American Society for Bone and Mineral Research* **17**, 1822-1831

23. Feng, J. Q., Clinkenbeard, E. L., Yuan, B., White, K. E., and Drezner, M. K. (2013) Osteocyte regulation of phosphate homeostasis and bone mineralization underlies the pathophysiology of the heritable disorders of rickets and osteomalacia. *Bone* **54**, 213-221

24. Feng, J. Q., Huang, H., Lu, Y., Ye, L., Xie, Y., Tsutsui, T. W., Kunieda, T., Castranio, T., Scott, G., Bonewald, L. B., and Mishina, Y. (2003) The Dentin matrix protein 1 (Dmp1) is specifically expressed in mineralized, but not soft, tissues during development. *Journal of dental research* **82**, 776-780

25. Feng, J. Q., Ward, L. M., Liu, S., Lu, Y., Xie, Y., Yuan, B., Yu, X., Rauch, F., Davis, S. I., Zhang, S., Rios, H., Drezner, M. K., Quarles, L. D., Bonewald, L. F., and White, K. E. (2006) Loss of DMP1 causes rickets and osteomalacia and identifies a role for osteocytes in mineral metabolism. *Nature genetics* **38**, 1310-1315

26. Feng, J. Q., Zhang, J., Dallas, S. L., Lu, Y., Chen, S., Tan, X., Owen, M., Harris, S. E., and MacDougall, M. (2002) Dentin matrix protein 1, a target molecule for Cbfa1 in bone, is a unique bone marker gene. *Journal of bone and mineral research : the official journal of the American Society for Bone and Mineral Research* **17**, 1822-1831

27. Fisher, L. W., and Fedarko, N. S. (2003) Six genes expressed in bones and teeth encode the current members of the SIBLING family of proteins. *Connect Tissue Res* **44 Suppl 1**, 33-40

28. Fisher, L. W., Torchia, D. A., Fohr, B., Young, M. F., and Fedarko, N. S. (2001) Flexible structures of SIBLING proteins, bone sialoprotein, and osteopontin. *Biochemical & Biophysical Research Communications* **280**, 460-465

29. Fox, C. H. (1992) New considerations in the prevalence of periodontal disease. *Current opinion in dentistry* **2**, 5-11

30. Fox, C. H., Jette, A. M., McGuire, S. M., Feldman, H. A., and Douglass, C. W. (1994) Periodontal disease among New England elders. *Journal of periodontology* **65**, 676-684

31. Franz-Odendaal, T. A., Hall, B. K., and Witten, P. E. (2006) Buried alive: how osteoblasts become osteocytes. *Developmental dynamics : an official publication of the American Association of Anatomists* **235**, 176-190

32. Galli, C., Passeri, G., and Macaluso, G. M. (2010) Osteocytes and WNT: the mechanical control of bone formation. *Journal of dental research* **89**, 331-343
33. George, A., Sabsay, B., Simonian, P. A., and Veis, A. (1993) Characterization of a novel dentin matrix acidic phosphoprotein. Implications for induction of biomineralization. *Journal of Biological Chemistry* **268**, 12624-12630
34. George, A., Sabsay, B., Simonian, P. A., and Veis, A. (1993) Characterization of a novel dentin matrix acidic phosphoprotein. Implications for induction of biomineralization. *The Journal of biological chemistry* **268**, 12624-12630
35. Hallmon, W. W., and Mealey, B. L. (1992) Implications of diabetes mellitus and periodontal disease. *The Diabetes educator* **18**, 310-315
36. Harada, H., Tagashira, S., Fujiwara, M., Ogawa, S., Katsumata, T., Yamaguchi, A., Komori, T., and Nakatsuka, M. (1999) Cbfa1 isoforms exert functional differences in osteoblast differentiation. *The Journal of biological chemistry* **274**, 6972-6978
37. Jawad, M. U., Fritton, K. E., Ma, T., Ren, P. G., Goodman, S. B., Ke, H. Z., Babij, P., and Genovese, M. C. (2013) Effects of sclerostin antibody on healing of a non-critical size femoral bone defect. *J Orthop Res* **31**, 155-163
38. Ke, H. Z., Richards, W. G., Li, X., and Ominsky, M. S. (2012) Sclerostin and Dickkopf-1 as therapeutic targets in bone diseases. *Endocrine reviews* **33**, 747-783
39. Khader, Y. S., Dauod, A. S., El-Qaderi, S. S., Alkafajei, A., and Batayha, W. Q. (2006) Periodontal status of diabetics compared with nondiabetics: a meta-analysis. *Journal of diabetes and its complications* **20**, 59-68
40. Kondoh, S., Inoue, K., Igarashi, K., Sugizaki, H., Shirode-Fukuda, Y., Inoue, E., Yu, T., Takeuchi, J. K., Kanno, J., Bonewald, L. F., and Imai, Y. (2013) Estrogen receptor alpha in osteocytes regulates trabecular bone formation in female mice. *Bone* **60C**, 68-77
41. Kuhr, A., Popa-Wagner, A., Schmoll, H., Schwahn, C., and Kocher, T. (2004) Observations on experimental marginal periodontitis in rats. *Journal of periodontal research* **39**, 101-106

42. Lee, T. Y., Lee, D. S., Kim, H. M., Ko, J. S., Gronostajski, R. M., Cho, M. I., Son, H. H., and Park, J. C. (2009) Disruption of Nfic causes dissociation of odontoblasts by interfering with the formation of intercellular junctions and aberrant odontoblast differentiation. *The journal of histochemistry and cytochemistry : official journal of the Histochemistry Society* **57**, 469-476

43. Lees, C. J., and Ramsay, H. (1999) Histomorphometry and bone biomarkers in cynomolgus females: a study in young, mature, and old monkeys. *Bone* **24**, 25-28

44. Li, R., Li, X., Zhou, M., Han, N., and Zhang, Q. (2012) Quantitative determination of matrix Gla protein (MGP) and BMP-2 during the osteogenic differentiation of human periodontal ligament cells. *Archives of oral biology* **57**, 1408-1417

45. Li, X., Ominsky, M. S., Niu, Q. T., Sun, N., Daugherty, B., D'Agostin, D., Kurahara, C., Gao, Y., Cao, J., Gong, J., Asuncion, F., Barrero, M., Warmington, K., Dwyer, D., Stolina, M., Morony, S., Sarosi, I., Kostenuik, P. J., Lacey, D. L., Simonet, W. S., Ke, H. Z., and Paszty, C. (2008) Targeted deletion of the sclerostin gene in mice results in increased bone formation and bone strength. *Journal of bone and mineral research : the official journal of the American Society for Bone and Mineral Research* **23**, 860-869

46. Li, X., Ominsky, M. S., Warmington, K. S., Morony, S., Gong, J., Cao, J., Gao, Y., Shalhoub, V., Tipton, B., Haldankar, R., Chen, Q., Winters, A., Boone, T., Geng, Z., Niu, Q. T., Ke, H. Z., Kostenuik, P. J., Simonet, W. S., Lacey, D. L., and Paszty, C. (2009) Sclerostin antibody treatment increases bone formation, bone mass, and bone strength in a rat model of postmenopausal osteoporosis. *J Bone Miner Res* **24**, 578-588

47. Ling, Y., Rios, H. F., Myers, E. R., Lu, Y., Feng, J. Q., and Boskey, A. L. (2005) DMP1 depletion decreases bone mineralization in vivo: an FTIR imaging analysis. *J Bone Miner Res* **20**, 2169-2177

48. Lorenz-Depiereux, B., Bastepe, M., Benet-Pages, A., Amyere, M., Wagenstaller, J., Muller-Barth, U., Badenhoop, K., Kaiser, S. M., Rittmaster, R. S., Shlossberg, A. H., Olivares, J. L., Loris, C., Ramos, F. J., Glorieux, F., Vikkula, M., Juppner,

H., and Strom, T. M. (2006) DMP1 mutations in autosomal recessive hypophosphatemia implicate a bone matrix protein in the regulation of phosphate homeostasis. *Nat Genet* **38**, 1248-1250

49. Lu, Y., Xie, Y., Zhang, S., Dusevich, V., Bonewald, L. F., and Feng, J. Q. (2007) DMP1-targeted Cre expression in odontoblasts and osteocytes. *Journal of dental research* **86**, 320-325
50. Lu, Y., Ye, L., Yu, S., Zhang, S., Xie, Y., McKee, M. D., Li, Y. C., Kong, J., Eick, J. D., Dallas, S. L., and Feng, J. Q. (2007) Rescue of odontogenesis in Dmp1-deficient mice by targeted re-expression of DMP1 reveals roles for DMP1 in early odontogenesis and dentin apposition in vivo. *Dev Biol* **303**, 191-201
51. Lu, Y., Yuan, B., Qin, C., Cao, Z., Xie, Y., Dallas, S. L., McKee, M. D., Drezner, M. K., Bonewald, L. F., and Feng, J. Q. (2011) The biological function of DMP-1 in osteocyte maturation is mediated by its 57-kDa C-terminal fragment. *Journal of bone and mineral research : the official journal of the American Society for Bone and Mineral Research* **26**, 331-340
52. Lu, Y., Zhang, S., Xie, Y., Pi, Y., and Feng, J. Q. (2005) Differential regulation of dentin matrix protein 1 expression during odontogenesis. *Cells Tissues Organs* **181**, 241-247
53. Manolagas, S. C. (1998) Cellular and molecular mechanisms of osteoporosis. *Aging (Milano)* **10**, 182-190
54. Martin, D. M., Hallsworth, A. S., and Buckley, T. (1978) A method for the study of internal spaces in hard tissue matrices by SEM, with special reference to dentine. *Journal of microscopy* **112**, 345-352
55. McClung, M. R., Grauer, A., Boonen, S., Bolognese, M. A., Brown, J. P., Diez-Perez, A., Langdahl, B. L., Reginster, J. Y., Zanchetta, J. R., Wasserman, S. M., Katz, L., Maddox, J., Yang, Y. C., Libanati, C., and Bone, H. G. (2014) Romosozumab in postmenopausal women with low bone mineral density. *N Engl J Med* **370**, 412-420

56. McColm, J., Hu, L., Womack, T., Tang, C. C., and Chiang, A. Y. (2014) Single- and multiple-dose randomized studies of blosozumab, a monoclonal antibody against sclerostin, in healthy postmenopausal women. *J Bone Miner Res* **29**, 935-943

57. Mealey, B. L., and Ocampo, G. L. (2007) Diabetes mellitus and periodontal disease. *Periodontology 2000* **44**, 127-153

58. Miller, S. C., Omura, T. H., and Smith, L. J. (1985) Changes in dentin appositional rates during pregnancy and lactation in rats. *Journal of dental research* **64**, 1062-1064

59. Nakashima, K., Zhou, X., Kunkel, G., Zhang, Z., Deng, J. M., Behringer, R. R., and de Crombrugghe, B. (2002) The novel zinc finger-containing transcription factor osterix is required for osteoblast differentiation and bone formation. *Cell* **108**, 17-29

60. Nakashima, T., Hayashi, M., Fukunaga, T., Kurata, K., Oh-Hora, M., Feng, J. Q., Bonewald, L. F., Kodama, T., Wutz, A., Wagner, E. F., Penninger, J. M., and Takayanagi, H. (2011) Evidence for osteocyte regulation of bone homeostasis through RANKL expression. *Nature medicine* **17**, 1231-1234

61. Nefussi, J. R., Sautier, J. M., Nicolas, V., and Forest, N. (1991) How osteoblasts become osteocytes: a decreasing matrix forming process. *Journal de biologie buccale* **19**, 75-82

62. Notelovitz, M. (2002) Overview of bone mineral density in postmenopausal women. *The Journal of reproductive medicine* **47**, 71-81

63. O'Brien, C. A., Nakashima, T., and Takayanagi, H. (2013) Osteocyte control of osteoclastogenesis. *Bone* **54**, 258-263

64. Ominsky, M. S., Vlasseros, F., Jolette, J., Smith, S. Y., Stouch, B., Doellgast, G., Gong, J., Gao, Y., Cao, J., Graham, K., Tipton, B., Cai, J., Deshpande, R., Zhou, L., Hale, M. D., Lightwood, D. J., Henry, A. J., Popplewell, A. G., Moore, A. R., Robinson, M. K., Lacey, D. L., Simonet, W. S., and Paszty, C. (2010) Two doses

of sclerostin antibody in cynomolgus monkeys increases bone formation, bone mineral density, and bone strength. *J Bone Miner Res* **25**, 948-959

65. Padhi, D., Jang, G., Stouch, B., Fang, L., and Posvar, E. (2011) Single-dose, placebo-controlled, randomized study of AMG 785, a sclerostin monoclonal antibody. *Journal of bone and mineral research : the official journal of the American Society for Bone and Mineral Research* **26**, 19-26
66. Parfitt, A. M. (1977) The cellular basis of bone turnover and bone loss: a rebuttal of the osteocytic resorption--bone flow theory. *Clinical orthopaedics and related research*, 236-247
67. Pihlstrom, B. L., Michalowicz, B. S., and Johnson, N. W. (2005) Periodontal diseases. *Lancet* **366**, 1809-1820
68. Preshaw, P. M., Alba, A. L., Herrera, D., Jepsen, S., Konstantinidis, A., Makrilakis, K., and Taylor, R. (2012) Periodontitis and diabetes: a two-way relationship. *Diabetologia* **55**, 21-31
69. Qin, C., D'Souza, R., and Feng, J. Q. (2007) Dentin matrix protein 1 (DMP1): new and important roles for biomineralization and phosphate homeostasis. *Journal of dental research* **86**, 1134-1141
70. Ren, Y., Han, X., Ho, S. P., Harris, S. E., Cao, Z., Economides, A. N., Qin, C., Ke, H., Liu, M., and Feng, J. Q. (2015) Removal of SOST or blocking its product sclerostin rescues defects in the periodontitis mouse model. *FASEB journal : official publication of the Federation of American Societies for Experimental Biology*.2015, pii: fj.14-265496.
71. Ren, Y., Lin, S., Jing, Y., Dechow, P. C., and Feng, J. Q. (2014) A novel way to statistically analyze morphologic changes in Dmp1-null osteocytes. *Connective tissue research* **55 Suppl 1**, 129-133
72. Rhee, Y., Allen, M. R., Condon, K., Lezcano, V., Ronda, A. C., Galli, C., Olivos, N., Passeri, G., O'Brien, C. A., Bivi, N., Plotkin, L. I., and Bellido, T. (2011) PTH receptor signaling in osteocytes governs periosteal bone formation and

intracortical remodeling. *Journal of bone and mineral research : the official journal of the American Society for Bone and Mineral Research* **26**, 1035-1046

73. Rios, H., Koushik, S. V., Wang, H., Wang, J., Zhou, H. M., Lindsley, A., Rogers, R., Chen, Z., Maeda, M., Kruzynska-Frejtag, A., Feng, J. Q., and Conway, S. J. (2005) periostin null mice exhibit dwarfism, incisor enamel defects, and an early-onset periodontal disease-like phenotype. *Molecular and cellular biology* **25**, 11131-11144
74. Rios, H., Koushik, S. V., Wang, H. Y., Wang, J., Zhou, H. M., Lindsley, A., Rogers, R., Chen, Z., Maeda, M., Kruzynska-Frejtag, A., Feng, J. Q., and Conway, S. J. (2005) periostin null mice exhibit dwarfism, incisor enamel defects, and an early-onset periodontal disease-like phenotype. *Molecular and Cellular Biology* **25**, 11131-11144
75. Rios, H. F., Ma, D., Xie, Y., Giannobile, W. V., Bonewald, L. F., Conway, S. J., and Feng, J. Q. (2008) Periostin is essential for the integrity and function of the periodontal ligament during occlusal loading in mice. *Journal of periodontology* **79**, 1480-1490
76. Rios, H. F., Ye, L., Dusevich, V., Eick, D., Bonewald, L. F., and Feng, J. Q. (2005) DMP1 is essential for osteocyte formation and function. *Journal of musculoskeletal & neuronal interactions* **5**, 325-327
77. Saini, V., Marengi, D. A., Barry, K. J., Fulzele, K. S., Heiden, E., Liu, X., Dedic, C., Maeda, A., Lotinun, S., Baron, R., and Pajevic, P. D. (2013) Parathyroid hormone (PTH)/PTH-related peptide type 1 receptor (PPR) signaling in osteocytes regulates anabolic and catabolic skeletal responses to PTH. *The Journal of biological chemistry* **288**, 20122-20134
78. Salvi, G. E., Carollo-Bittel, B., and Lang, N. P. (2008) Effects of diabetes mellitus on periodontal and peri-implant conditions: update on associations and risks. *Journal of clinical periodontology* **35**, 398-409
79. Souza, D. M., Prado Fde, A., Prado Mde, A., Rocha, R. F., and Carvalho, Y. R. (2010) Evaluation of two morphometric methods of bone loss percentages caused

by periodontitis in rats in different locations. *Journal of applied oral science : revista FOB* **18**, 493-497

80. Sun, Y. Q., McLeod, K. J., and Rubin, C. T. (1995) Mechanically induced periosteal bone formation is paralleled by the upregulation of collagen type one mRNA in osteocytes as measured by in situ reverse transcript-polymerase chain reaction. *Calcified tissue international* **57**, 456-462
81. Taut, A. D., Jin, Q., Chung, J. H., Galindo-Moreno, P., Yi, E. S., Sugai, J. V., Ke, H. Z., Liu, M., and Giannobile, W. V. (2013) Sclerostin antibody stimulates bone regeneration after experimental periodontitis. *Journal of bone and mineral research : the official journal of the American Society for Bone and Mineral Research* **28**, 2347-2356
82. Toyosawa, S., Shintani, S., Fujiwara, T., Ooshima, T., Sato, A., Ijuhin, N., and Komori, T. (2001) Dentin matrix protein 1 is predominantly expressed in chicken and rat osteocytes but not in osteoblasts. *Journal of bone and mineral research : the official journal of the American Society for Bone and Mineral Research* **16**, 2017-2026
83. van Bezooijen, R. L., Roelen, B. A., Visser, A., van der Wee-Pals, L., de Wilt, E., Karperien, M., Hamersma, H., Papapoulos, S. E., ten Dijke, P., and Lowik, C. W. (2004) Sclerostin is an osteocyte-expressed negative regulator of bone formation, but not a classical BMP antagonist. *The Journal of experimental medicine* **199**, 805-814
84. Veis, A., and Dorvee, J. R. (2012) Biomineralization Mechanisms: A New Paradigm for Crystal Nucleation in Organic Matrices. *Calcif Tissue Int*
85. Wilde, J., Yokozeki, M., Terai, K., Kudo, A., and Moriyama, K. (2003) The divergent expression of periostin mRNA in the periodontal ligament during experimental tooth movement. *Cell and tissue research* **312**, 345-351
86. Windahl, S. H., Borjesson, A. E., Farman, H. H., Engdahl, C., Moverare-Skrtic, S., Sjogren, K., Lagerquist, M. K., Kindblom, J. M., Koskela, A., Tuukkanen, J., Divieti Pajevic, P., Feng, J. Q., Dahlman-Wright, K., Antonson, P., Gustafsson, J.

A., and Ohlsson, C. (2013) Estrogen receptor-alpha in osteocytes is important for trabecular bone formation in male mice. *Proceedings of the National Academy of Sciences of the United States of America* **110**, 2294-2299

87. Xiong, J., Onal, M., Jilka, R. L., Weinstein, R. S., Manolagas, S. C., and O'Brien, C. A. (2011) Matrix-embedded cells control osteoclast formation. *Nature medicine* **17**, 1235-1241

88. Ye, L., MacDougall, M., Zhang, S., Xie, Y., Zhang, J., Li, Z., Lu, Y., Mishina, Y., and Feng, J. Q. (2004) Deletion of dentin matrix protein-1 leads to a partial failure of maturation of predentin into dentin, hypomineralization, and expanded cavities of pulp and root canal during postnatal tooth development. *The Journal of biological chemistry* **279**, 19141-19148

89. Ye, L., Mishina, Y., Chen, D., Huang, H., Dallas, S. L., Dallas, M. R., Sivakumar, P., Kunieda, T., Tsutsui, T. W., Boskey, A., Bonewald, L. F., and Feng, J. Q. (2005) Dmp1-deficient mice display severe defects in cartilage formation responsible for a chondrodysplasia-like phenotype. *The Journal of biological chemistry* **280**, 6197-6203

90. Zarrinkalam, M. R., Mulaibrahimovic, A., Atkins, G. J., and Moore, R. J. (2012) Changes in osteocyte density correspond with changes in osteoblast and osteoclast activity in an osteoporotic sheep model. *Osteoporosis international : a journal established as result of cooperation between the European Foundation for Osteoporosis and the National Osteoporosis Foundation of the USA* **23**, 1329-1336

91. Zhang, R., Lu, Y., Ye, L., Yuan, B., Yu, S., Qin, C., Xie, Y., Gao, T., Drezner, M. K., Bonewald, L. F., and Feng, J. Q. (2011) Unique roles of phosphorus in endochondral bone formation and osteocyte maturation. *Journal of bone and mineral research : the official journal of the American Society for Bone and Mineral Research* **26**, 1047-1056

APPENDIX

FIGURES

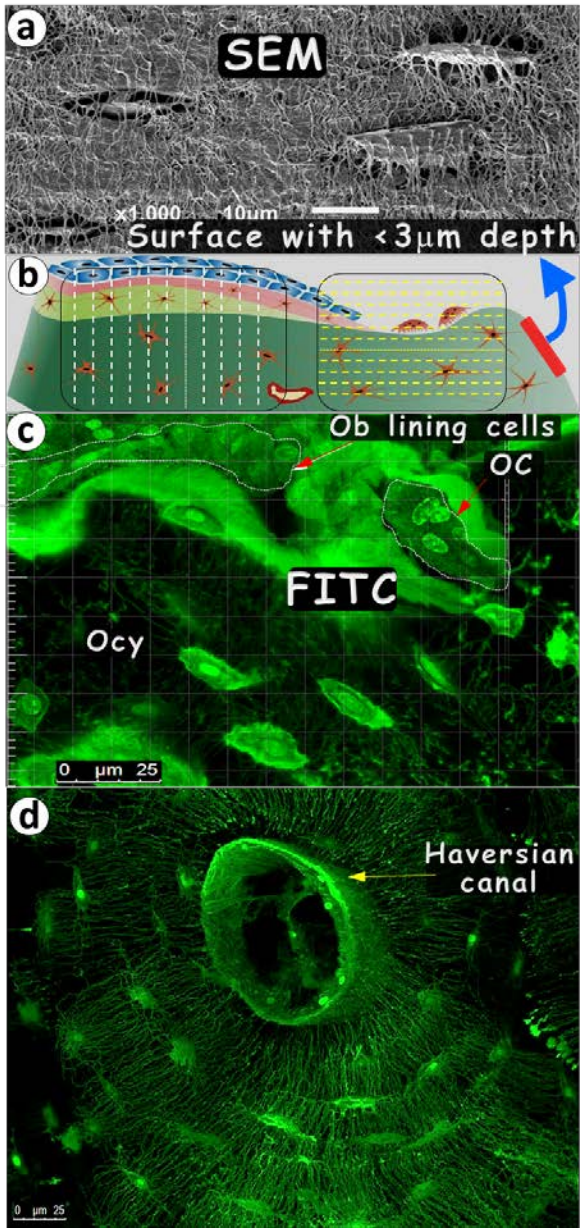

Figure 1-1. ***Pros and cons of acid-etched SEM and FITC techniques in imaging bone cells.*** (a) Acid-etched, high-resolution SEM image displayed resin-casted osteocyte (Ocy)-canalicular system on the bone surface; (b) The diagram reveals the difference between the SEM and FITC imaging techniques with the former showing mineral-buried Ocy on

the surface only and the latter technique imaging cells from the bone surface to inside the bone to a depth up to 450 mm with any region, angle or direction interested; (c) An example of an FITC image of the 6-mon-old rat tibia cortical bone revealing osteocyte (Ocy), osteoblast (Ob) lining cells, and osteoclast (OC); and (d) An example of a FITC-osteon image of the 30-year-old femur cortical bone showing the Ocy-dendritic system surrounding the Haversian canal. (Published by Ren. Etc. on Connective Tissue Research 2014 Aug;55)

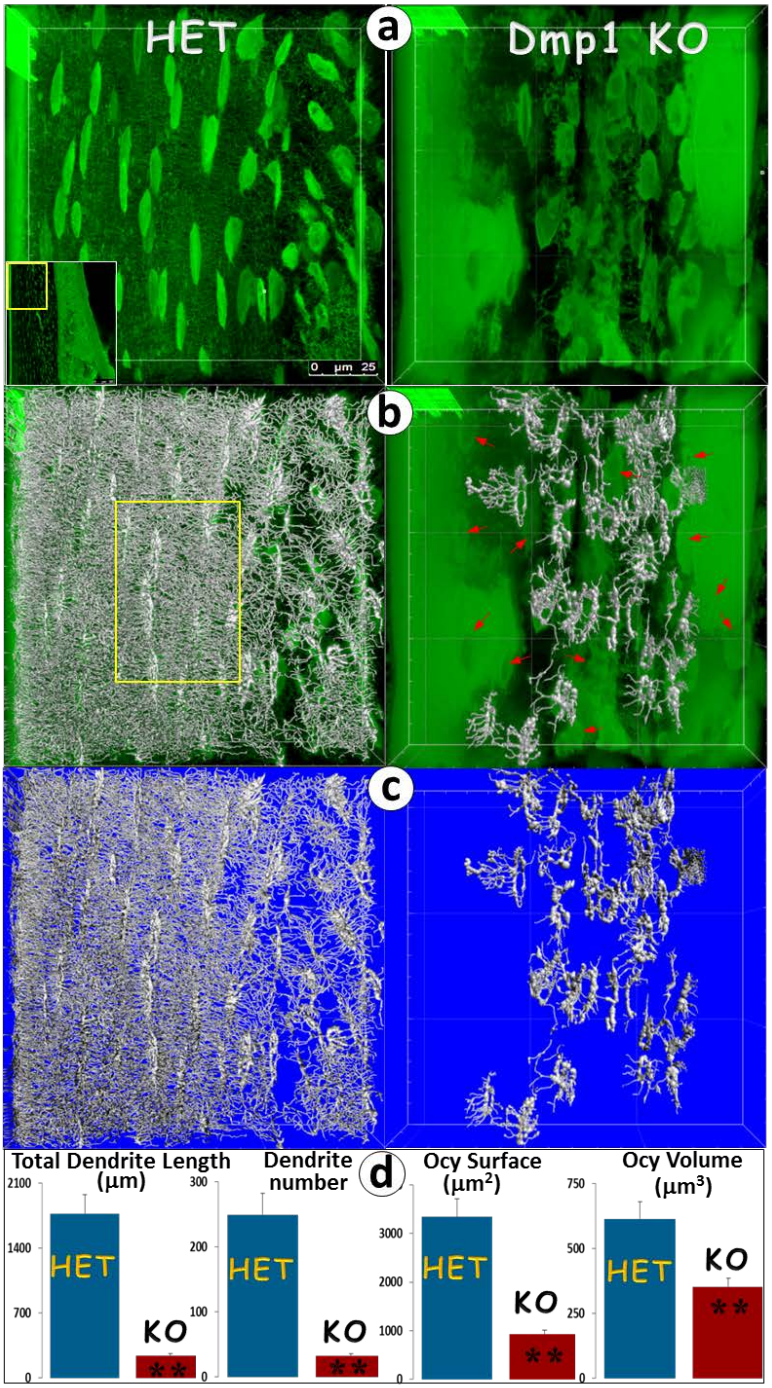

Figure 1-2. ***Quantitation of osteocyte changes in the 8-wk-old Dmp1-null (KO) compared to the age-matched control (HET) mice using the FITC-Imaris technique.*** (a) Confocal FITC image shows spindle-shaped osteocytes with numerous dendrites in a well-

organized arrangement along the longitudinal axis in the HET (left) compared to the KO osteocytes, which are buried in poorly mineralized matrices (right) with much enlarged cell bodies that are less organized in structure and distribution, plus a few dendrites; (b) FITC confocal image reconstructed with the Imaris software revealed dense dendrites shown in artificial silver color (left, HET) compared to the KO tibia, in which there were 20 osteocytes with dendrites selected and reconstructed, and the rest of them were not (red arrows, right); (c) The original FITC confocal images were removed, with the Imaris-reconstructed images displayed only; and (d) The statistical analysis using Imaris software unveils a significant difference in total dendrite length, number, osteocyte surface area and total cell volume between the KO (n ¼ 20) and the HET control bone (n ¼ 25). (Published by Ren. Etc. on Connective Tissue Research 2014 Aug;55)

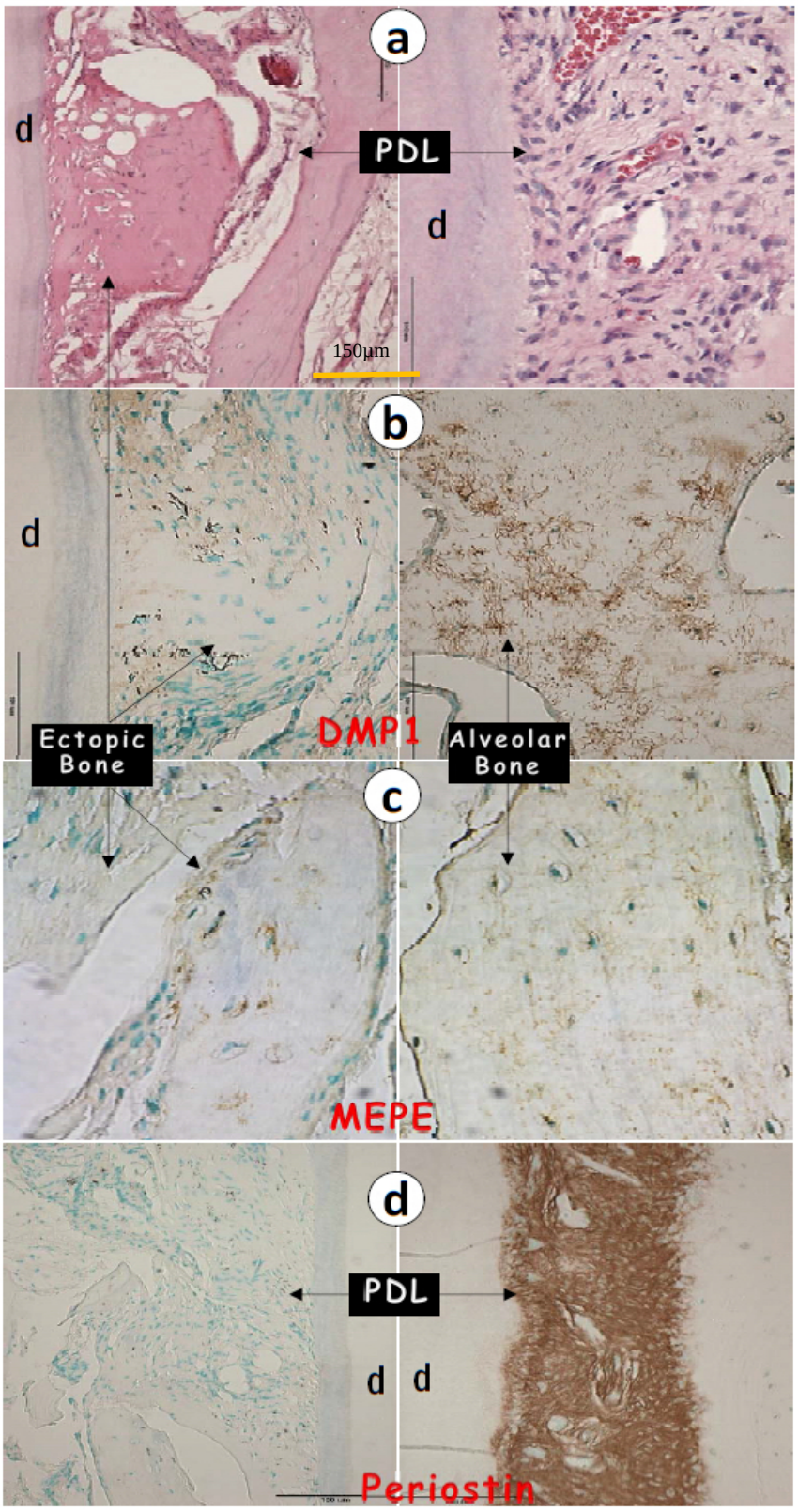
a
d
PDL
d
150μm
b
d
Ectopic Bone
DMP1
Alveolar Bone
c
MEPE
d
PDL
d d
Periostin

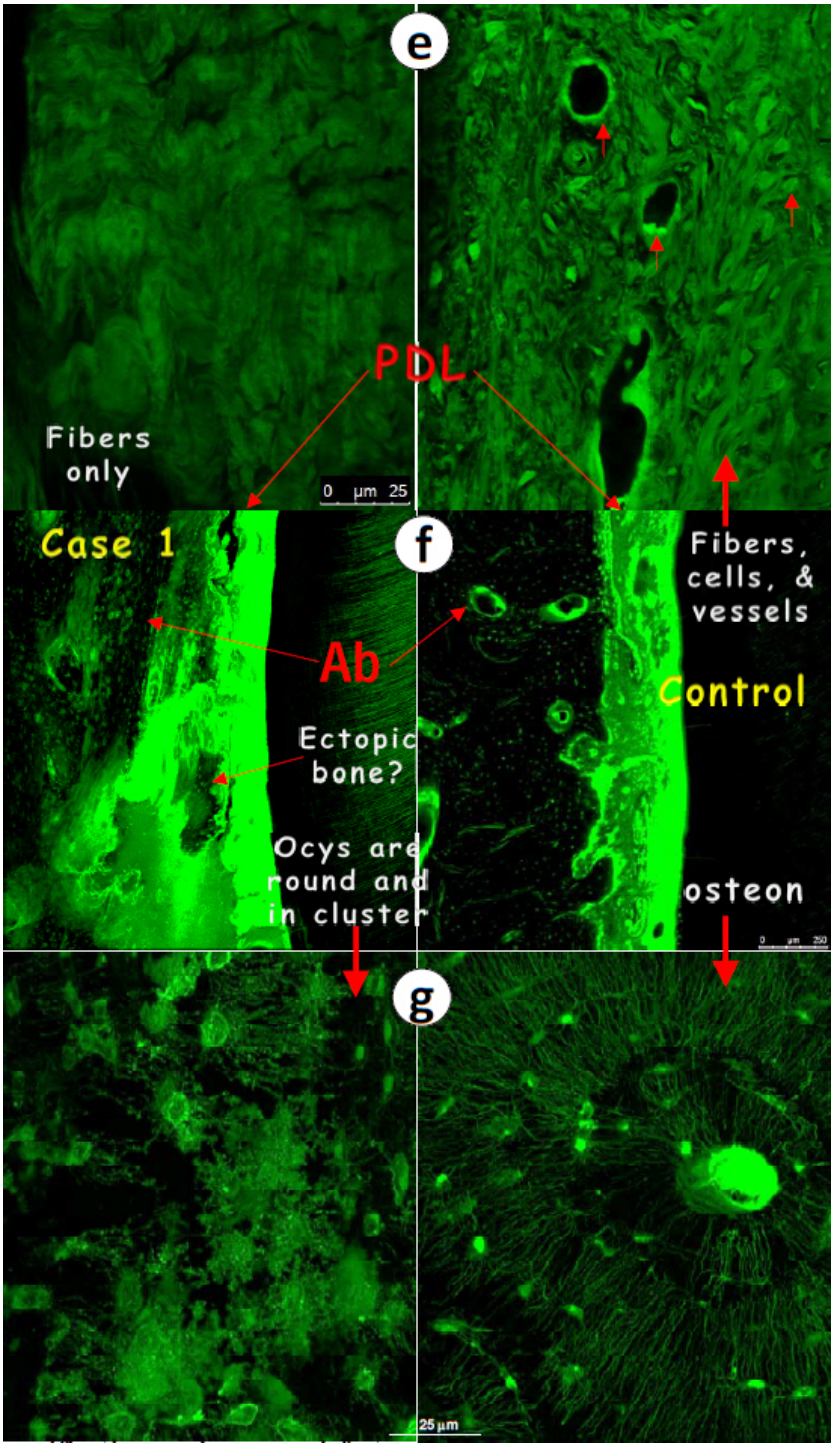

Figure 2-1 ***Ectopic ossification and severe defects of osteocytes and PDL in a patient with severe periodontitis.*** (a) The H&E stained images showed a poor PDL structure and

ectopic ossification (left)compared to a control subject (right); (b-d) A very low level expression of DMP1 (b), MEPE (c), and periostin (d) compared to the alveolar bone or the control subject (right); and (e-g) FITC confocal images revealed a loss of PDL cells (e), and abnormalities of osteocytes (f-g, the cell body in expanded round shape and distributed in cluster with few dendrites) (g, full of fibers with few cells and vessels) in the same patient (left) d dentin

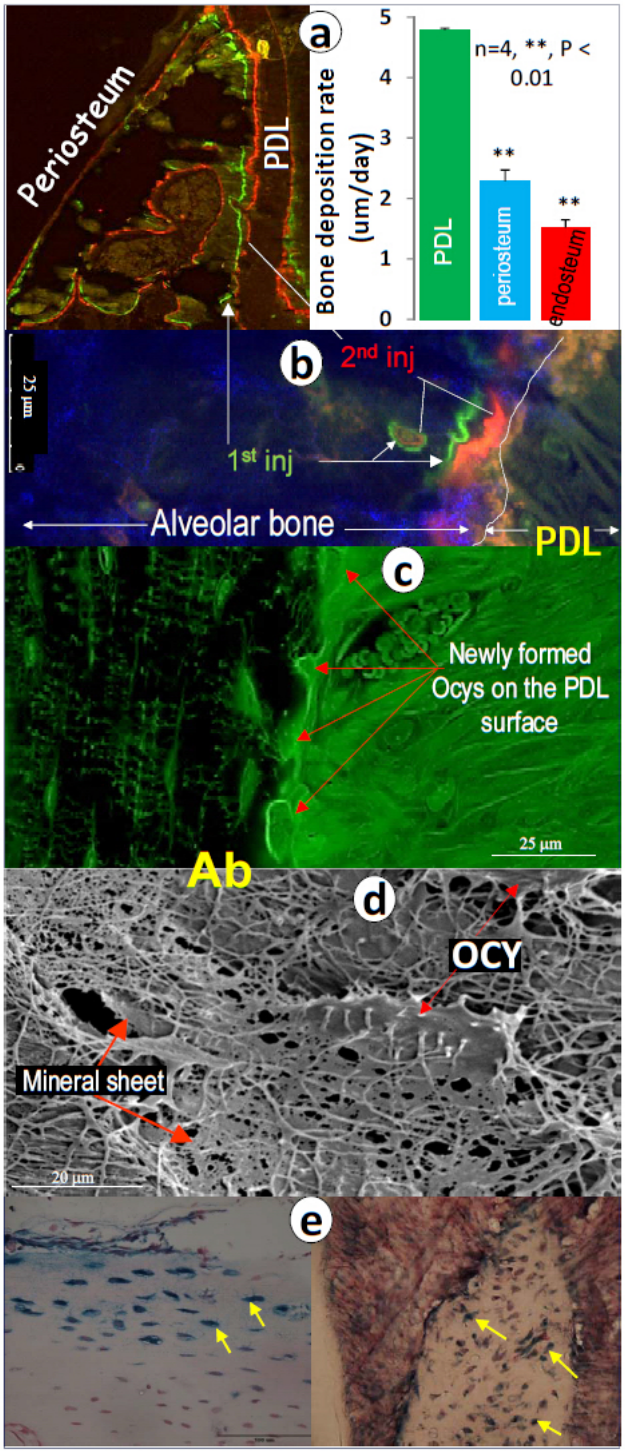

Figure 2-2 ***PDL is the major resource of progenitors in alveolar bone formation (1-mon-old mandible).*** (a) The double labeling confocal images showed the widest distance between green (calcein) and red (alizarin red) lines in PDL-alveolar bone surface than

periosteum and endosteum with a statistical difference; (b) The enlarge fluorochrome image revealed a double labeling layers surrounding the osteocyte (Ocy) plus yellow color minerals (overlaps of green and red labels) on the PDL-alveolar bone (Ab) surface, indicating a contribution of OCYs in mineralization and trace amount of minerals in the PDL- alveolar bone surface; (c) FTIC confocal images displayed a few newly formed Ocys on the Ab-PDL surface, supporting the possibility of the bone cells originated from PDL; (d) The acid-etched SEM image unveiled a mineral sheet closely linked to the Ocy and its dendrites; and (e) The X-gal stained jaw bone, in which a one-time adenovirus local infection in periosteum and PDL was performed 5 days before sample harvests. The blue cells reflect their origins from either the periosteum or PDL progenitors.

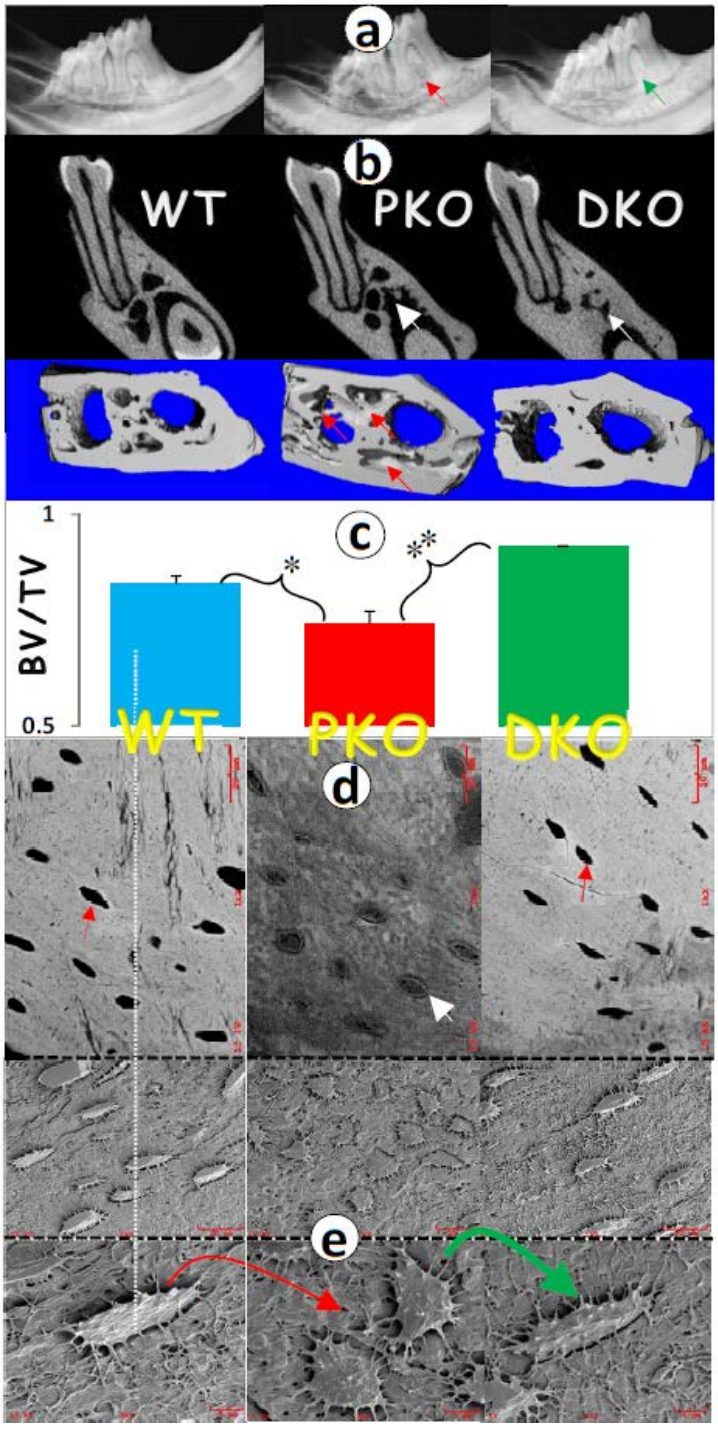

Figure 2-3 ***Restoration of bone loss and Ocy morphological shapes from round to spindle.*** (**a**) Representative radiographs revealed a restoration of bone loss in PKO jaw bones by removing *Sost* gene(*right; DKO, double knockout*); (**b**) Backscattered SEM

images confirmed the rescue of bone loss in DKO mice (*right*); (**c**) qualitative (*upper panels*) and quantitative (*lower panels*) mCT data supported the above observation (*right*); and (**d-e**) Both backscattered SEM images (**d**) and acid etched SEM images (**e**) documented a direct correlation between changes of Ocy shapes and surrounding matrices in PKO (defects, *middle*) and DKO (rescue, *middle*) compared to the age-matched control (*left*).**, $p<0.01$; *,$p<0.05$; n=5.

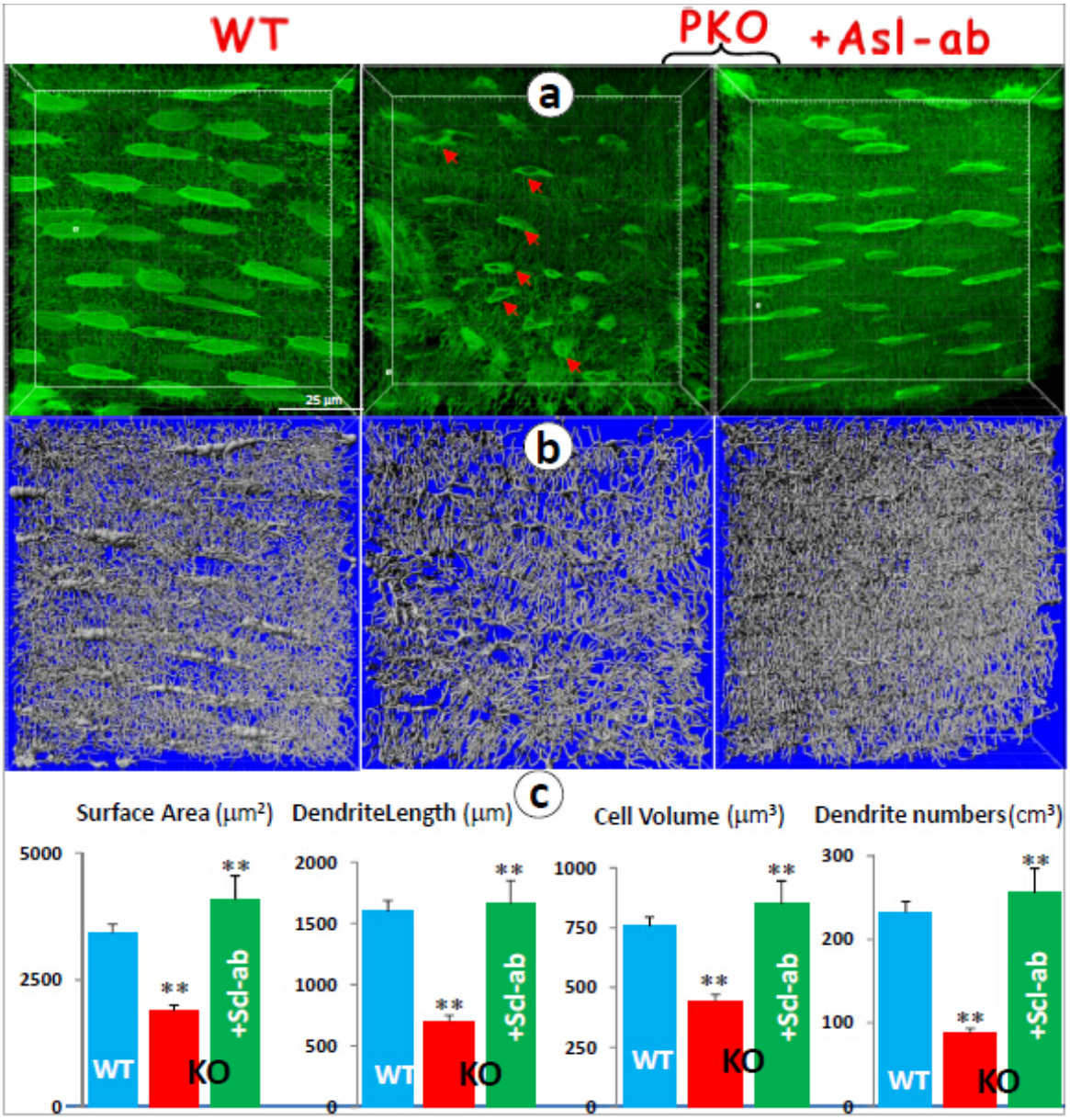

Figure 2-4 ***Rescue of Ocy morphological shapes from round to spindle.*** (**a**)Representative radiographs revealed a restoration of bone loss in PKO jaw bones by removing *Sost* gene (*right; DKO, double knockout*); (**b**) Backscattered SEM images confirmed the rescue of bone loss in DKO mice (*right*); (**c**) qualitative (*upper panels*) and quantitative (*lower panels*) µCT data supported the above observation (*right*); and (**d-e**)

Both backscattered SEM images (**d**) and acid etched SEM images (**e**) documented a direct correlation between changes of Ocy shapes and surrounding matrices in PKO(defects, *middle*) and DKO (rescue, *middle*) compared to the age-matched control (*left*).**, $p<0.01$; *,$p<0.05$; n=5.

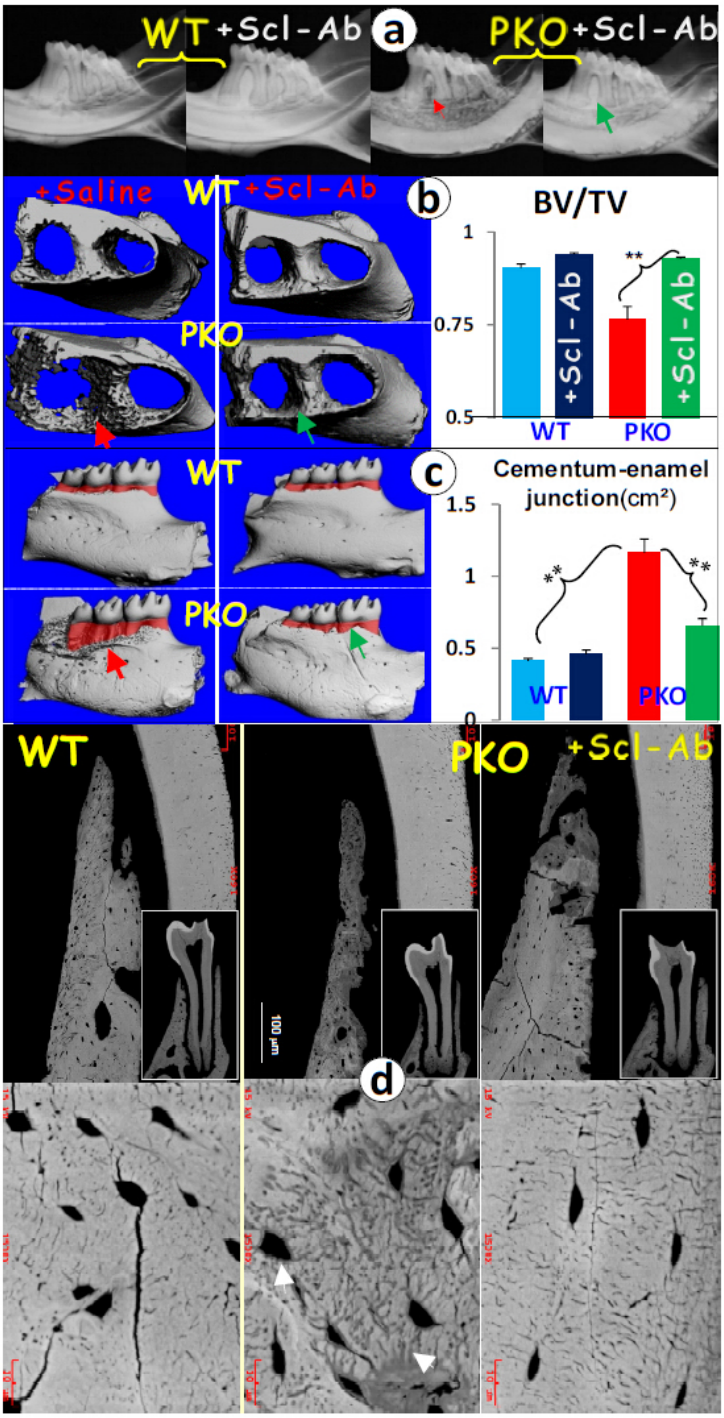

Figure 2-5 ***Restoration of bone loss, changes of the cementum-enamel junction(CEJ) area, and Ocy morphology in the 5-monthold periostin KO (PKO) after Scl-ab treatment for 8 weeks*****. (a).** Representative radiograph images displayed a severe bone loss in the

non-treat jaw bone (red arrow) and recovery of bone loss in the treated group (green arrow); **(b).** The μCT images confirmed the radiograph observation *(left),* and quantitative μCT data showed that this changes is statically significant; **(c).** Representative μCT images displayed an increase of CEJ area (pink) in the PKO mice, which was restored in the antibody treatment group (green arrow); and quantitative analyses showed that the CEJ changes in PKO mice are significant compared to either the age-matched control or treatment group. Note that 5 animals per group were selected for μCT scan. The images were rotated in a way crown pulp and root pulp are connected and perpendicular to the horizontal plane for estimation of CEJ area (red color) through over 100 "cutting" slides across the mandible (**, $p<0.01$; $n=5$). **(d).** Representative backscattered SEM image revealed an expanded canalicular and lacunar system in non-treat group, which is fully reversed in the treated group.

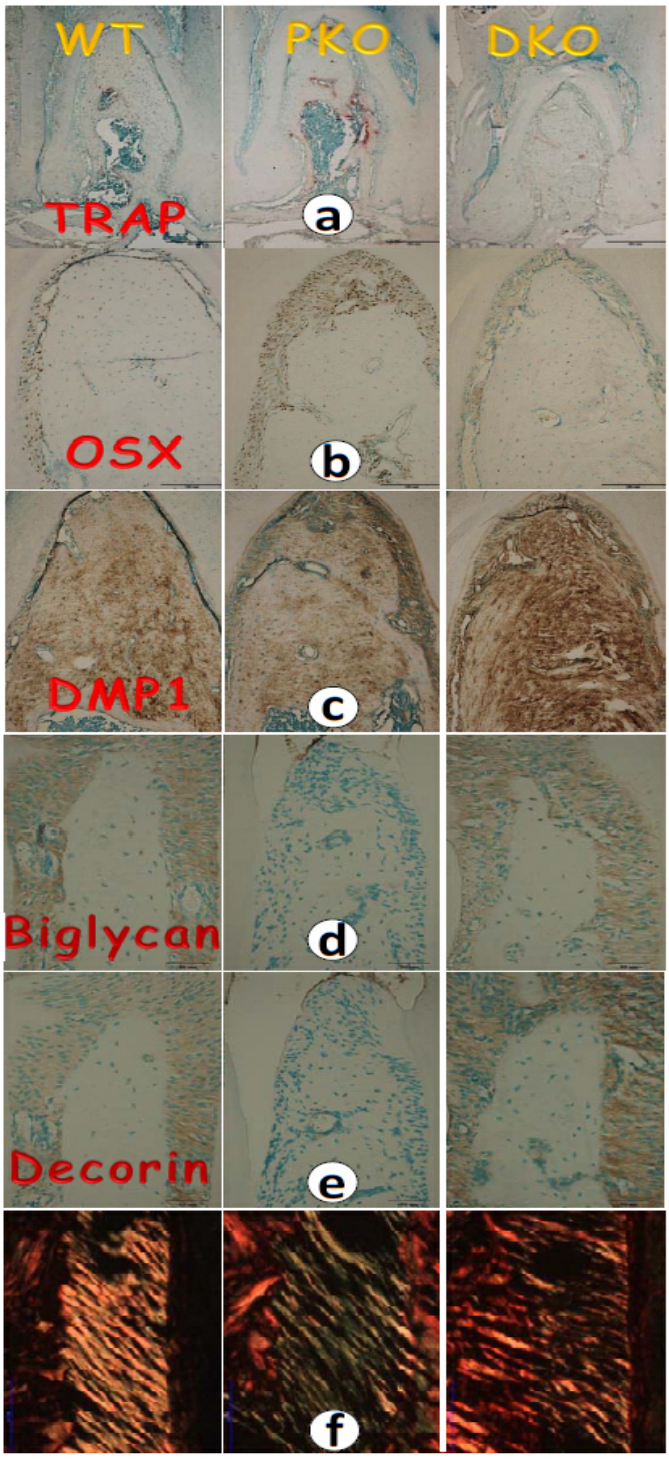

Figure 2-6 ***Restoration of molecular markers and collagen in double knockout (DKO) mice.*** (**a**) TRAP stains revealed a reduction of osteoclast number in *DKO* jaw bones; (**b-**

e) restorations of molecular markers in DKO mice by immunohistochemistry, including OSX (**b**),DMP1 (**c**), biglycan (**d**), and decorin (**e**); and (**f**) Dr. Ho's data showed thinner bundling of fibers in PKO PDL, and restoration of PDL in DKO.

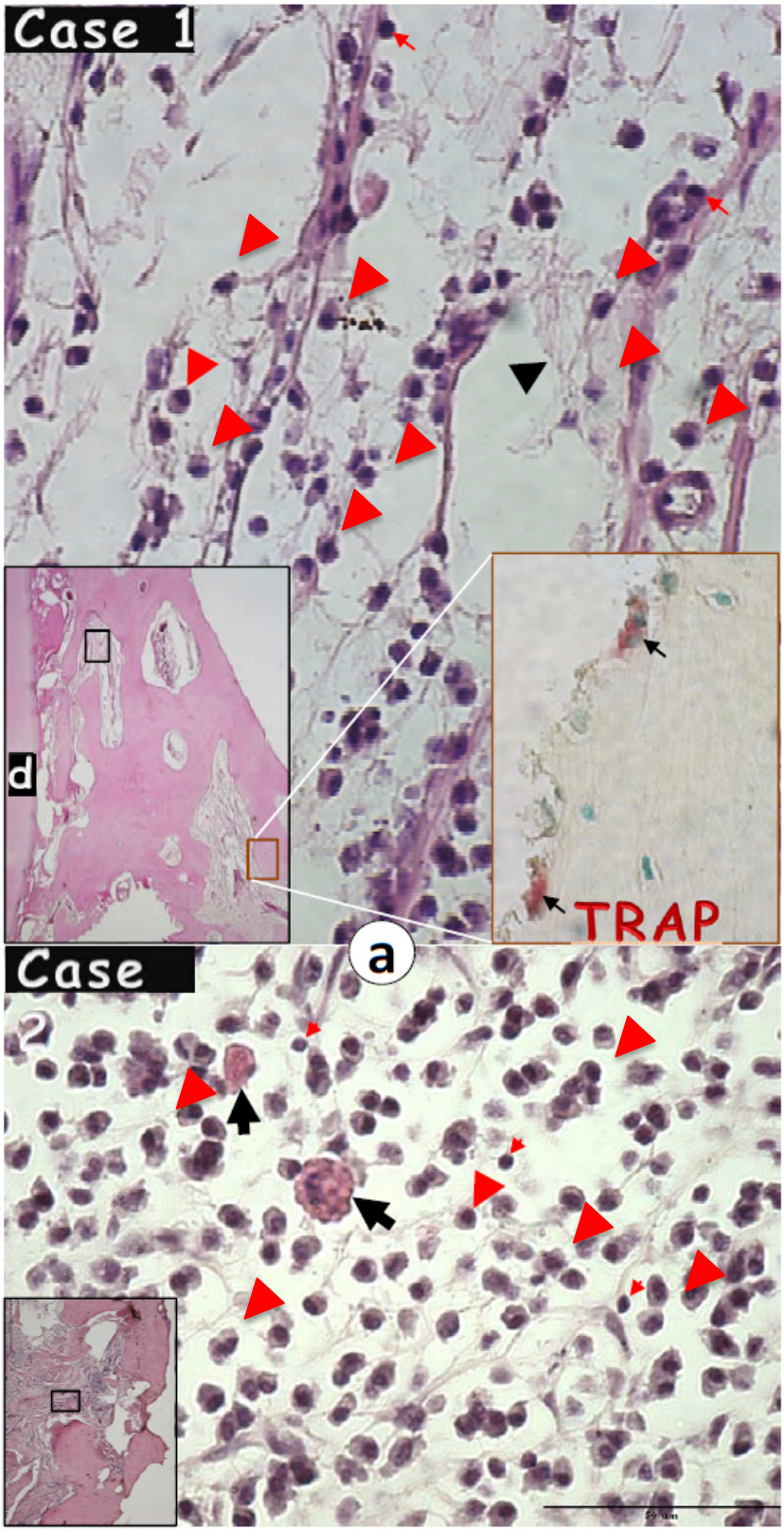
Case 1
d
TRAP
a
Case
2

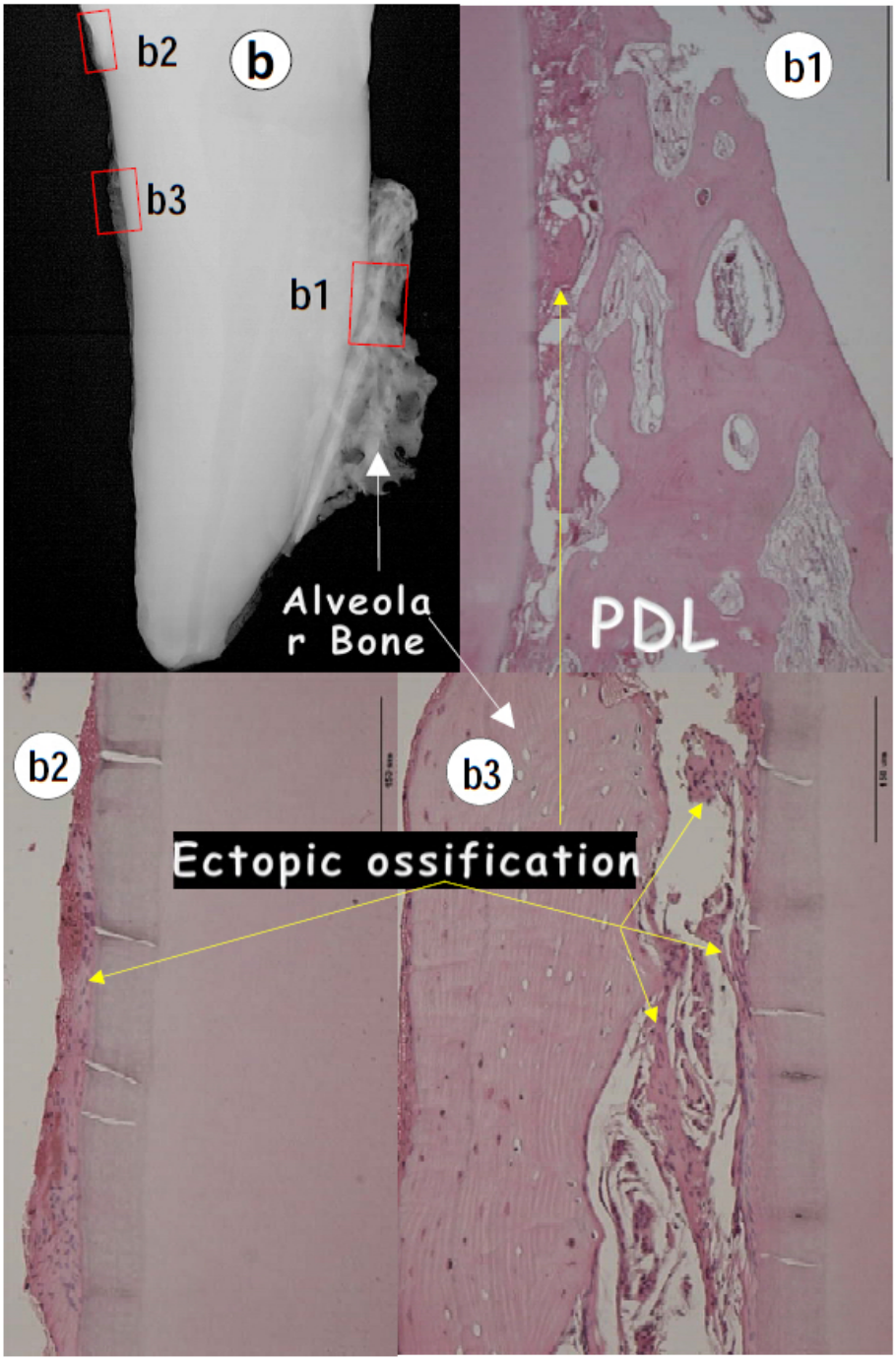

Figure 2-S1 Fig. S1. ***Chronic inflammation and ectopic ossification in the patients with severe periodontitis.*** (a).In the case 1 (*upper panel*), the enlarged H&E image showed a

mixture of many plasma cells(red arrow head) and few lymphocytes (arrows) with marrow fibrosis (black arrow head) from the infected alveolar bone adjacent to PDL(the low magnification of the extracted tooth and its surrounding tissues). The TRAP (Tartrate-resistant acid phosphatase) assay revealed two active osteoclasts on the bone surfaces. In case 2(below), the bone marrow in the extracted alveolar bone, which was adjacent to the canine tooth, is filled with the mixture of huge amount of plasma cells (red arrow head) and few lymphocytes (arrows) plus Russell bodies (black arrows, plasma cells undergoing excessive synthesis of immunoglobulin and characteristic of the distended endoplasmic reticulum) with no sign of red blood cells. (**b**) The radiograph image of the canine extracted; and (**b1-3**) with b1, b2 and b3 areas for H&E stains, in which the PDL structure was substantially destroyed with few cells observed. There were numerous calcified tissues that are darker in color compared to the existing alveolar bone. d, dentin.

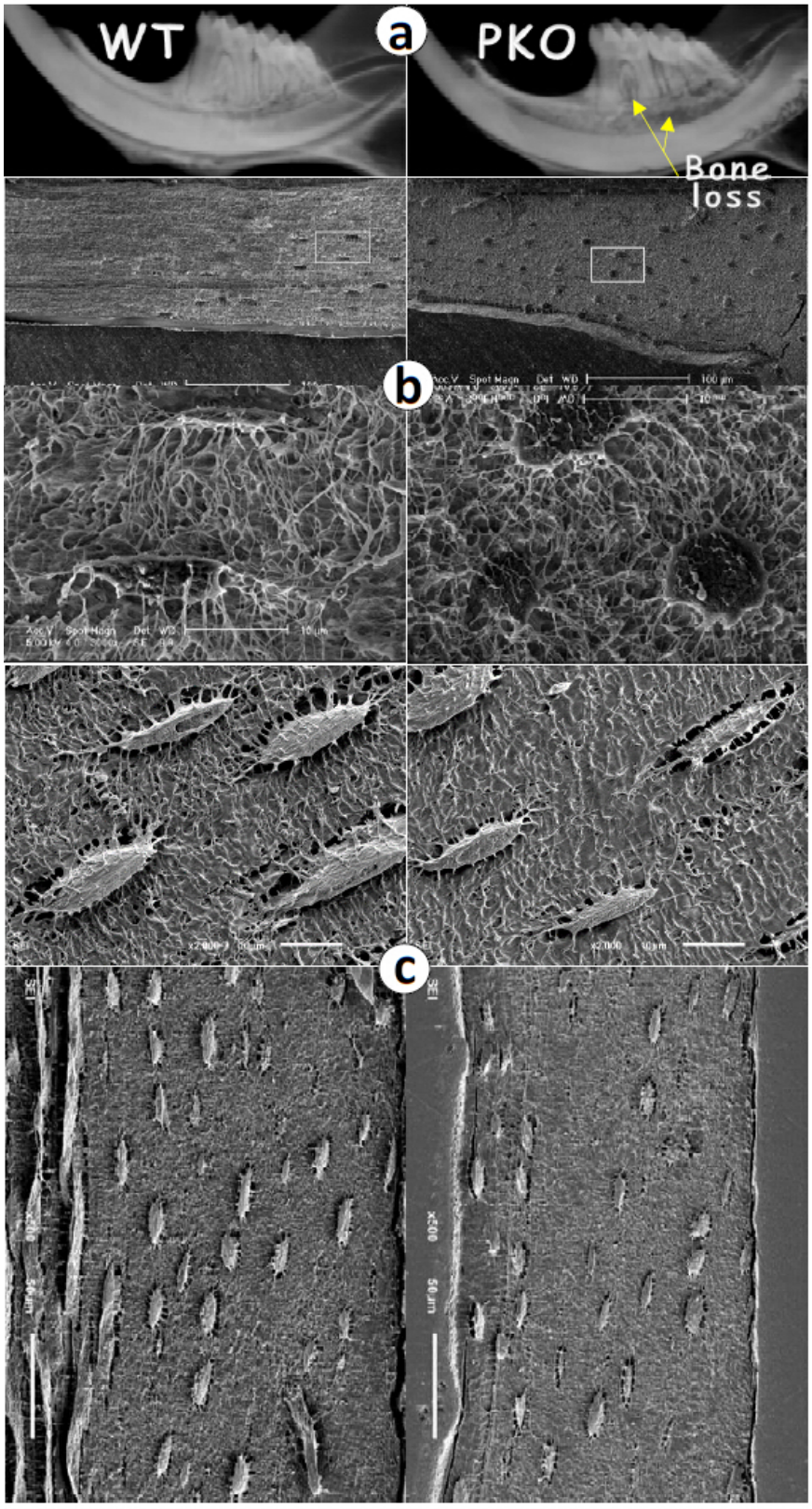
WT
a
PKO
Bone loss
b
c

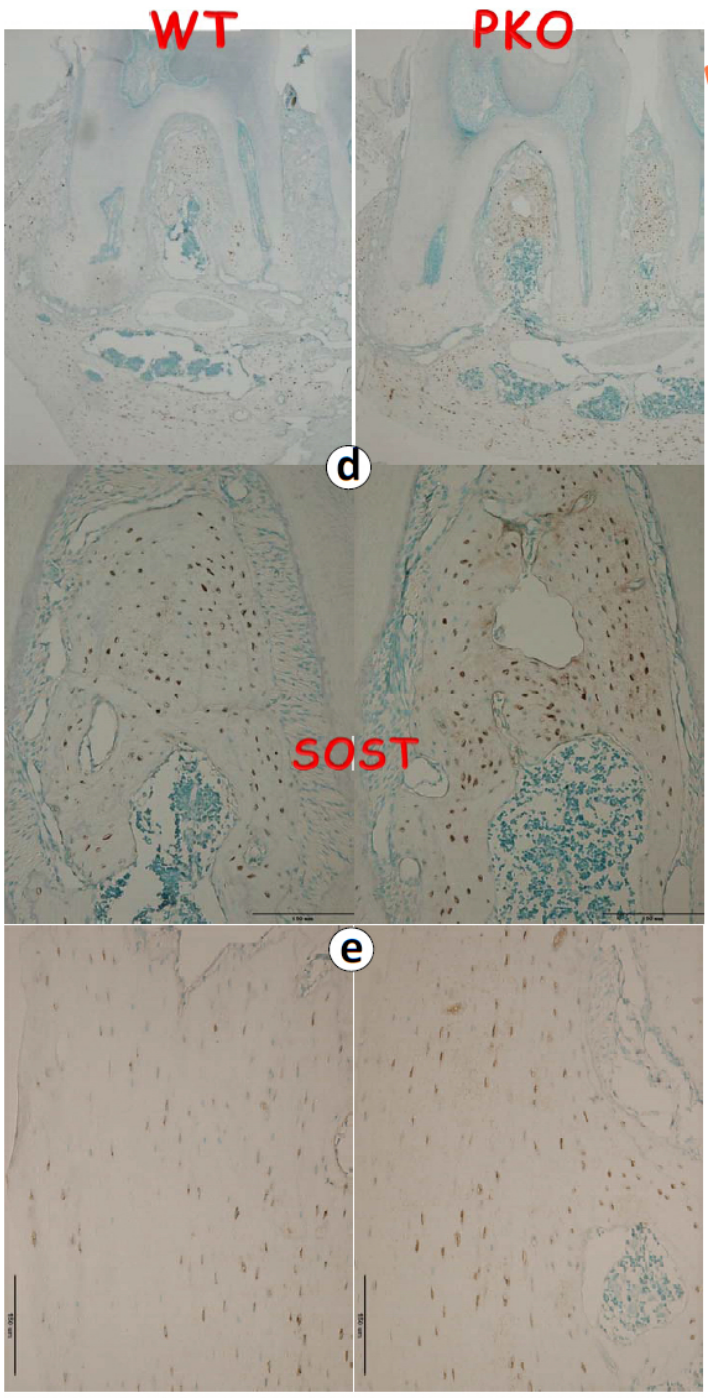

Figure 2-S2 Fig. S2 ***Deletion of periostin (PKO) lead to local changes of osteocytes (Ocys) and a sharp increase in SOST in the PKO jaw bone but not in long bone***.(**a**) Representative radiographs revealed bone loss in PKO alveolar bone (*right*); (**b**) Acid

etched SEM images displayed a sharp change of Ocys in jaw bone from spindle to round in PKO mice; (**c**) Acid etched SEM images displayed no apparent change of Ocys in PKO long bone; and (**d-e**) The immunohistochemistry stain images displayed a dramatic increase in SOST in the mandibular bone (**d**, *rights*) but a very mild change in the long bone(*right*). The above data support a link between the bone loss and the local changes of Ocy morphologies and an increase in SOST in the PKO jaw bone.

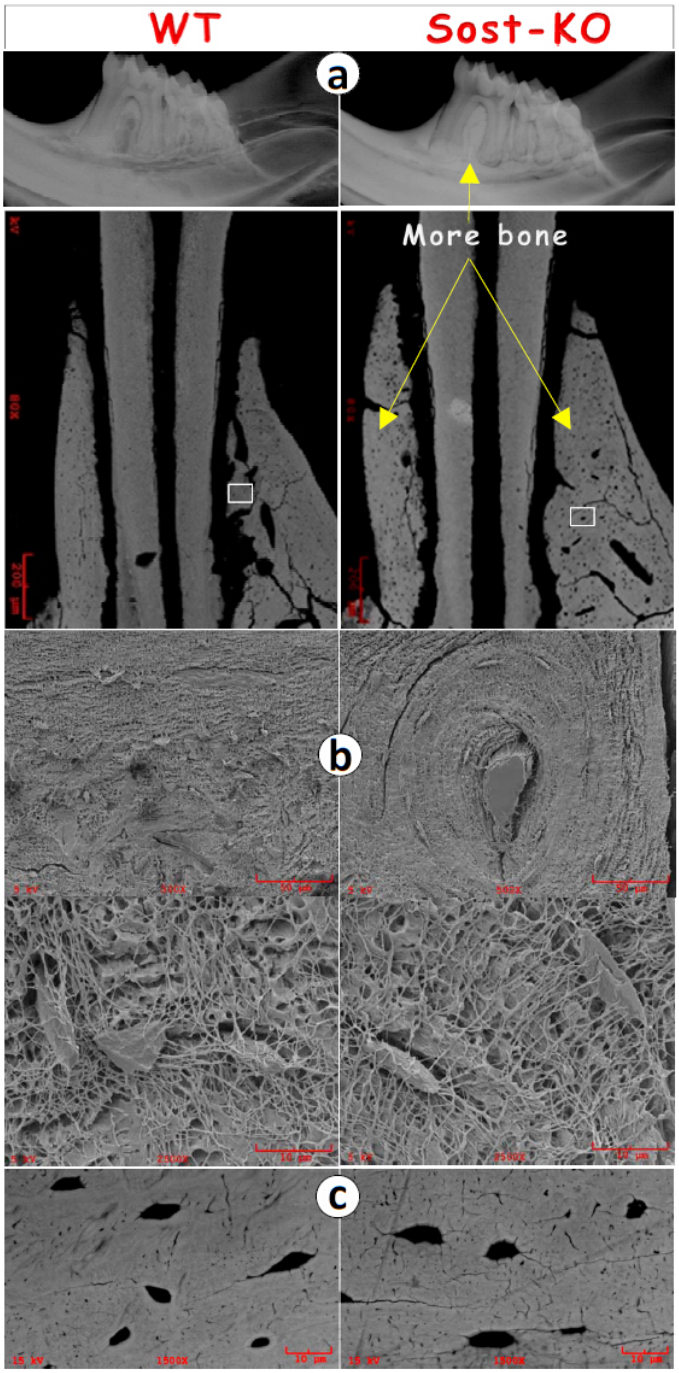

Figure 2-S3 ***Deletion of Sost KO leads to changes of Ocy morphologies***.(**a**) Representative radiographs revealed an increase in Sost KO alveolar bone (*right*); (**b**) Acid

etched SEM images displayed an osteon (the basic bone unit in mammalian but not in rodents) with a better Ocy organization in *Sost* KO mice (*right*); and (**c**) Backscattered SEM images revealed more defined Ocy structures in the Sost KO jawbone.

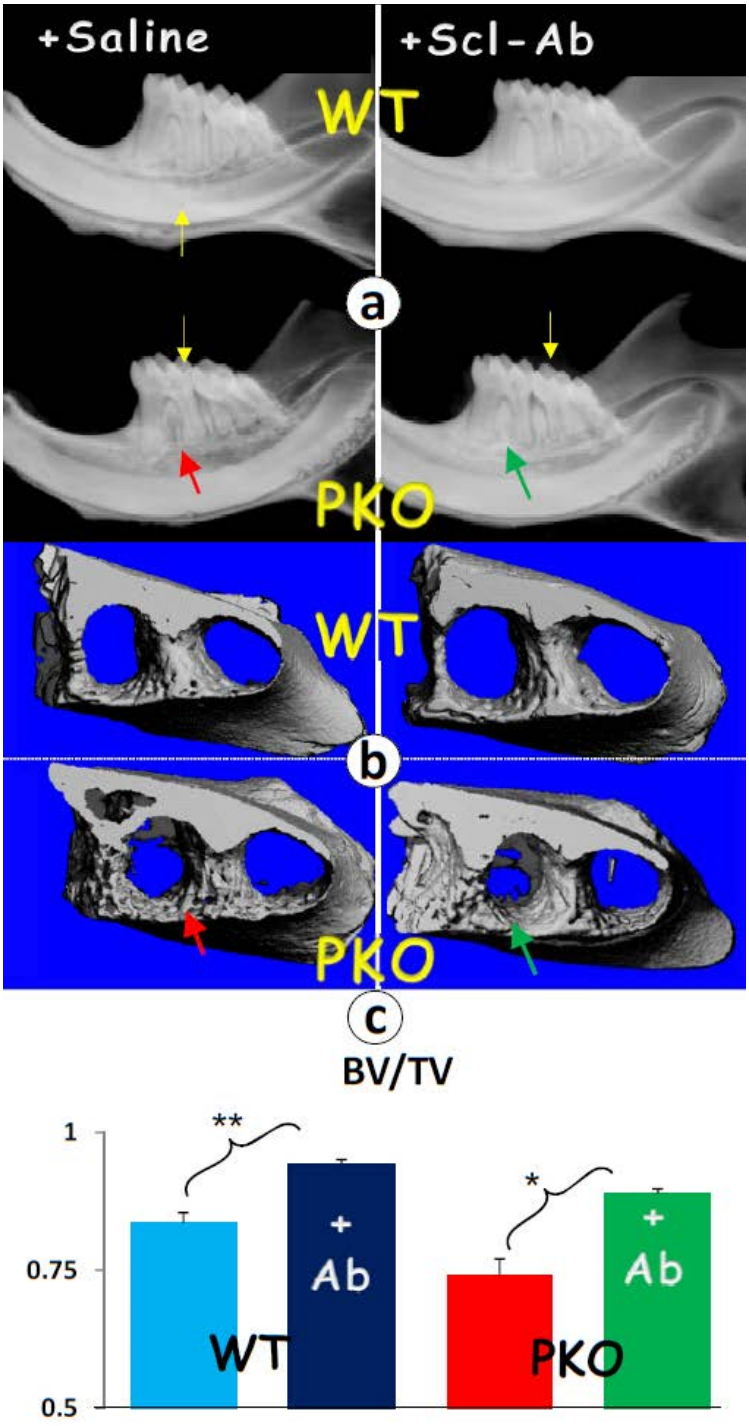

Figure 2-S4 Prevention of bone loss in PKO mice using Scl-ab for 8 weeks. (a). Representative radiograph images displayed bone loss at the age of 3-month (red arrow),

which was fully prevented by using Scl-Ab for 8 weeks (green arrow); **(b).** Representative uCT images confirmed the radiograph observation*;* and **(c).**quantitative data showed that this changes is statically significant. *, $p<0.05$; **, $p<0.01$; and n=4-5.

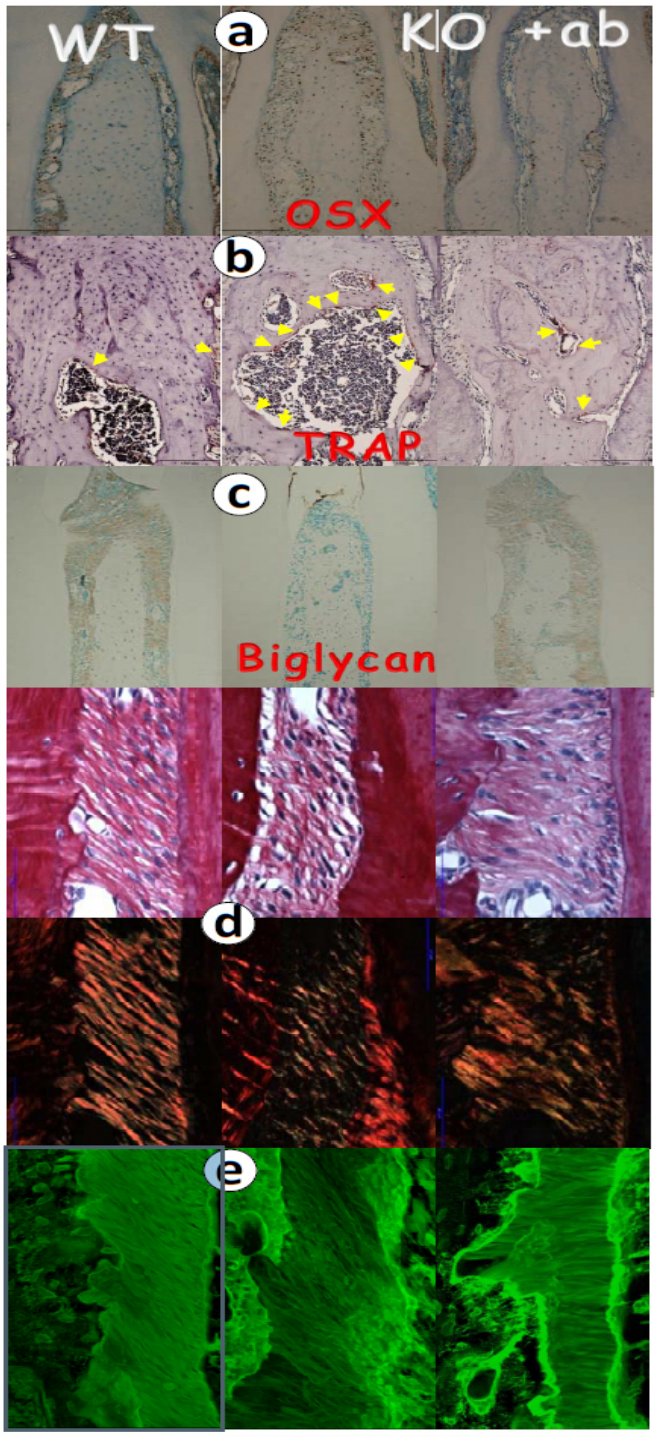

Figure 2-S5 ***Restorations of osteoblast, osteoclast, and periodontal ligament (PDL) markers after treatment of periostin knockout mice (PKO) with Scl-ab for 8 weeks in the 12-wk-old group***. (**a).** Representative OSX immunohistochemistry stains in WT (*left*),

PKO (*middle*) PKO treated with Scl-ab (*right*); (**b**) TRAP stain images in these three groups; (**c**) Biglycan stain images in these three groups; (**d**) Sirius stain images by regular microscopy (upper) and polarized microscopy (lower) in these three groups; and(**e**) FITC stain images in these three groups. The data showed improvement of all these markers and PDL fibers in the PKO treated group.

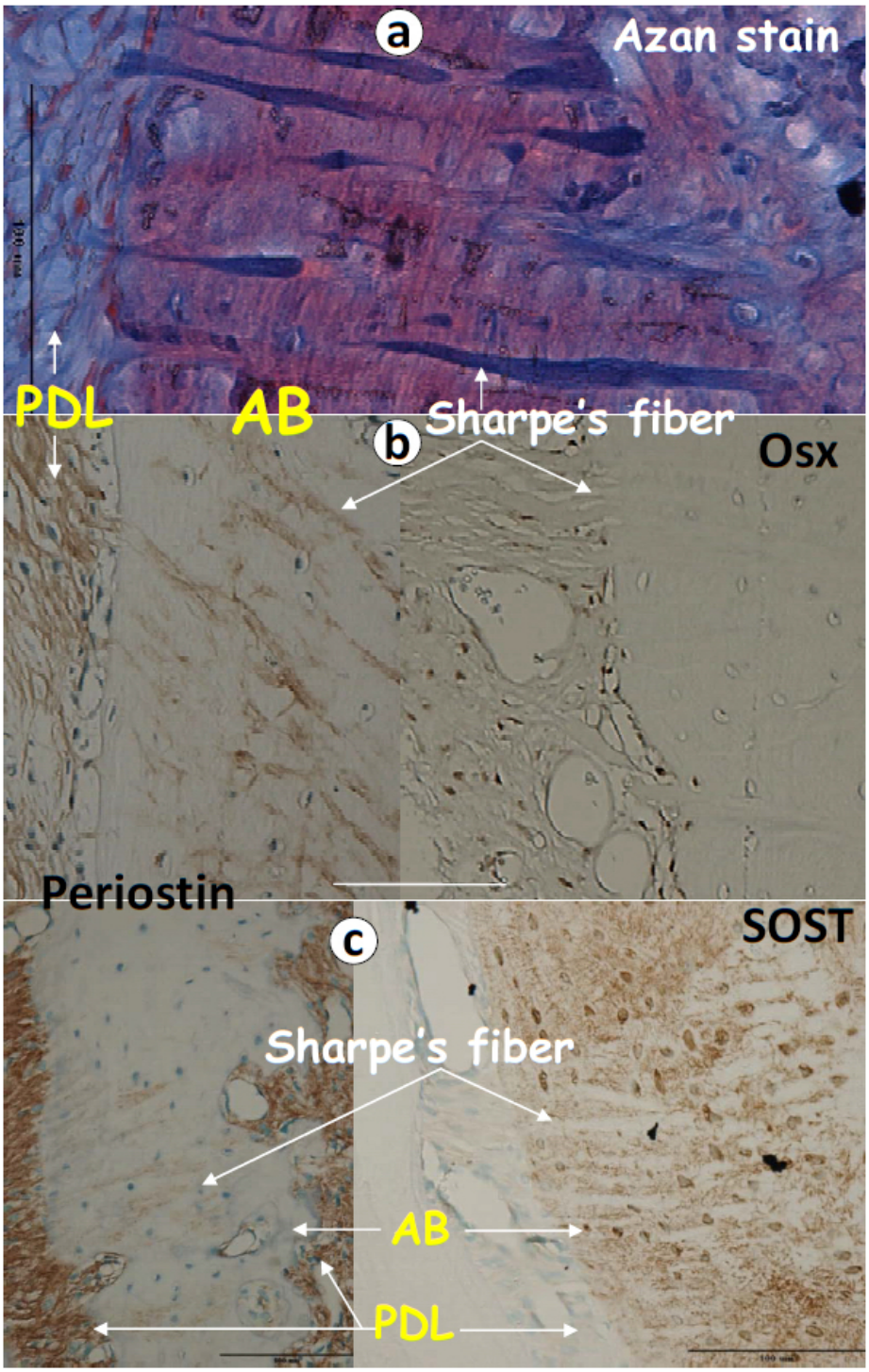

Figure 2-S6 ***A close link between PDL and alveolar bone through Sharpe's fibers.*** (**a**) A representative Azan stain image revealed Sharpe's fibers in blue in the 10-month-old

dog alveolar bone (AB); (**b**).Immunohistochemistry images displayed a high level of periostin in the dog PDL and Sharpe's fiber (*left*), and osterix (Osx) in PDL progenitor and osteoblast cells (*right*); and (**c**). Immunohistochemistry images presented a high level of periostin in the mouse PDL and Sharpe's fiber (*left*), and sclerostin(SOST) in osteocytes (*right*).

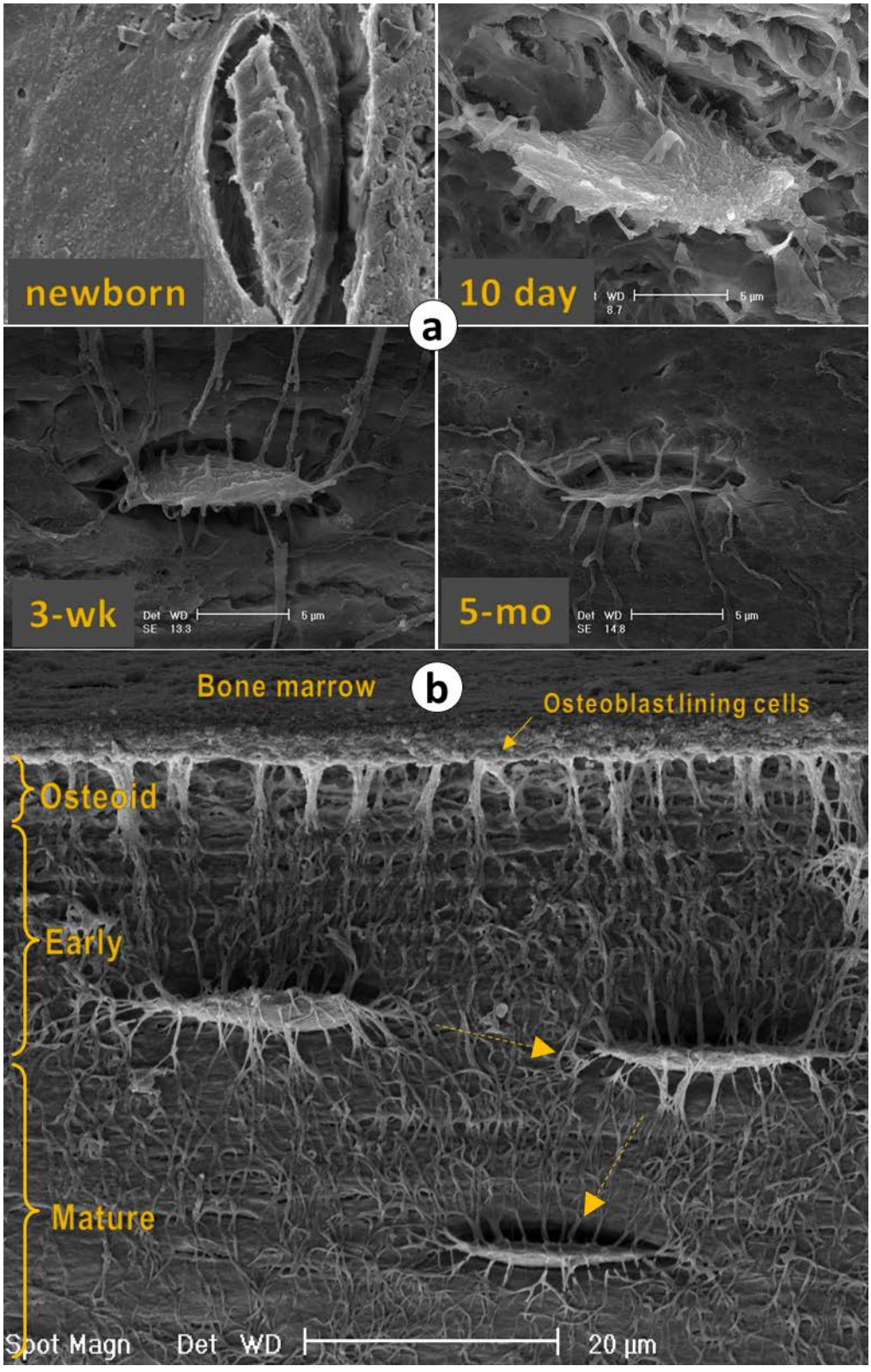
newborn
10 day
WD 8.7
5 µm
a
3-wk
Det WD SE 13.3
5 µm
5-mo
Det WD SE 14.8
5 µm
Bone marrow
b
Osteoblast lining cells
Osteoid
Early
Mature
Spot Magn Det WD
20 µm

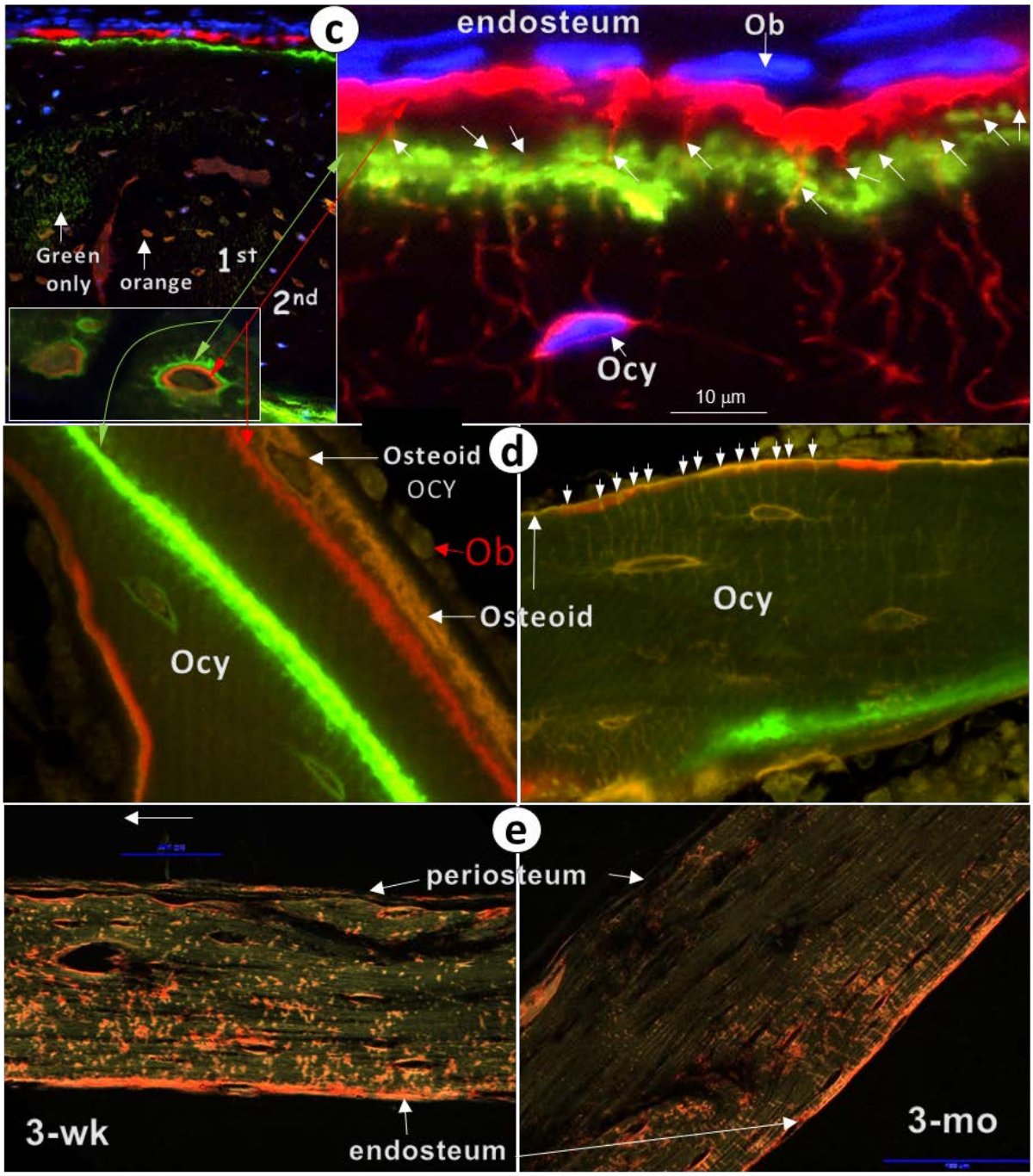

Figure 3-1 ***Murine bone mineralization is a prolonged process directly linked to Ocy maturation.*** **a**. SEM images of murine bone calvariae (0-10 days) revealed absent or multiple etched holes, indicative of poor mineralization and inadequate Ocy maturation

and reflected by plump irregularly shaped cells and few flat dendrites per cell. In contrast, murine bone calvariae (3 wk -5 mon) revealed resistance to acid etching and few holes in the matrix, due to enhanced matrix mineralization, which is evidence of progressive Ocy maturation, including a more complex dendritic network and eventual reduction in the cell volume and the transformation into a spindle shape, which is characteristic of a mature cell. **b**. SEM image of acid-etched cortical long bone from a 2 mon old mouse showed poor mineralization in the osteoid layer (evidenced by abundant holes in the matrix) and Ocy immaturity (plump Ocys with few flat dendrites), which progressed in the mature matrix to well-established mineralization (with resistance to acid etching from abundant calcium) and Ocy maturity (spindle-shaped cells with reduced volume). **c**. Confocal images of fluorochrome labeling counter-stained with DAPI displayed green, orange or green and red, and red-stained osteocytes and canaliculi; **d**. Double labeled images revealed an orange-labeled osteoid region in the more active trabecular bone, whose mineral deposition mainly originated from inner Ocys; and **e**. Polarized light image showing immature collagen in the entire 3-week-old cortical bone area, whereas the collagen was largely undetectable in the mature tibia region.

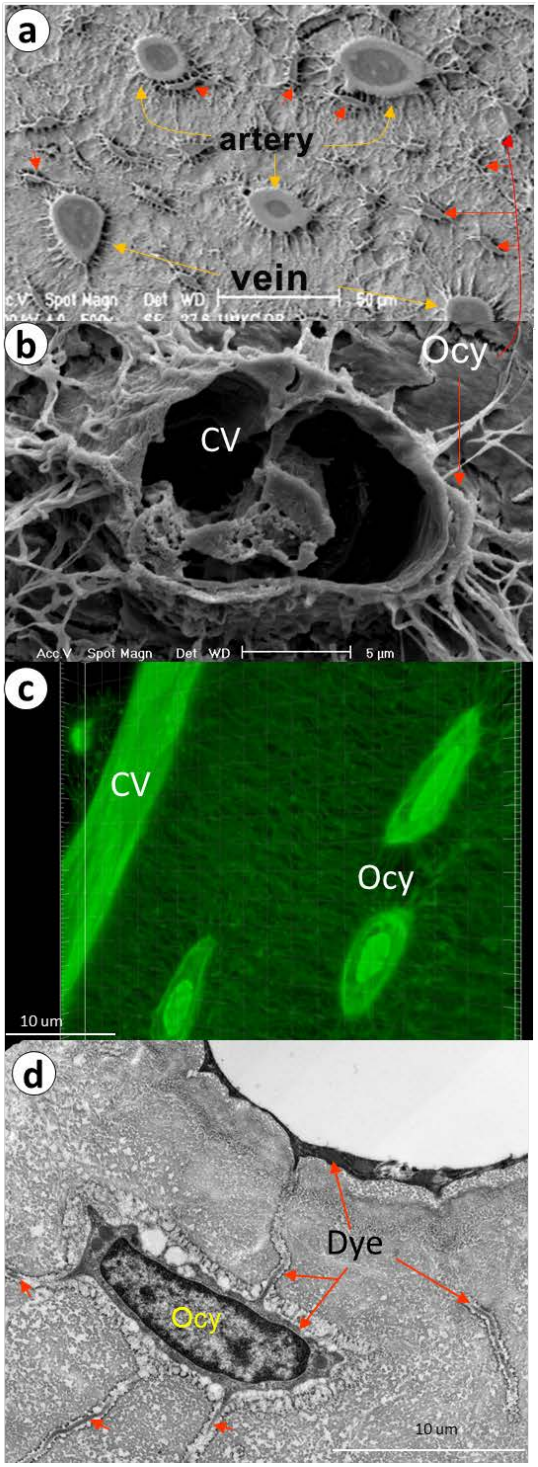

Figure 3-2 ***Abundant connections between osteocytes and blood vessels.*** **a**. A representative acid-etched SEM image displayed numerous Ocy dendritic connections to

both arteries and veins in cortical bone; **b**. A representative acid-etched SEM image also revealed Ocy dendritic connections to a capillary vessel (CV) in cortical bone; **c**. A FITC confocal image of trabecular bone likewise displayed identical Ocy dendritic connections to a CV; and **d**. A TEM image of an Ocy adjacent to the endothelial cells in the wall of a CV documenting dye stain (black) trapped in the endothelial cells and in the Ocy cytoplasm and dendrites <2 minutes after dye injection into the rabbit abdominal aorta.

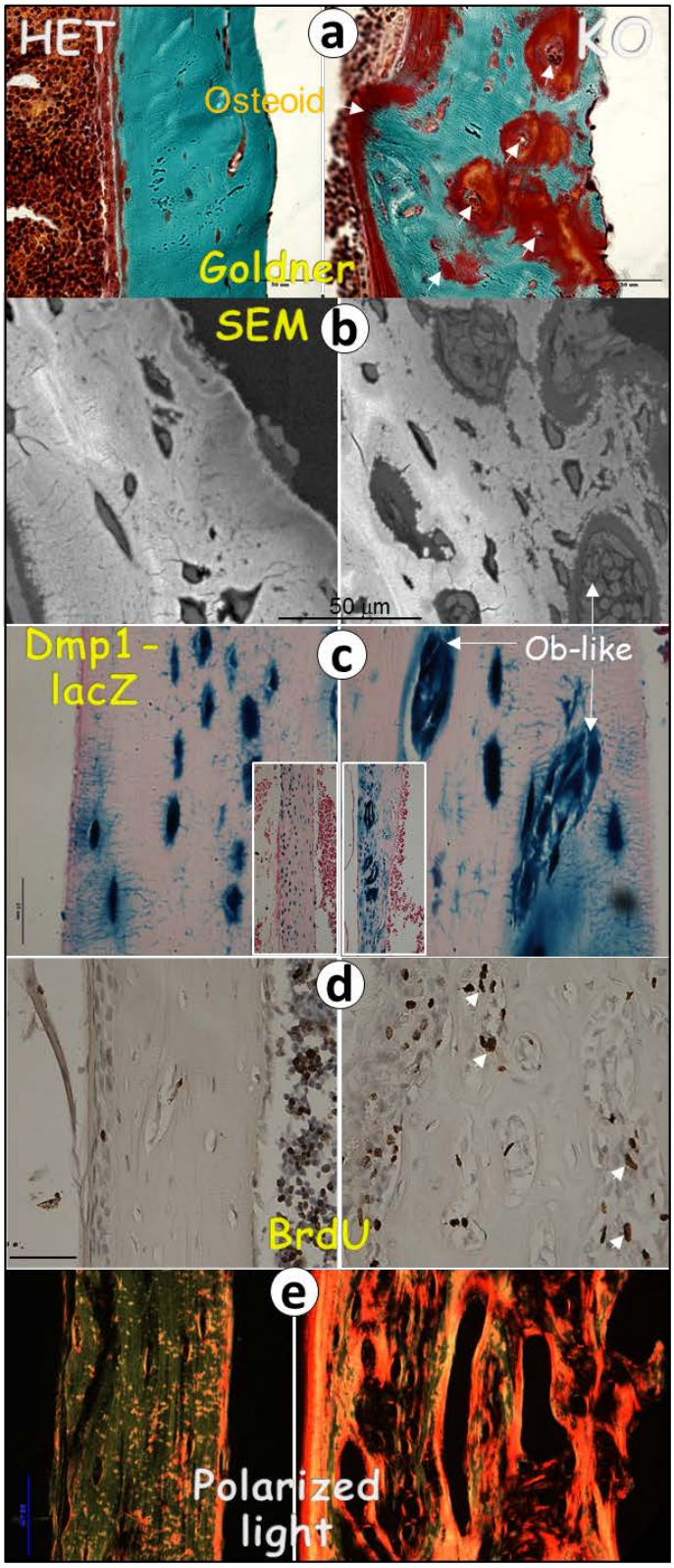
HET
a
KO
Osteoid
Goldner
SEM
b
50 µm
Dmp1-
lacZ
c
Ob-like
d
BrdU
e
Polarized
light

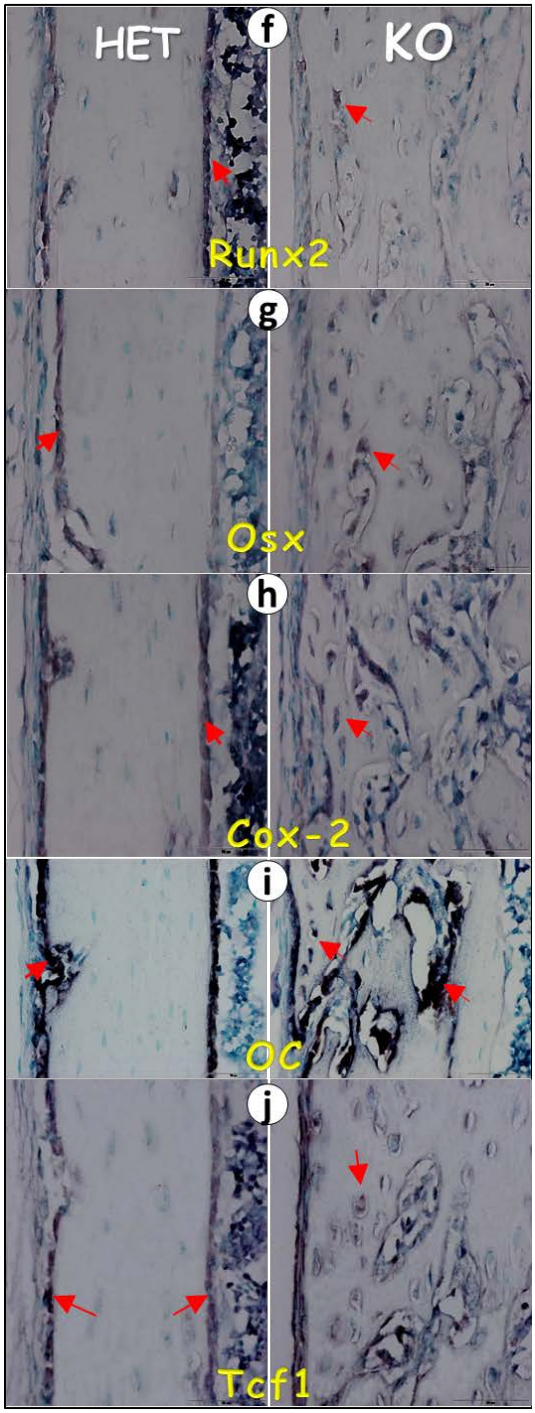

Figure 3-3 ***Impaired transition of osteoblasts into osteocytes is responsible for osteomalacia in Dmp1-null (KO) mice.*** **a**. Goldner stained images of cortical tibial bone

from KO mice showed unique morphology, compared to heterozygous *Dmp1* control mice, including cells (arrows) embedded in abundant osteoid and; **b**. Backscattered SEM images revealed that the embedded cells in the KO mice were cuboidal and similar in appearance to osteoblasts; **c**. X-gal stained images of a tibia from heterozygous *Dmp1* control mice (with a *lacZ* knockin) showed the *lacZ* signal only in Ocys, while comparable *Dmp1* KO mice exhibited *lacZ* positive cells in both Ocys and Ob-like cells, consistent with impaired transition of the osteoblasts into osteocytes; **d**. BrdU-stained images revealed that the Ob-like cells in the osteoid of KO mice had high cell proliferation (arrows), whereas no proliferation was detected in specimens from the heterozygous mice; **e**. Polarized light images of cortical bone showed abundant but poorly organized collagen in the KO mice; **f-j**) In situ hybridization revealed dramatic increases in Ob markers, *Runx2* (**f**), *Osx* (**g**), *Cox2* (**h**), *OC* (**i**), and *Tcf1* (**j**).

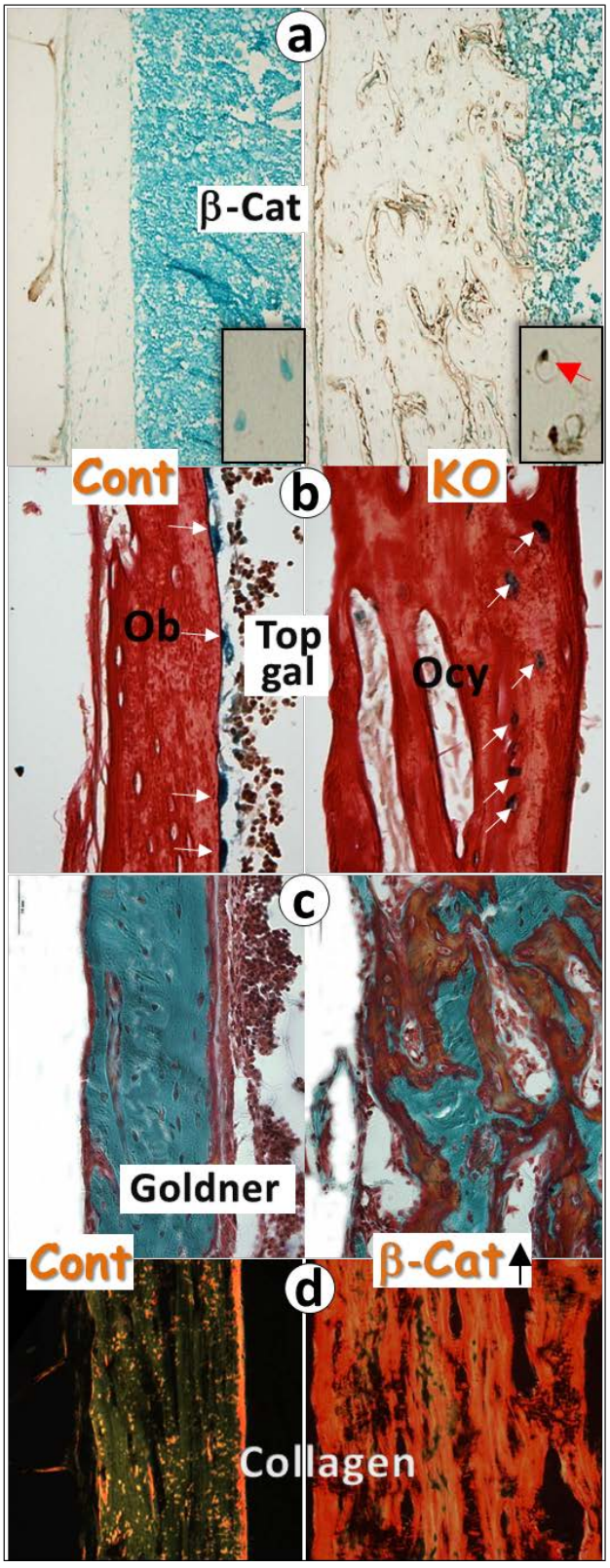
a
β-Cat
Cont
b
KO
Ob
Top
gal
Ocy
c
Goldner
Cont
β-Cat
d
Collagen

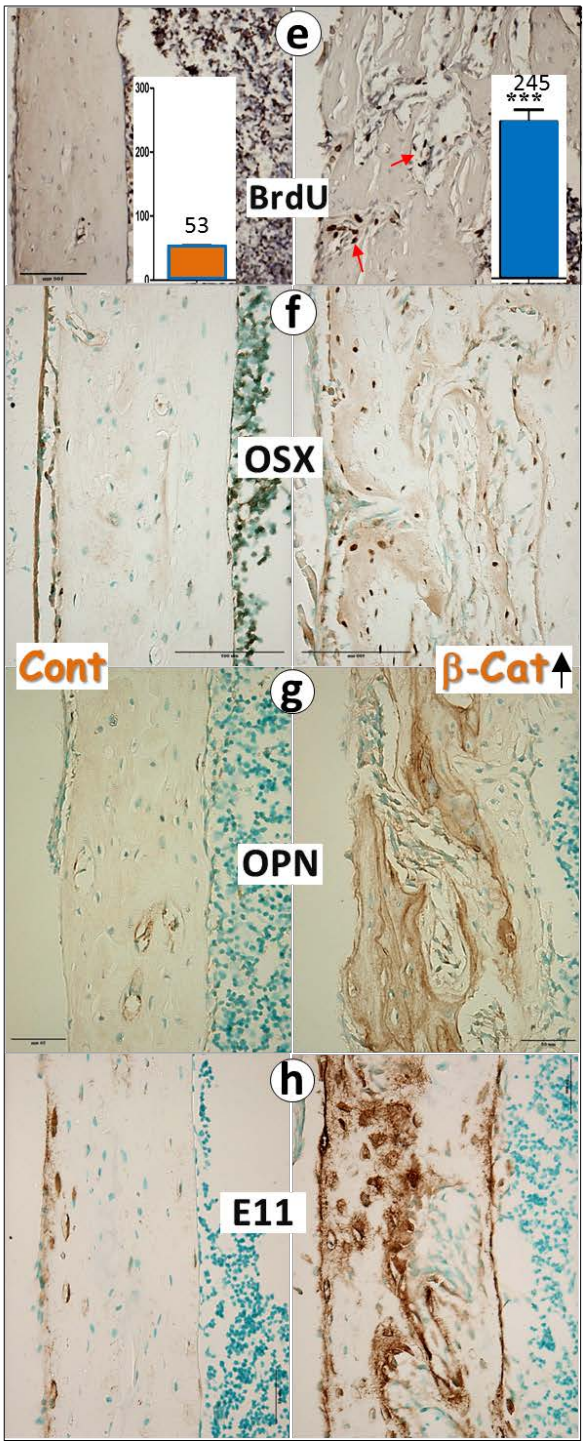

Figure 3-4 ***Sharp increases in Wnt-β-catenin signaling led to development of osteomalacia.*** **a-b**. Elevated β-catenin levels in *Dmp1 KO* mice were documented by

immunostaining (**a**), and X-gal stain (**b**); **c-h**. Elevated β-catenin levels in offspring of *Dmp1-Cre* X *Ctnnb1*^{ex3flox} mice resulted in osteomalacia indistinguishable from that in *Dmp1* KO mice, as evidenced by: Goldner stained sections of bone, which exhibited abundant red-staining osteoid (**c**), polarized light images that showed increased disorganized collagen (**d**), BrdU staining that documented increased proliferation of the Ob-like cells in the osteoid (**e**), and immunostains of Ob and early osteocyte markers, such as osterix (**f**), osteopontin (**g**), and E-11(**j**).

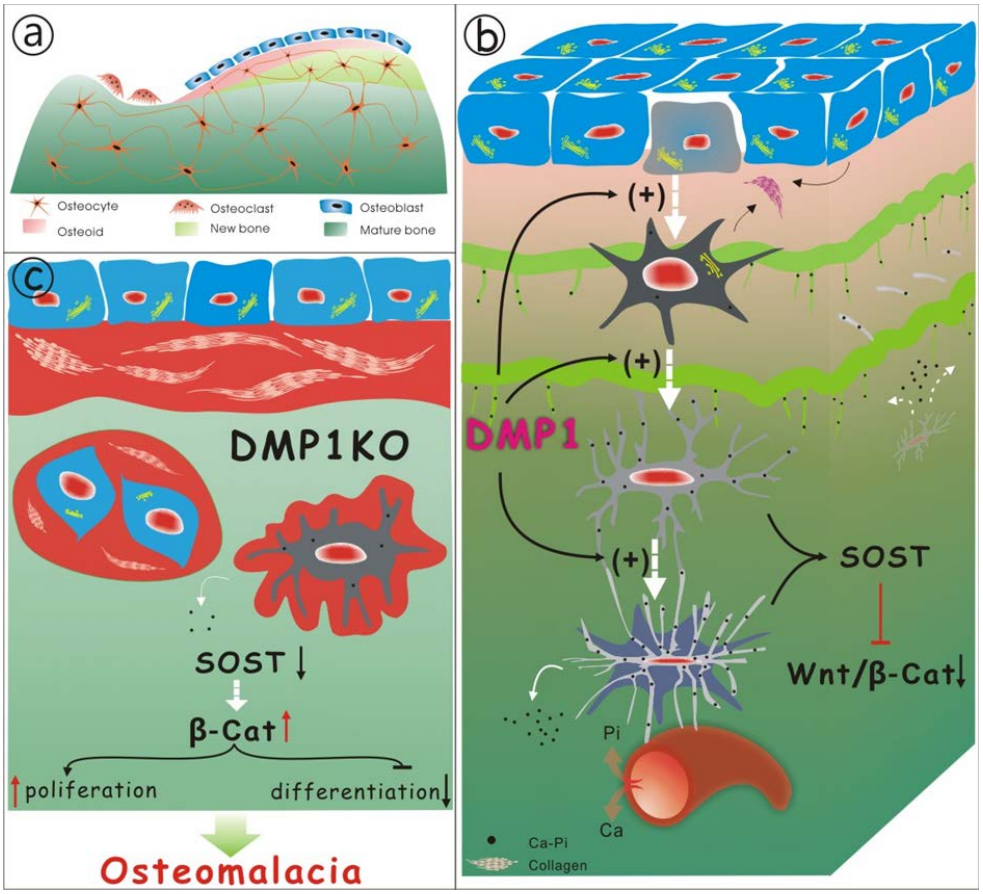

Figure 3-S1 ***Osteocytes (Ocys) form mineralized bone.*** a. The prevailing theory in bone biology is that osteoblasts (Obs) form mineralized bone. b. A new model of bone formation, suggested by our novel finding, indicates that the role of the Obs is to differentiate into Ocys, which play a primary role in mineralized bone, as reflected by: i) Nascent Ocys (dark grey) produce and secrete collagen into the bone matrix and deposit small amounts of mineral (Ca-Pi) in the matrix; ii) Working together, the well-formed Ocys (light grey) and the mature Ocys (white) deposit Ca-Pi in the bone matrix, "pump" Ca-Pi through dendrites to the bone surface (two *green lines with numerous "thorns", bearing mineral secreted by the Ocys located in the calcified bone matrix*), and deposit mineral in the matrix space created by the volume reduction of the Ocy cell body; iii) Ca, Pi and nutrients are rapidly transported from surrounding blood vessels to Ocys; iv) DMP1 controls the transition of Obs to Ocys and Ocys maturation; and v) the mature Ocys

produce SOST (sclerostin), a potent inhibitor of Wnt-β-catenin, which modulates Ocy-maturation and consequently mineralization (See Figure 3-1c). c. In the *Dmp1*-null (KO) mouse (a model of osteomalacia) immature bone cells release large amounts of β-catenin, which accelerates Ob proliferation, while inhibiting cell differentiation, resulting in arrest at the Ob stage (although preserving high activity; blue stain) or the immature Ocy stage (grey stain) and failure to pump adequate Ca-Pi to surrounding bone matrix and bone surface (red stain-osteoid; green stain-calcified bone).

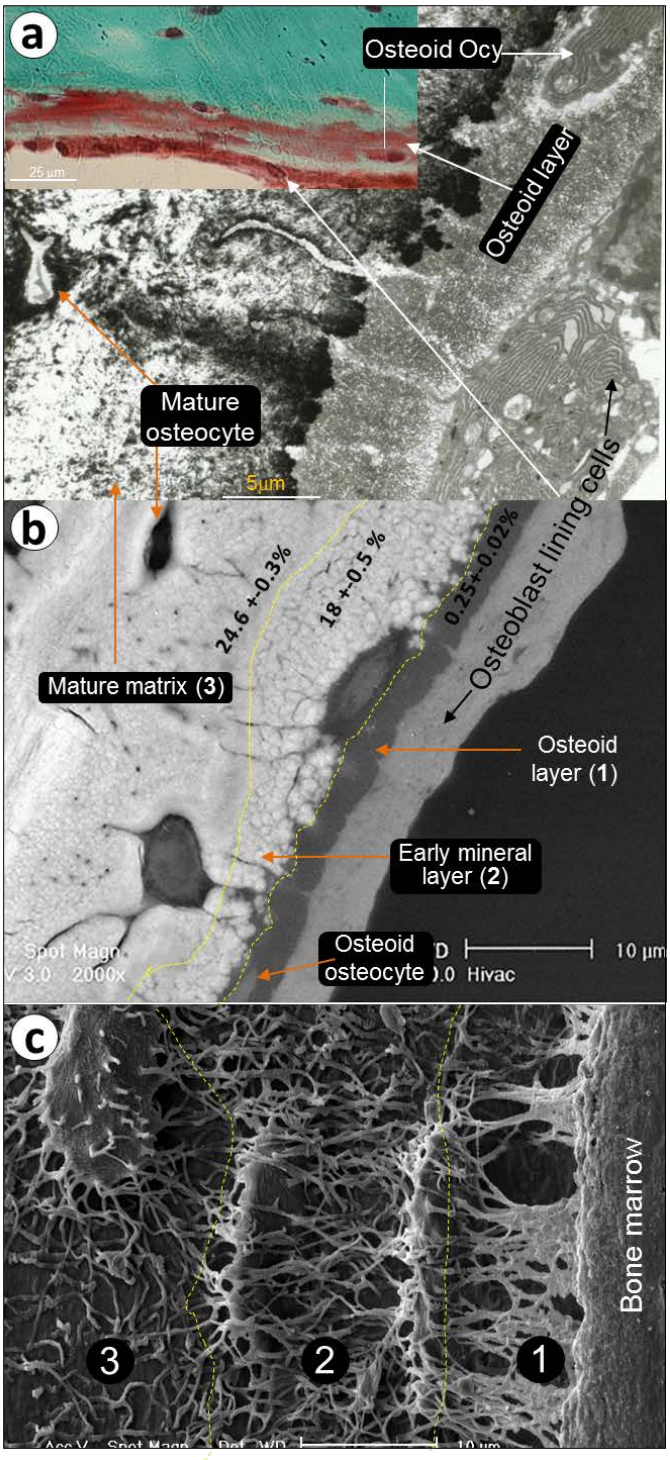

Figure 3-S2 ***Mineralization is directly linked to various phases of Ocy maturation.*** a. TEM and Goldner stained (insert) images, displaying an osteoblast (Ob) lining cell layer

and an osteoid layer, in which the osteoid Ocys, like the Ob lining cells, are rich with rough endoplasmic reticulum and Golgi complexes, indicating that the Ocys may produce and secrete collagen. b. A backscattered SEM image, exhibiting a distinct mineral distribution pattern, wherein no mineral deposits are present in the surrounding matrix of the Ob lining cells (light grey color), small amounts of mineral are present in the osteoid layer (dark grey), a poorly formed mineral layer with a poorly organized sphere-like mineral structure is found in the early mineral layer (white color), and confluent mineral deposits are present in the mature matrix, in which the Ocys are well defined; Energy dispersive X-ray spectroscopy analyses of 10 random spots in each layer quantitatively confirmed these observations; and c. The acid-etched SEM image revealed: i) large holes (indicative of relatively complete removal of calcium) in the osteoid layer, as well as numerous newly formed Ocy dendrites that appear flat and clumped, ii) moderate removal of calcium in the poorly organized early mineral layer, uncovering a relatively well defined system of Ocy-dendrites that pierce deeply into the bone; and iii) limited removal of calcium in the highly calcified mature matrix, with exposure of only surface Ocy-dendrites.

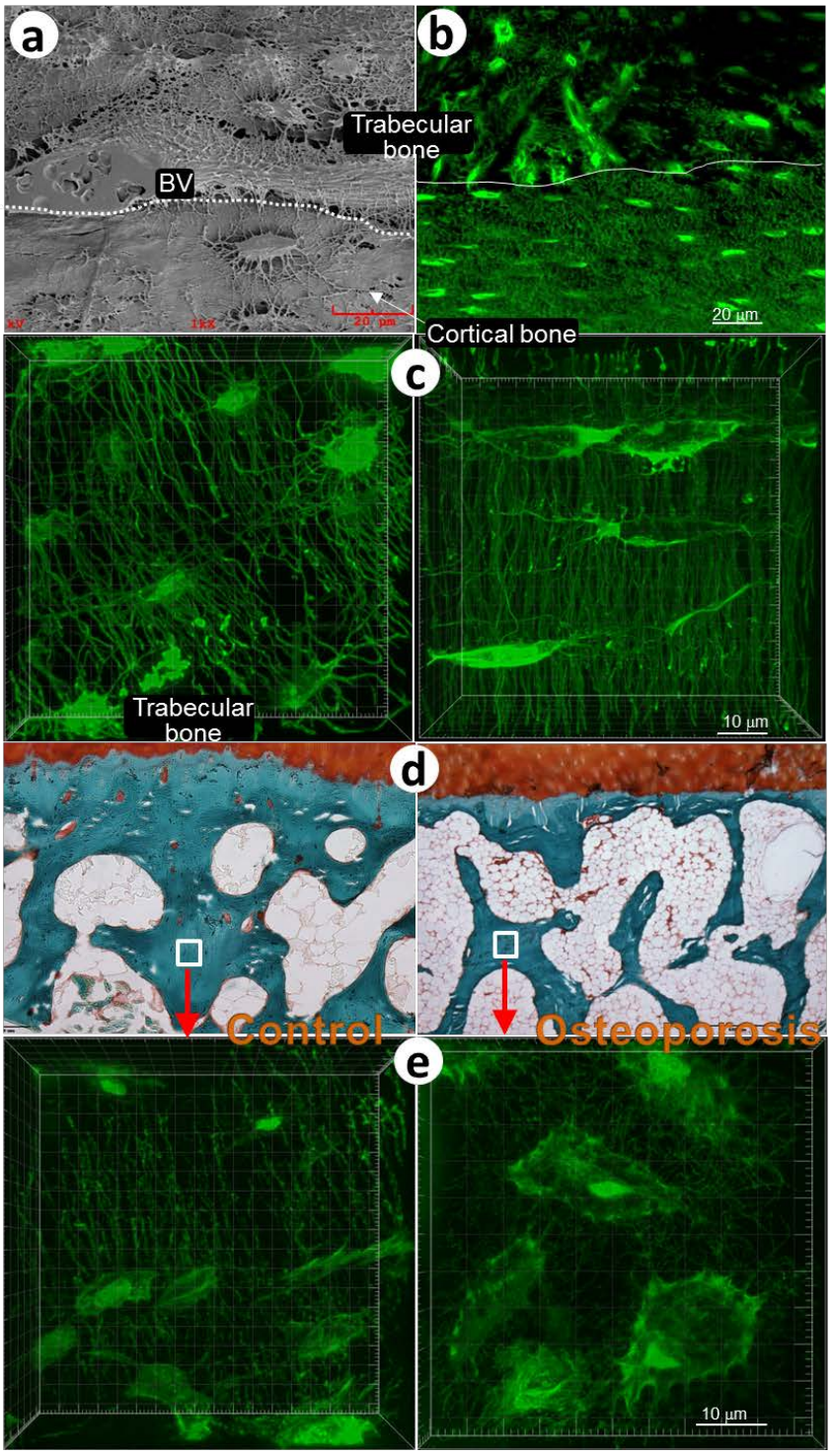

Figure 3-S3 ***Mineralization quality is closely associated with the osteocyte shape and its dendrite numbers*** **a**, The acid-etched SEM images showed porotic bone in the mouse

trabecular bone (upper) compared to the cortical bone (lower); **b**, a FITC confocal image, a "mirror" of **a**, displayed spindle-Ocys with numerous dendrites in the cortical bone region, whereas in the trabecular bone, there are few dendrites, and the Ocys are irregularly shaped in a non-organized pattern (left); **c**, the human FITC confocal images revealed a similar pattern in the trabecular (left) and cortical bone (right); **d**, Goldner images showed bone loss in a 99-year-old female femur (right) compared to the control (37-year-old male, left), although no apparent other bone changes observed by this technique; and **e**, the enlarged FITC images from the trabecular bone in white boxes revealed a dramatic changes of osteocytes from spindle in the control (left image) to round with much enlarged cytoplasm (i.e., more mineral matrices lost, right image), which are responsible for poor bone quality in the osteoporosis patient. Of note is that both samples were obtained from cadaver bodies.

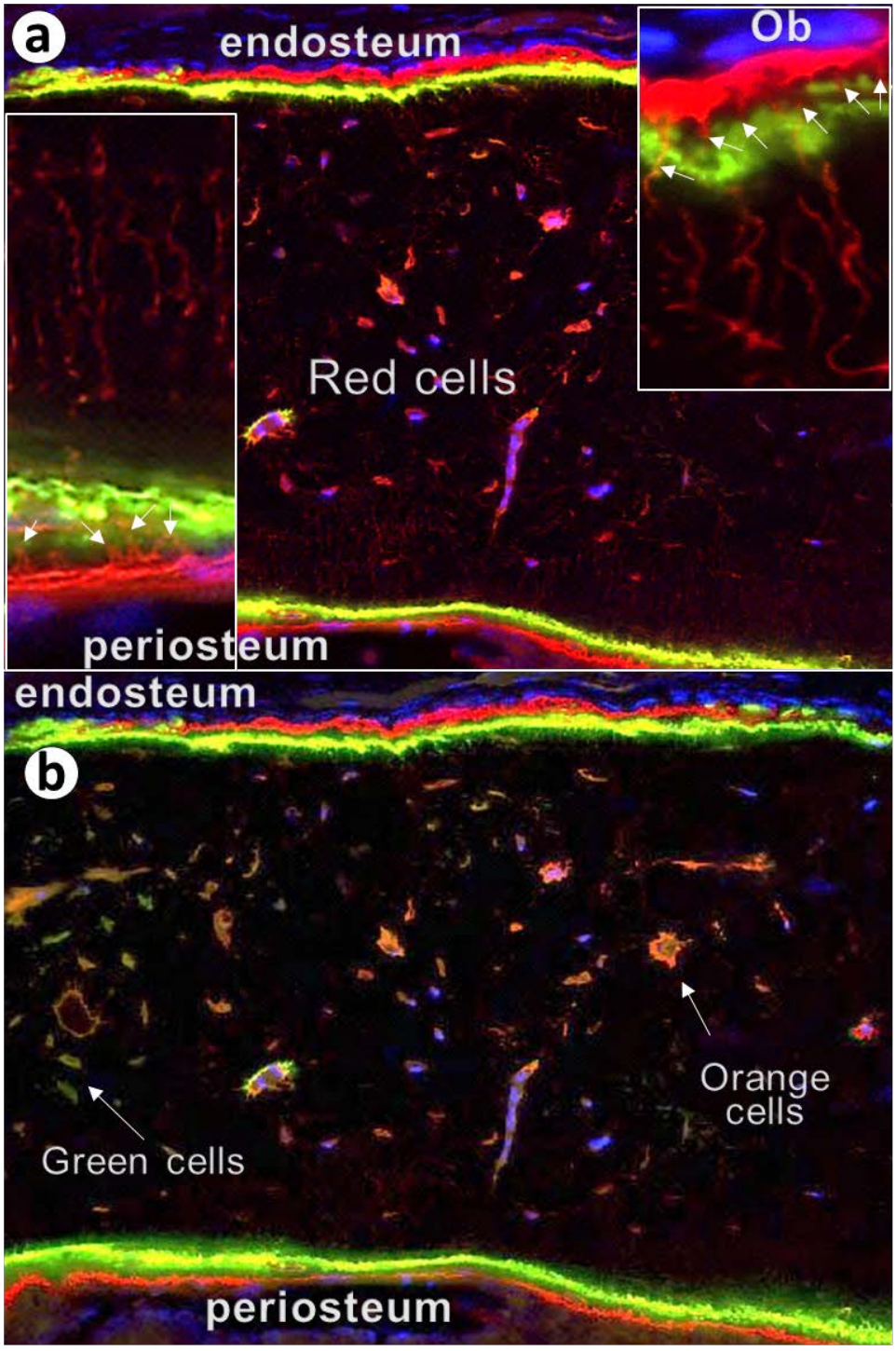

Figure 3-S4 ***Bones grow from the inside to the outside.*** Calcein was injected into 7-wk-old WT mice followed by Alizarin Red 5 days later, and the mice were sacrificed at age

of 8 wk. A series of 10-mm sections of a plastic-embedded long bone was counter stained with DAPI stain followed by confocal imaging. a. The surface sagittal section displayed double-labelled mineralized fronts plus numerous red stained osteocytes and their dendrites (arrows), suggesting that osteocytes continuously deposit minerals in bone matrices and bone surfaces of the endosteum and periosteum (inserts) with no mineral contributions from the osteoblast (Ob) on bone surfaces; b. The deep bone section displayed two color-stained osteocytes: green (indicating mineral deposition at an early phase) and orange (suggesting these cells deposit minerals at both phases).

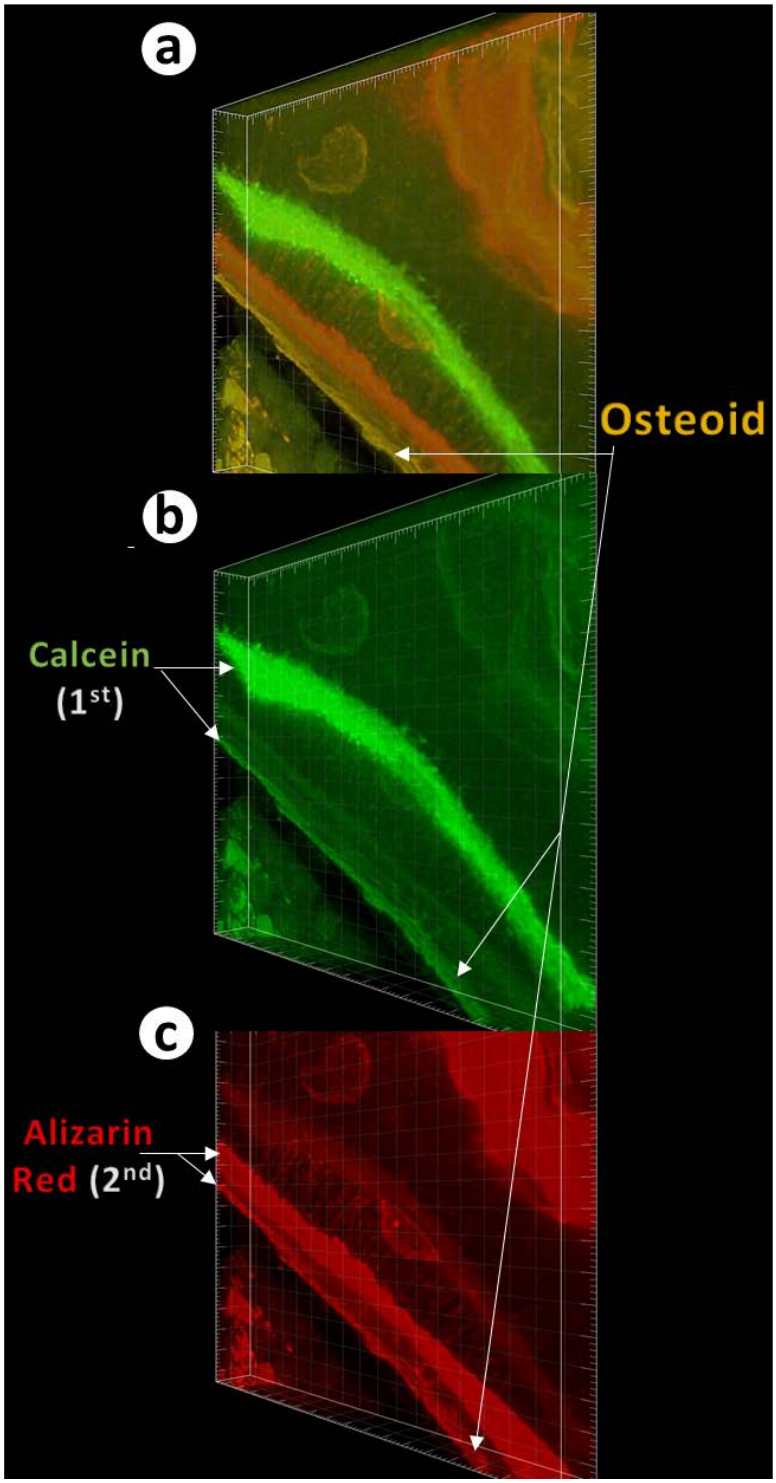

Figure 3-S5 ***There is a small amount of Mineral in the osteoid layer is mainly formed from inner Ocys.*** Calcein was injected into 7-wk-old WT mice followed by Alizarin Red

5 days later, and the mice were sacrificed at age of 8 wk. a. Overlapping both red and green lights revealed an orange line, reflecting contributions of inner Ocys for a small amount mineral in the osteoid layer. b. The green light view only, showing one bolt line and one thin surface line; and c. The red light view only, showing one bolt line and one thin surface line.

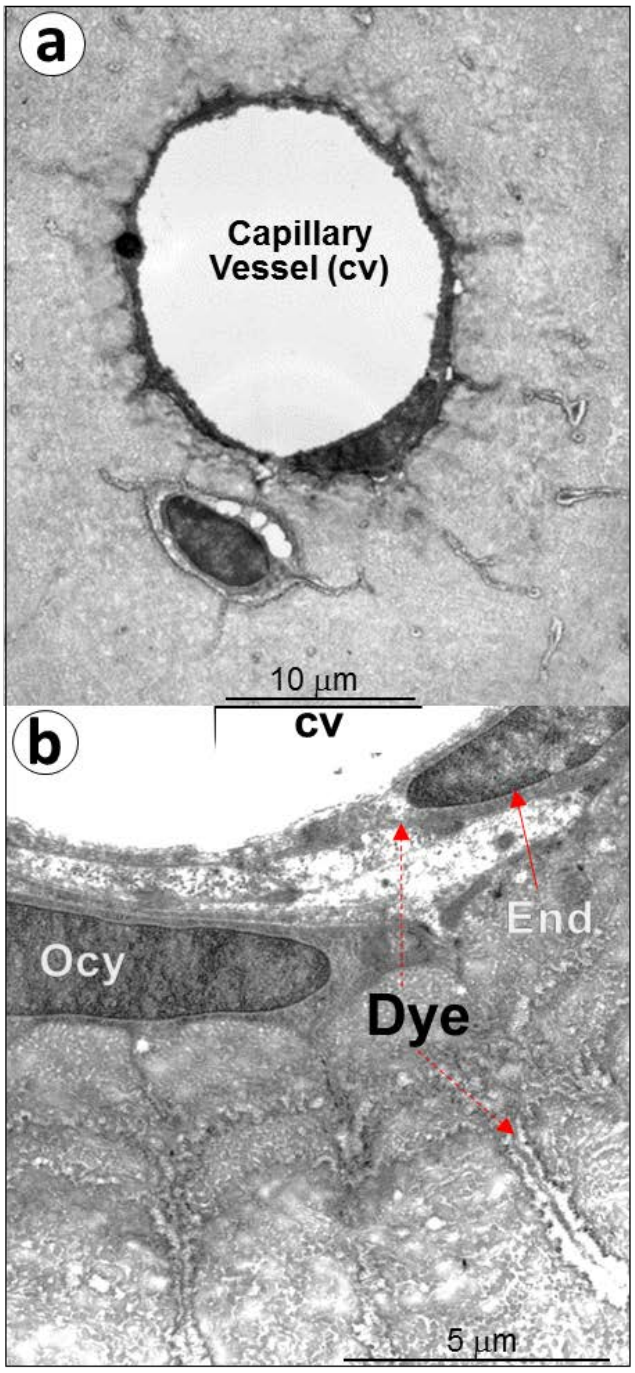

Figure 3-S6 ***Direct communication between capillary vessels and osteocytes (Ocy).*** An adult rabbit was under intravenous anesthesia with pentobarbital (30 mg/kg), followed by

catheter placement into the abdominal aorta. Ten ml of PBS was used to flush out blood, and then a 5% sodium metaperiodate solution (dye with molecular weight of 213.89) was injected into the bloodstream, followed by immediate fixation with less than a 2-minute delay. a. The TEM image showed a capillary vessel surrounded by numerous Ocy-dendrites Most of the dye filled the cytoplasm of the Ocy-dendrites with dye (black color) filled in the cytoplasm of the cell body and dendrites but not in matrices. b. The enlarge TEM image displayed dye in the cytoplasm of endothelial (End) and Ocy-dendrites (arrows).

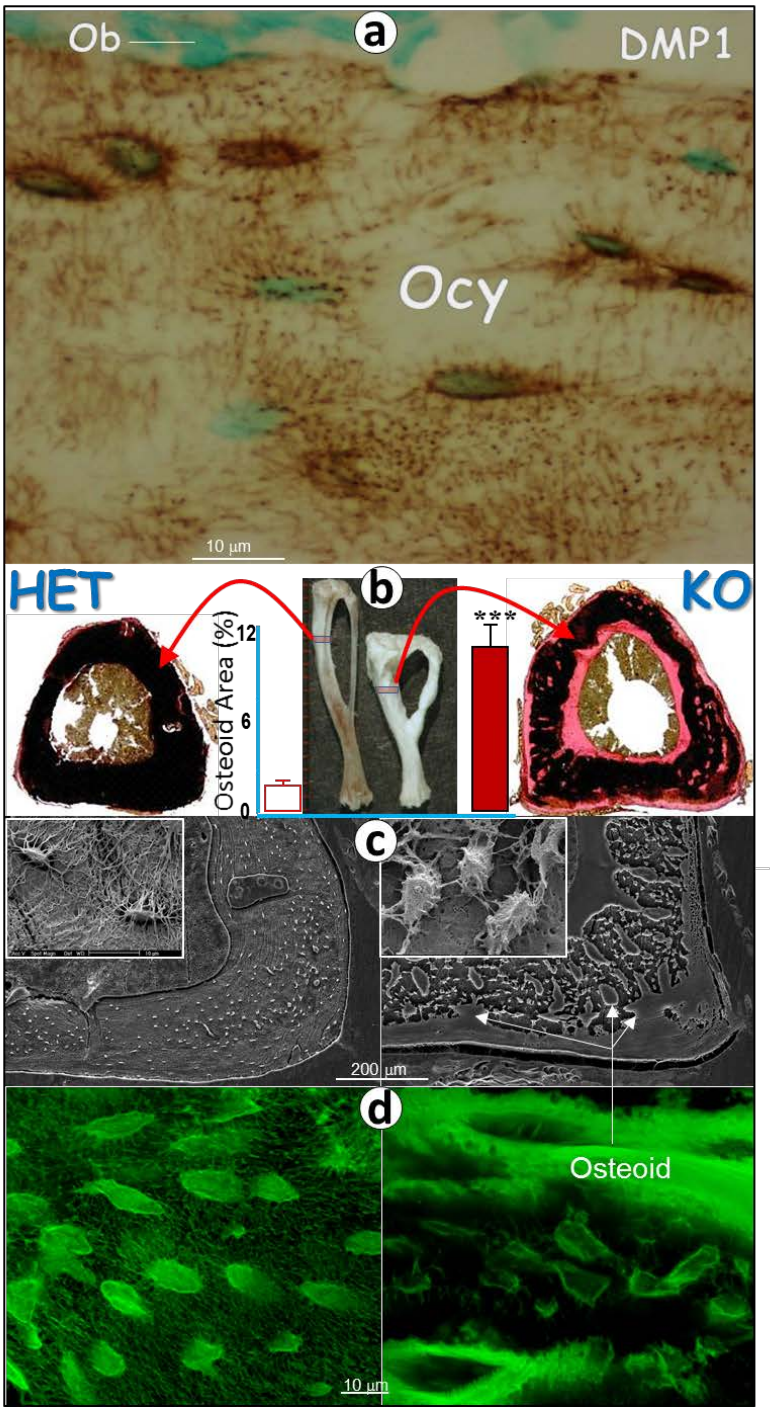

Figure 3-S7 ***Loss of Dmp1, a gene highly expressed in osteocytes (Ocys), leads to an osteomalacic phenotype*****. a**. a representative immunostain image displays a high level of

DMP1 in the extracellular matrix surrounding the Ocy and dendrites but not in the matrix surrounding osteoblast (Ob); **b**. Photographs of 3-month old tibias (mid) showed dramatic changes in *Dmp1* knockout (KO) bone in size and shape; the Von Kossa stain images revealed a sharp increase in osteoid (red, right image) content (10-fold higher than heterozygous control, HET, n=4, $p<0.001$). **c**. Representative acid-etched SEM images display a large amount of osteoid in the KO long bone (a cross sectional view, arrows) compared to that in *Dmp1* HET control bone (left). The *Dmp1* KO image (insert) shows a great morphological change in the KO's Ocy bodies with few dendrites and loss of surrounding matrices, indicating poor mineral content directly linked to morphological changes of the KO Ocys; **d**. FITC confocal images further confirmed a large amount of osteoid and malformed Ocy with few dendrites in the KO mouse bone (right) compared to that in the HET (left) mice.

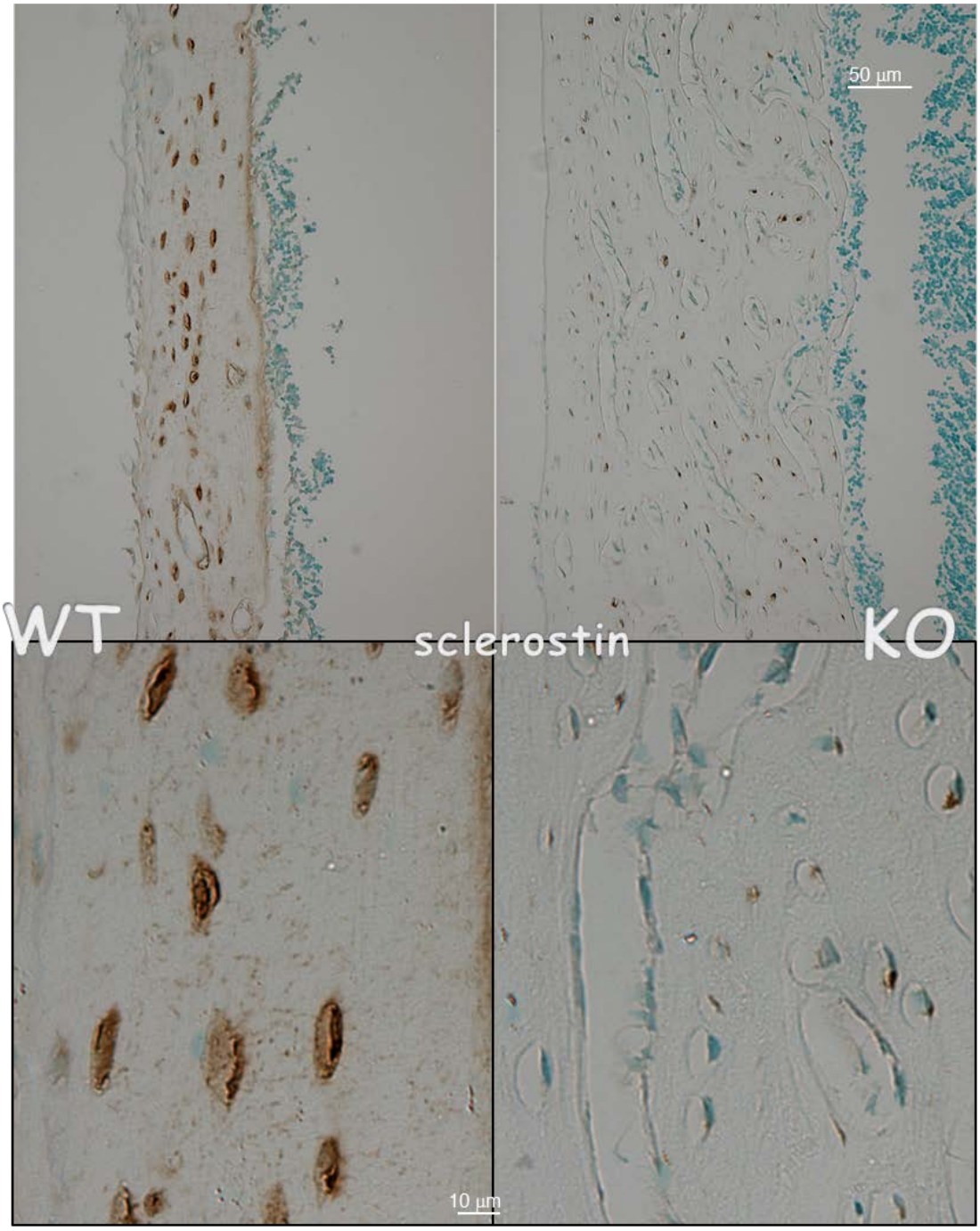

Figure 3-S8 ***A sharp reduction of sclerostin expression in a 3-wk old Dmp1-null (KO) tibia.*** The representative immunostain image displays a high level of sclerostin in the

mature osteocytes and dendrites (left) compared to the age matched KO tibia, where sclerostin was largely undetectable (right images). (Unpublished Data from Shuxian Lin)

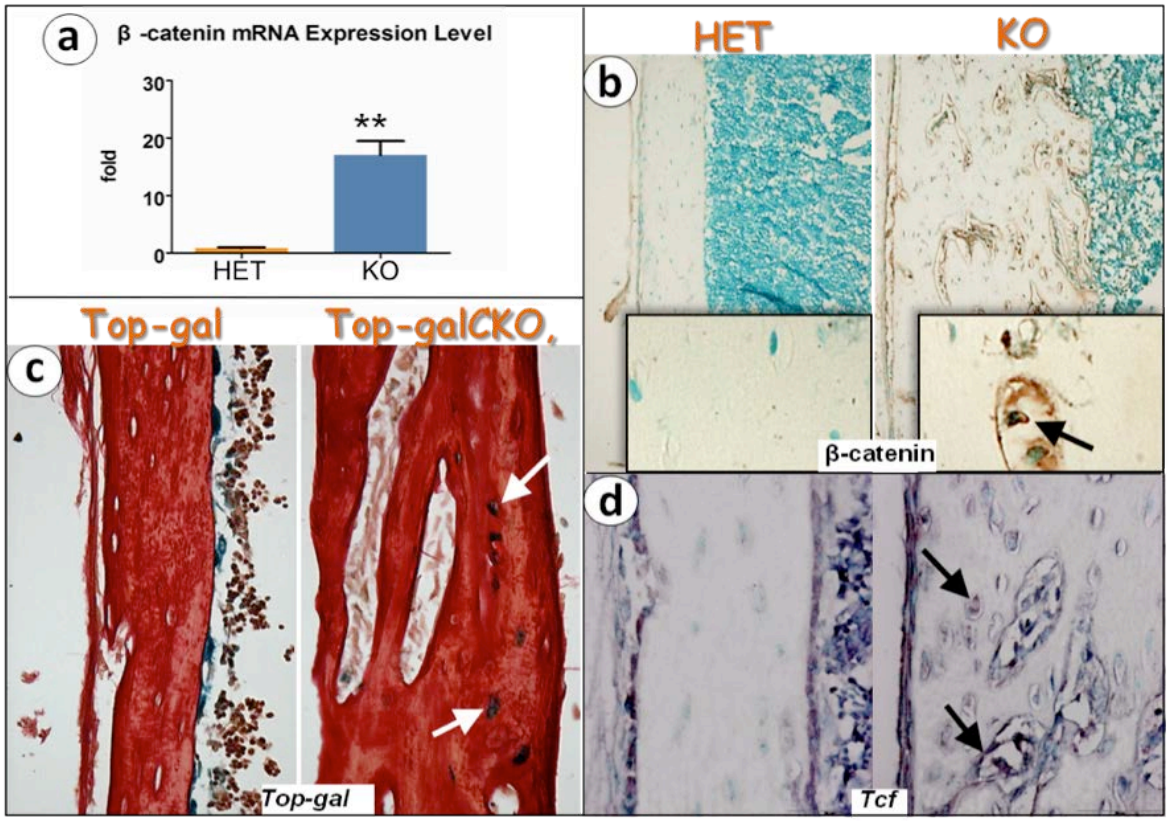

Figure 4-1 ***Wnt/β-catenin signaling was up-regulated in the osteocyte of Dmp1-null mice.*** (**a**) The mRNA expression level of β-catenin showed a more than 15-fold up-regulation in *Dmp1*-null mice compared to the controls. Data are presented as mean ± SEM; n=6 in each group; *P<0.05; **P<0.01. (**b**) Immunohistochemistry staining of β-catenin revealed an increased expression of β-catenin in the osteocytes. The arrow in the magnified box indicated a nuclear localization of β-catenin. (**c**) X-gal positive osteocytes were found in the *Dmp1* conditional knockout (*3.6 kb Col1 Cre; Dmp1*$^{fx/fx}$; Top-gal+) mouse long bones (arrows), compared to few positive osteocytes in the control group (*Dmp1*$^{fx/fx}$; Top-gal+). Note the *β-galactosidase* gene was driven by a TCF-β-catenin responsive promoter in the Top-gal mouse, so canonical Wnt activity was detected by X-gal staining. (**d**) *In situ* hybridization staining demonstrated the *Tcf* expression that was up-regulated in the osteocytes of *Dmp1*-null mice (arrows). (Unpublished data from Shuxian Lin)

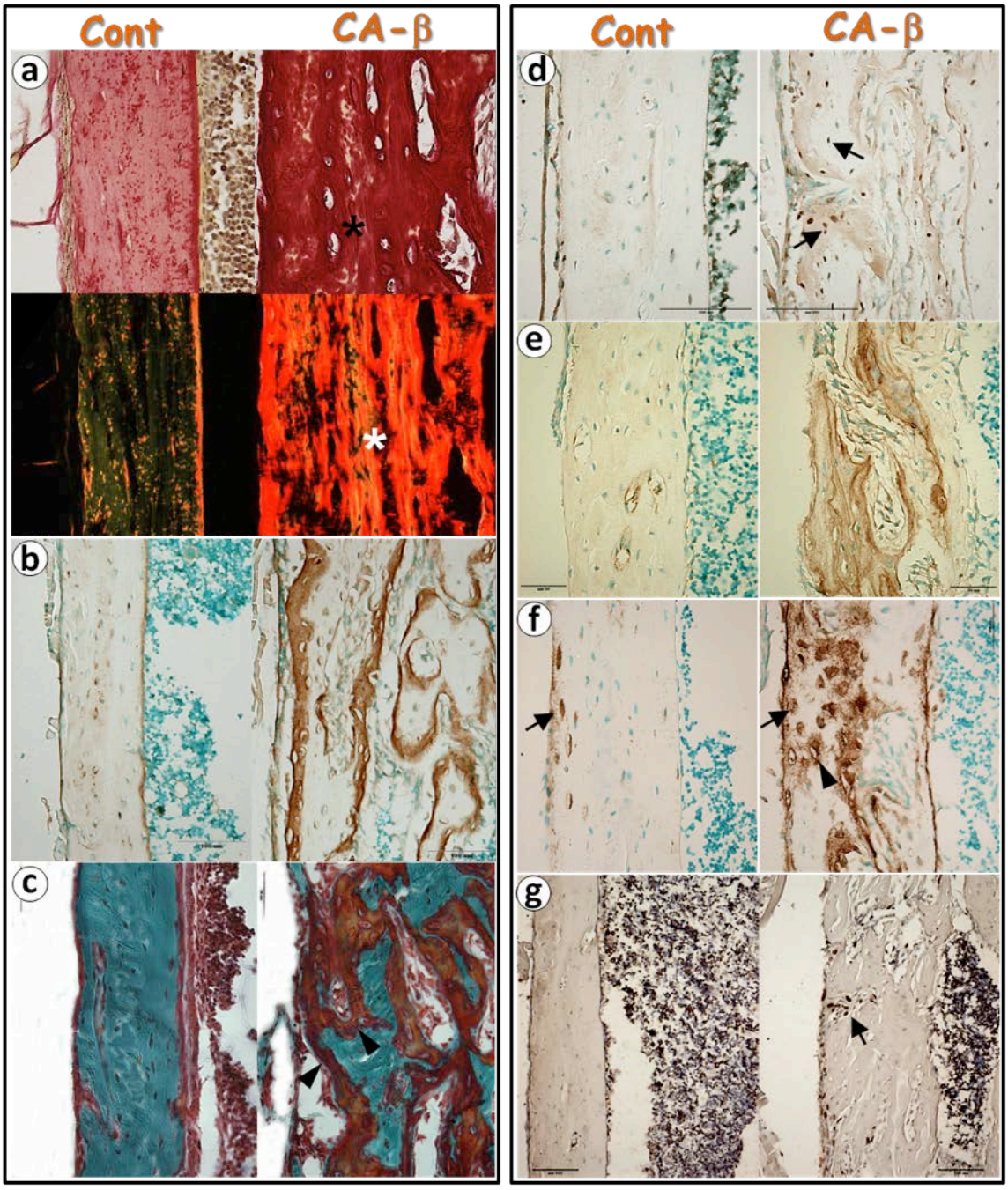

Figure 4-2 ***Constitutive stabilization of β-catenin in osteocytes recaptured osteomalacia phenotype and displayed deformed osteocytes.*** (**a-c**) Elevated β-catenin levels in offspring of CA-β (*Dmp1-Cre*; β-cat$^{ex3loxP/+}$) mice resulted in osteomalacia indistinguishable from that in *Dmp1*-KO mice, as evidenced by: polarized light images, in which green means

thinner collagen fibers such as reticular fibers, whereas red or orange indicates larger collagen fibers such as collagen type I, showing increased disorganized collagen (**a**); Biglycan staining that appeared more positively stained area (**b**); Goldner-stained sections of bone, which exhibited abundant red-staining osteoid (**c**). (**d-g**) Increased β-catenin levels in osteocytes caused maturation defects, as supported by immunostains of osteoblast and early osteocyte markers, such as OSX (**d**), OPN (**e**), and E11 (**g**) showed apparently elevated expressions; BrdU staining that documented increased proliferation of the immature osteocytes in the osteoid (**g**). (Unpublished data from Shuxian Lin)

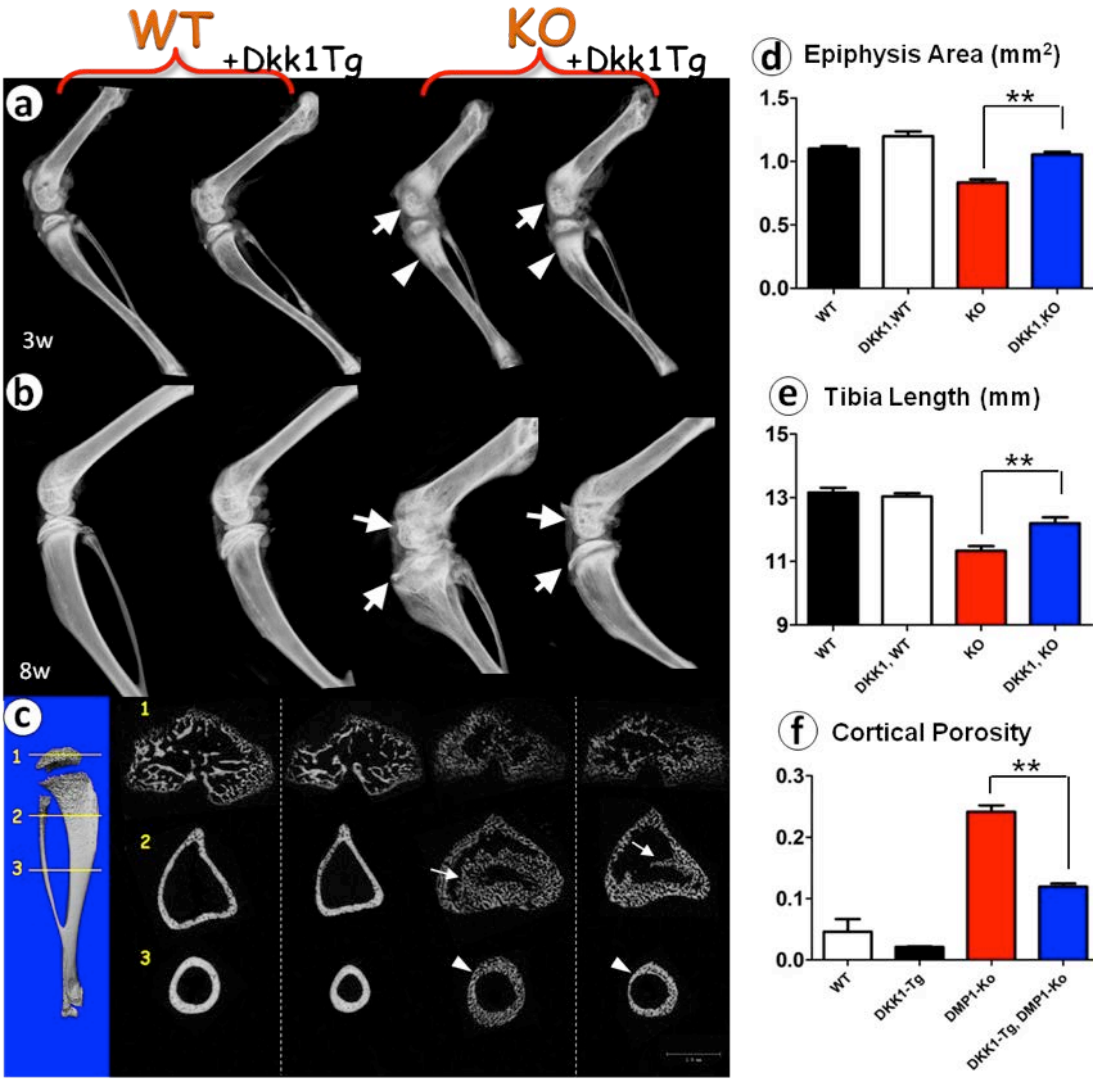

Figure 4-3 ***Normalizing the Wnt/β-catenin activity greatly improves the bone morphology.*** (**a-b**) Representative radiographs of 3-wk (**a**) and 8-wk (**b**) groups. Note the long bone shape was better formed in the DKK1; KO mice, compared to the KO groups. Also, in the KO mice, the bone accumulation appeared in the metaphysis (arrowhead) and the epiphyseal structures were disorganized and malformed (arrows), but were notably improved by *Dkk1*-Tg. (**c**) μ-CT images of different tibia cross sections indicated malformed epiphysis structure, obvious bone accumulation in the metaphysis (arrow), and porous cortical bone (arrowhead) in the KO mice, which was partially rescued by *Dkk1*-Tg. (**d-f**) Statistical analysis of epiphysis area (**d**), tibia length (**e**), and cortical porosity (**f**)

indicated significances between KO and DKK1; KO groups. Data are presented as mean ± SEM; n=5 in each group; *P<0.05; **P<0.01. (Unpublished data from Shuxian Lin)

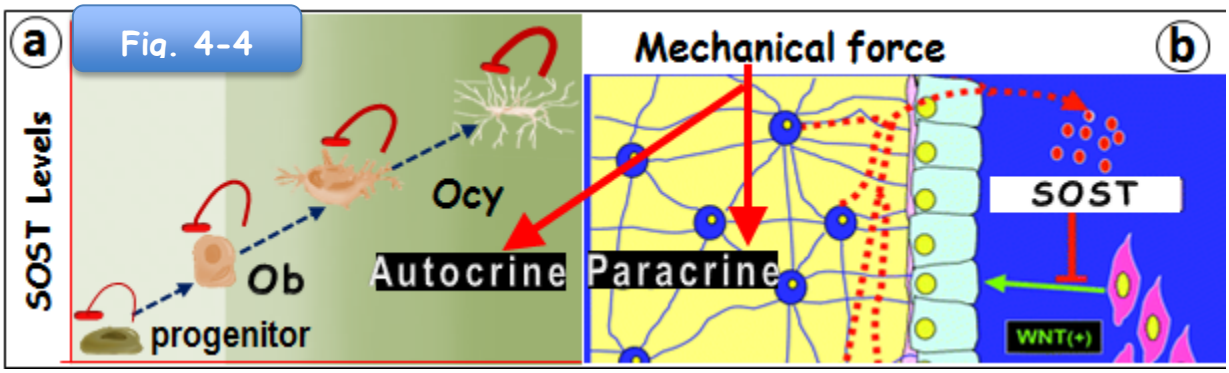

Fig 4-4. ***SOST function in a autocrine manner and target on its own cell to regulate gene expression.*** (a). Through the maturation from osteo-progenitor cells to osteocytes, SOST expression increases as the cell mature and target the cell itself. (b), old dogma showed SOST works as a paracrine and secreted by mature osteocyte to target on bone lining osteoblasts and progenitor cells in response to mechanical forces.

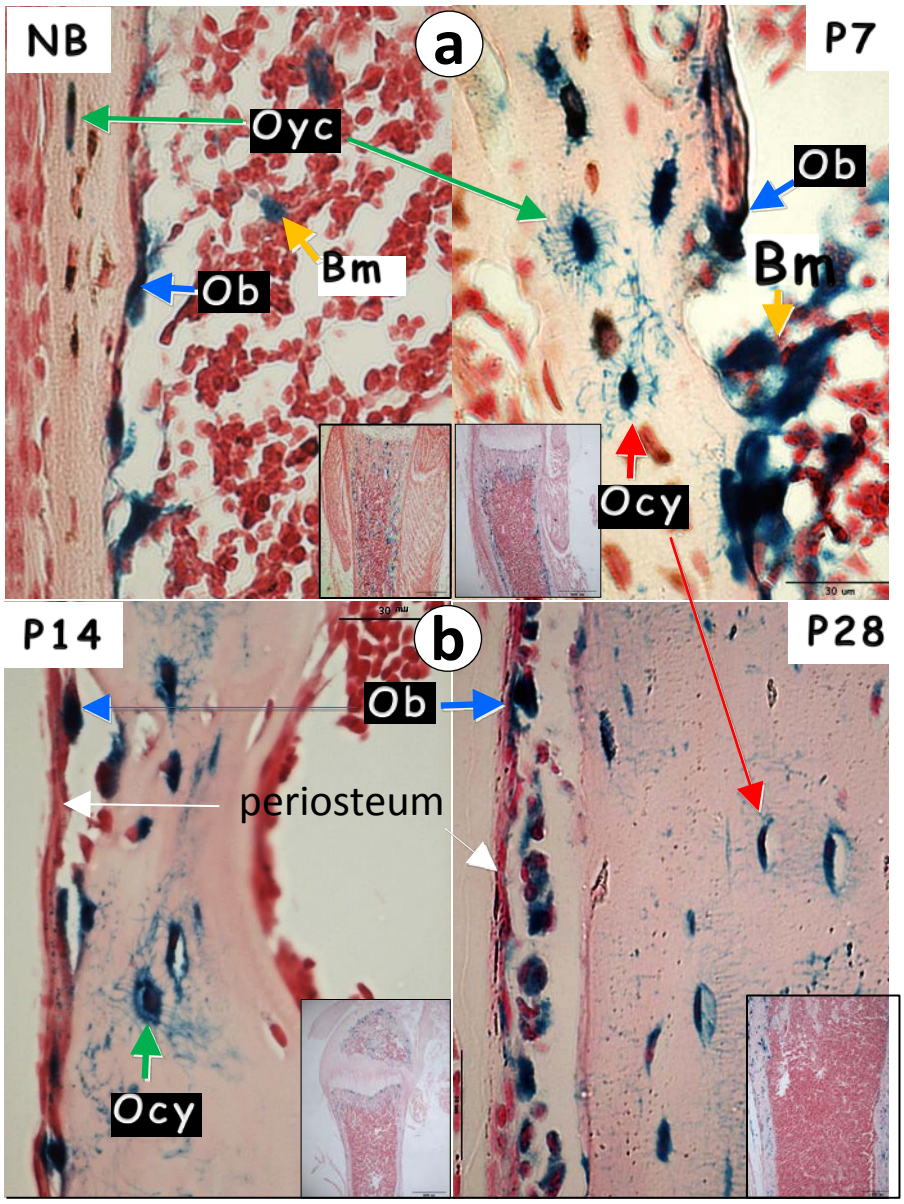
NB
a
P7
Oyc
Ob
Bm
Ob
Bm
Ocy
P14
b
P28
Ob
periosteum
Ocy

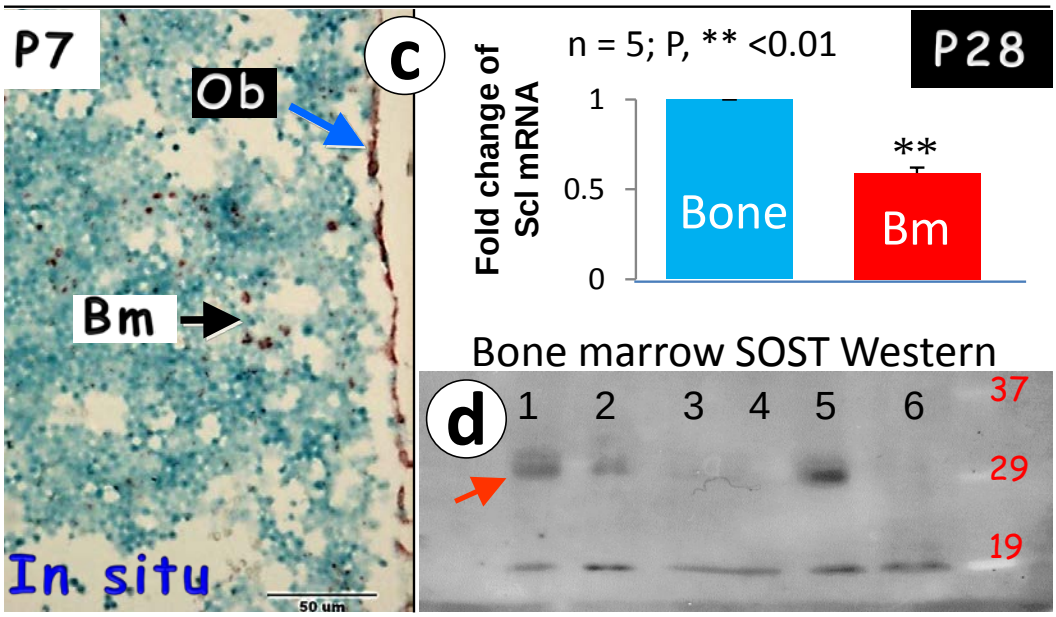

Figure 4-5 ***SOST is expressed in bone marrow and osteoblast cells, as well as in osteocytes.*** **a)** The X-gal-stained image of Sost-lacZ knock-in HET bone revealed SOST-lacZ expressions in bone marrow (Bm), osteoblast (Ob) and osteocyte cells at the ages of newborn (NB) and day 7; **b**) The X-gal-stained image of Sost-lacZ knock-in HET bone revealed SOST-lacZ expressions in the periosteum and cortical bone at the ages of days 14 and 28; **c**) *In situ* hybridization showed Sost mRNA (red) in the bone marrow and osteoblast lining cells (left image), and quantitative RT-PCR data showed Sost expression in cortical bone (with both periosteum and endosteum removed) and bone marrow cells; and **d**) Western blot from the cultured primary mesenchymal cells obtained from mouse bone marrows (lines 1-2) and rat bone marrows (line 5) showed SOST expressions compared to the tooth pulp primary cells (lines 3-4 are from mouse and line 6 is from rat). Altogether, the above data highlight a new source of SOST in bone marrow and osteoblast cells, which are not released from osteocytes as commonly speculated.

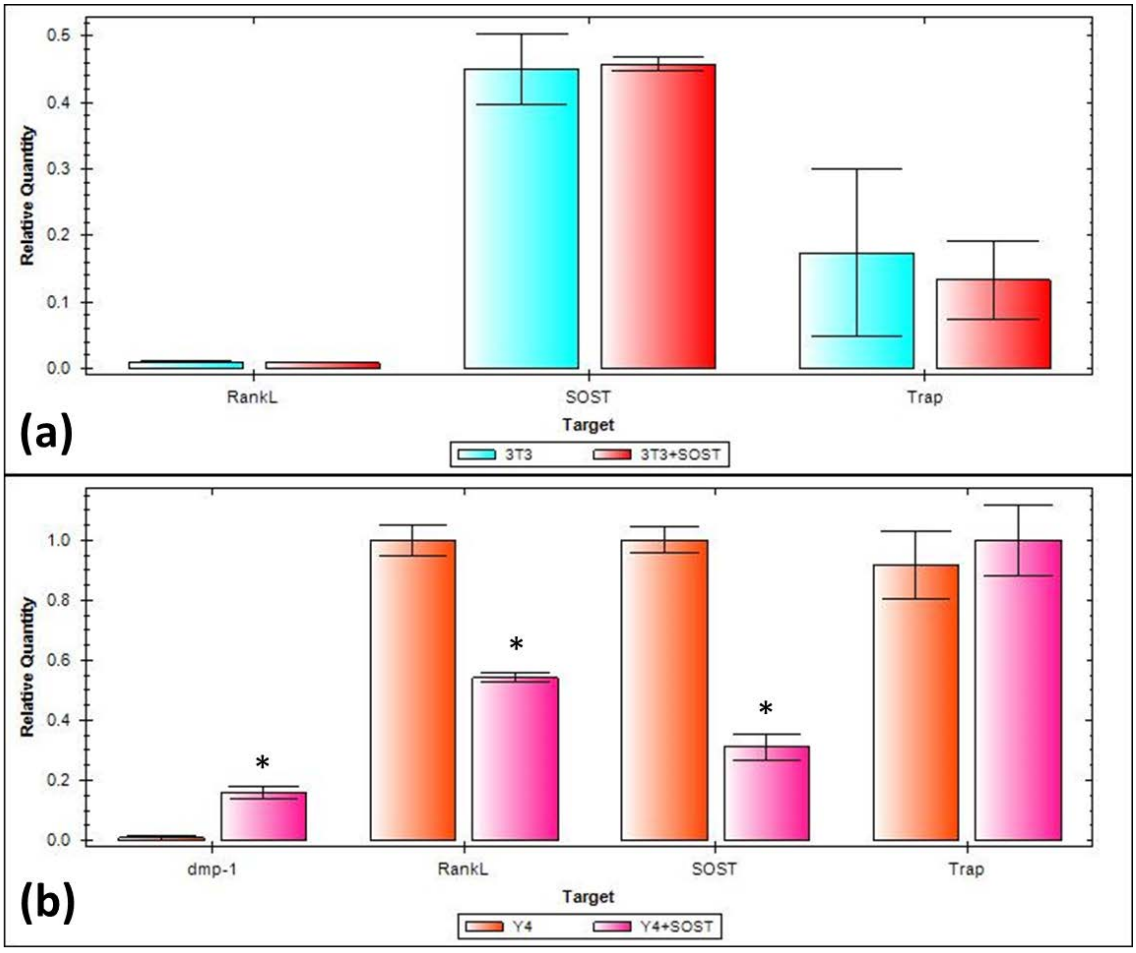

Figure 4-6 ***Gene expression changes of MC3T3 (Ob) cell line and MLOY4 (Ocy) cell line 36 hours after Scl-Ab administration (500ng/ml)***. (a) Anti-SOST antibody on osteoblast cell line (MC3T3) revealed no significant gene expression level changes including SOST. (b). Anti-SOST antibody down-regulated SOST expression by close to 70% in MLOY4 Osteocyte cell line, and significantly decreased RankL and increased Dmp1 expression.